eman ta zabal zazu

Universidad del País Vasco
Euskal Herriko Unibertsitatea

FACULTY OF ENGINEERING VITORIA-GASTEIZ
UNIVERSITY OF THE BASQUE COUNTRY

Advanced Control of Piezoelectric Actuators

by

Cristian M. Napole

a dissertation submitted in partial fulfillment
of the requirements for the degree of

Doctoral Programme in
Control, Automation and Robotics
University of the Basque Country (UPV-EHU)

September, 2022

Resumen en Español

A lo largo de las últimas décadas, la ingeniería de precisión ha tenido un papel importante como tecnología puntera donde la tendencia a la reducción de tamaño de las herramientas industriales ha sido clave. Los procesos industriales comenzaron a demandar precisión en el rango de nanómetros a micrómetros. Pese a que los actuadores convencionales no pueden reducirse lo suficiente ni lograr tal exactitud, los actuadores piezoeléctricos son una tecnología innovadora en este campo y su rendimiento aún está en estudio en la comunidad científica.

Los actuadores piezoeléctricos se usan comúnmente en micro y nanomecatrónica para aplicaciones de posicionamiento debido a su alta resolución y fuerza de actuación (pueden llegar a soportar fuerzas de hasta 100 Newtons) en comparación con su tamaño. Todas estas características también se pueden combinar con una actuación rápida y rigidez, según los requisitos de la aplicación. Por lo tanto, con estas características, los actuadores piezoeléctricos pueden ser utilizados en una amplia variedad de aplicaciones industriales.

Los efectos negativos, como la fluencia, vibraciones y la histéresis, se estudian comúnmente para mejorar el rendimiento cuando se requiere una alta precisión. Uno de los efectos que más reduce el rendimiento de los PEA es la histéresis. Esto se produce especialmente cuando el actuador está en una aplicación de guiado, por lo que la histéresis puede inducir errores que pueden alcanzar un valor de hasta 22%. Este fenómeno no lineal se puede definir como un efecto generado por la combinación de acciones mecánicas y eléctricas que depende de estados previos. La histéresis se puede reducir principalmente mediante dos estrategias: rediseño de materiales o algoritmos de control tipo feedback. El rediseño de material comprende varias desventajas por lo que el motivo principal de esta tesis está enfocado al diseño de algoritmos de control para reducir la histéresis.

El objetivo principal de esta tesis es el desarrollo de estrategias de control avanzadas que puedan mejorar la precisión de seguimiento de los actuadores

piezoeléctricos comerciales. Aunque se utilizó un actuador piezoeléctrico comercial, la idea es que estas estrategias puedan ser aplicadas en sistemas similares con histéresis como principal fenómeno no-lineal. Además de que los algoritmos deben generar una señal de control adecuada para proteger el hardware, también deben cumplir con una complejidad de cálculo numérico limitada. Las características comunes en cuanto a la comparativa de estrategias, están basadas en:

- Desarrollo de estrategias de control avanzadas destinadas a reducir la histéresis de actuadores piezoeléctricos comerciales. Los modelos de control tienen entradas correspondientes a la señal de posición y error obtenidos de la posición del actuator.

- Implementación y validación teórica y experimental de los algoritmos de control. La implementación se realizó en un piezoelectrico comercial a modo de evaluación aunque es posible escalar las estrategias a otros actuadores similares que posean histeresis.

- Evaluación de la medición del error de seguimiento a través de métricas de rendimiento. Las comparativas visuales pueden no ser suficientes y la generación de medidas númericas puede representar una ventaja para mostrar ventajas explicitas en una comparación entre dos esquemas.

- Diseño de cada controlador con señales de actuación que no aumenten el desgaste del actuador y teniendo en cuenta la comparación de los requerimientos de cómputo. Otras caracteristicas importantes que se tuvieron en cuanta estan relacionadas con un diseño de arquitectura sencilla para la implementación, bajo consumo, precisión, estabilidad y robustez.

La comparativa con métodos clásicos e industriales, permitieron analizar las ventajas de las estructuras planteadas. Es por ello que se utilizó un control PID ya que tiene un diseño intuitivo y simple que permite que la señal de pocisionamiento se mantenga próxima a la referencia. Los parámetros del controlador se ajustan tras el análisis de dicha respuesta. Es por esto que este tipo de control es el más utilizado porque es un control sencillo que proporciona unos resultados aceptables. Sin embargo, en el caso de sistemas complejos con dinámica fuertemente no lineal como la histeresis que es un efecto no-lineal dependiente del tiempo. El funcionamiento del sistema mejoró, en gran medida, utilizando técnicas de control avanzadas.

La disminución de la histéresis y la disminución del error de seguimiento se realizó en combinación entre esquemas feedback-feedforward. La compensación feedforward tiene como objetivo mapear la no linealidad del dispositivo para compensar la histeresis; en esta investigación se ha demostrado que esta técnica es efectiva. Por otro lado, la reducción de errores, los cambios dinámicos y los efectos desconocidos son propiedades que aunque el control que feedforward no logra compensar, pueden abordarse con una estrategia de retroalimentación (o feedback). Este último ofrece una solución que puede aumentar la precisión del controlador, aunque su uso puede resultar en un margen de ganancia bajo que restringe el uso de controladores de alta ganancia. En esta investigación se optó principalmente por una combinación de ambos marcos (feedback-feedforward) para el análisis e implementación. Los controladores feedback-feedforward aumentaron la precisión del actuador a través de las ventajas que ambas técnicas pueden proporcionar por separado. Las estrategías feedback-feedforward se pueden combinar de diferentes formas. En este trabajo, la histéresis se compensó principalmente con redes neuronales artificiales combinadas con controladores convencionales, de lógica difusa y control de modo deslizante.

Las redes neuronales artificiales pretenden imitar la plasticidad neuronal del cerebro humano para el aprendizaje de distintos conceptos. Se ha definido una red neuronal como un sistema compuesto por muchos elementos de procesamiento (neuronas) que operan en paralelo, cuya función es determinada por la estructura de la red, las conexiones y el procesamiento realizado por los elementos computacionales o nodos. Las redes neuronales pueden aprender a partir de conjuntos de datos de entrenamiento que se reflejan en la estructura de la red en modo de un conjunto de funciones lineales cuyos parámetros son obtenidos a partir de un proceso estadístico con los datos. Se ha demostrado que las redes neuronales pueden ser usadas con efectividad y precisión para la identificación y el control de sistemas con dinámicas complejas, especialmente para plantas no lineales que varían en el tiempo y que resultan más difíciles de regular con métodos convencionales. En la vida real la mayoría de los procesos industriales pertenecen a esta categoría, de ahí la necesidad de métodos inteligentes para controlar esos sistemas. El interés creciente en las redes neuronales se debe a su gran versatilidad y al continuo avance en los algoritmos de entrenamiento de redes y en el hardware, lo que ha sido posible gracias a que cada vez es más fácil disponer de computadores extremadamente rápidos, a un precio competitivo, para implementar estos algoritmos. La mayoría de las aplicaciones desarrolladas hasta ahora lo han sido en áreas de cálculo

intensivo. Dentro del control hay también áreas con esos requerimientos como la identificación en tiempo real y el control de grandes estructuras flexibles, o en robótica, donde el uso de las redes neuronales pueden conseguir mejores resultados. El desarrollo hardware de redes neuronales puede llevar a una nueva revolución en las aplicaciones del control, similar a la producida con la aparición de los microprocesadores.

La lógica borrosa o fuzzy, introducida por Lofti A. Zadeh (1965), es una forma matemática de representar la imprecisión inherente al lenguaje natural. La teoría de conjuntos borrosos resulta muy útil en aquellas situaciones en que los datos y sus relaciones no pueden escribirse en términos matemáticos precisos. Los conjuntos borrosos son una generalización de la lógica clásica y contienen objetos que pertenecen de forma imprecisa o gradual al conjunto. El grado de pertenencia viene definido por una función de pertenencia, que usualmente toma valores entre 0 y 1. La primera aplicación de la lógica borrosa al control fue realizada por Mamdani, en 1974. Su aspecto novedoso está en que pretende emular la estrategia de control que seguiría un experto humano en el control manual de un proceso más que el controlador en sí, y en que utiliza información descrita en términos lingüísticos. Es una de las aproximaciones más populares hoy en día en la industria, especialmente en Japón y se ha ido consolidando, aunque más lentamente en USA y Europa. Tanto la teoría como las aplicaciones de la lógica borrosa siguen actualmente en desarrollo, y ha sido implementada con éxito en numerosas aplicaciones prácticas (como en este trabajo de investigación), si bien sigue siendo también en algunos casos un tema de controversia en la comunidad científica.

El control de modo deslizante (o SMC, por sus siglas en inglés) es un enfoque no lineal cuya principal ventaja es que proporciona una respuesta rápida, robustez, estabilidad en entornos indeterminados y requiere bajos recursos computacionales. Esta técnica posee una ley de control que cambia la dinámica de un sistema en base a una superficie deslizante que asegura la convergencia. Sin embargo, un inconveniente de esta estrategia es que los estados pueden tardar en alcanzar un estado de equilibrio. Otro inconveniente del control deslizante es la generación de vibraciones (o chattering) causada por la discontinuidad propia del esquema. El chattering se puede atenuar con el uso de derivadas de la superficie deslizante que pueden ayudar a disminuir este efecto. Está técnica se ha denominado como controlador de modo deslizante de orden superior (o HOSMC, por sus siglas en inglés). Cuando se utilizan derivadas, la convergencia de tiempo finito está garantizada al origen, mientras que el SMC convencional solo cede a la estabilidad asintótica. Leonid Fridman

definió una segunda generación de SMC, denominada bajo el nombre de algoritmo de torsión (o TA, por sus siglas en inglés) en la que se emplean derivadas. Sin embargo, el uso de derivadas puede inducir un alto nivel de ruido en un esquema feedback. En este escenario, el algoritmo de super-torsión (STA, por sus siglas en inglés) intenta contrarrestar estos problemas utilizando términos integrales y evitando utilizar derivadas de orden elevado. Además, otra estructura no convencional que también se encontró es la ley de convergencia prescrita, que es un algoritmo de segundo orden conocido por su tasa de convergencia y capacidades de seguimiento.

Estas combinaciones han sido analizadas en la plataforma comercial seleccionada. Los resultados se difundieron a través de diversas publicaciones que se resumen a continuación:

- Control PID con compensaciones avanzadas tipo feedforward: En este estudio se estudio una estructura de control tipo PID con distintas estrategias de compensación a través de una identificación inversa del sistema. En este sentido, se utilizaron tanto una estrategia lineal simple como el uso de una red neuronal pre-entrenada. Finalmente se generó un algoritmo puramente neuronal que contempla un PID neuronal con una compensación de red neuronal.

- Compensación con identificador Hammerstein-Wiener (HW) y lógica borrosa como controlador: Se utilizó una compensación de HW, el cual es un método de identificación cuya estructura contempla una combinación de bloques lineales y no lineales donde los parámetros se pueden hallar por estimación comparativa con datos experimentales. Por lo tanto, se diseñó y se implementó un controlador realimentado con lógica borrosa tipo 1 compensado con HW. Se realizaron comparativas con un controlador tipo PID donde se midió la performance a través de la medición del IAE, raíz del error cuadrático medio (RMSE) y raíz del error cuadrático medio relativo (RRMSE). Los resultados obtenidos fueron favorables para la estructura propuesta tanto en la precisión como el comportamiento de la señal de control.

- Desarrollo de un algoritmo deslizante tipo super-twisting basado en redes neuronales: Los controladores surper-twisting pertenecen a los deslizantes de orden superior y se desarrollaron para reducir el chattering generado por los controladores deslizantes convencionales. La innovación de esta investigación fue la propuesta de un controlador tipo deslizante de orden

superior con una red neuronal entrenada con datos experimentales para reemplazar el término equivalente de un controlador deslizante convencional. Además, se demostró la estabilidad teórica mediante un desarrollo de Lyapunov así como la experimental donde se midió IAE, RMSE y RRMSE. Los resultados mostraron una ventaja significativa para el controlador propuesto al igual que una señal de control adecuada.

- Desarrollo de un algoritmo deslizante tipo cuasi-continúo basado en redes neuronales: Continuando con la tendencia del controlador explicado anteriormente, esta vez se realizó una estrategia similar, pero utilizando un controlador deslizante cuasi-continuo. Este mismo fue diseñado para reducir el chattering de un deslizante convencional y mantener la robustez. La red neuronal se entrenó de nuevo con datos experimentales para reemplazar el término equivalente de un controlador deslizante convencional. La comparativa se realizó con un control PID en un esquema experimental y se obtuvo una mayor precisión, utilizando como indicadores el IAE y el RMSE. Además, se midió el chattering de manera numérica y se obtuvo un valor también favorable el algoritmo planteado.

- Control de lógica difusa tipo 1 y 2 con compensación neuronal: en función a la investigación y experiencia previa, se optó por probar nuevas estrategias aún más avanzadas. En este sentido, se utilizaron controles difusos de tipo-1 y tipo-1 en combinación con una red neuronal pre-entrenada. En la comparativa se utilizó un controlador industrial tal como un PID y se analizó, en base a datos experimentales, las ventajas de las estrategias con y sin compensación feedforward. Esto generó como conclusión que los controladores difusos con compensación tienen una significativa mejora frente a la reducción del error y señal de control. También se concluyó que la estructura de lógica difusa tipo 2 en conjunto con la red neuronal, generó los mejores resultados en este estudio.

- Controladores neuronales avanzados de modo deslizante: En esta investigación, se compararon varios enfoques de control, basados en la combinación de control de modo deslizante y redes neuronales. Esto permitió hacer frente a las no linealidades, mejorar la precisión y robustez del posicionamiento del actuador. En particular, se analizó la aplicación de diversas técnicas de control de modo deslizante de distintos ordenes, como twisting, super-twisting y prescribed convergence law, en combinación con redes neuronales. Estas técnicas se validaron experimental-

mente y se verificó la reducción del error entre los algoritmos de super-twisting y prescribed convergence law. Finalmente, se evaluó el consumo de tiempo computacional para las estrategias de control presentadas.

Abstract

Piezoelectric actuators are micro electro-mechanical devices frequently employed in applications where nano- microdisplacement is required, because of their high-precision performance that comes also with large actuation forces. However, the positioning is affected substantially by non-linear effects being hysteresis the most relevant one. The objective of this study is to enhance the tracking accuracy of a commercial piezoelectric stack actuator. Hence, the proposal is based on control algorithms that could compensate the hysteresis. Different combinations and variations of sliding mode control strategies, fuzzy logic and proportional-integral-derivative with feedforward compensations (like Hammerstein-Wiener and artificial neural networks) were studied. Additionally, experimental results were performed in a test bench with different comparisons of the proposed control approaches. The outcomes showed enhancements in terms of error reduction, generated control signal and robustness, which were analysed in depth with the contrasted techniques for each case.

To my family and friends.

Contents

Listing of figures

Acknowledgments

First, I would like to say thanks to Dr. Oscar Barambones and Dr. Isidro Calvo for their support during this research period. Words cannot describe my gratitude to they. Also, to the University of the Basque Country (UPV/EHU) for the opportunity to develop this research.

Secondly, I would like to say thanks to my family and friends who support me during these years. Their accompaniment was very important for me. Also to my new friends that I met in Vitoria who had give me a huge encouragement at any time.

Last but not least, I would like to say thanks to my friend Dr. Mohamed Derbeli for his support, ideas shared and hard-work capabilities. He has been an important partner in this research and a great team player from whom I had the pleasure to work with.

Acronyms

AFM: Atomic force microscope
ANN: Artificial Neural Network
BB: Black-box
BW: Bouc-Wen
EKM: Enhanced Karnik-Mendel
FF: Feed-forward
FLC: Fuzzy logic control
FLC-T1: Fuzzy logic control type-1
FLC-T2: Fuzzy logic control type-2
FOU: Footprint of Uncertainty
HOSMC: High order sliding mode control
HW: Hammerstein-Wiener
IAE: Integral of the absolute error
IASC: Iterative algorithm with stop condition
ISMC: Integral Sliding mode control
LCP: Lower converging point
LM: Levenberg-Marquardt
LQG: Linear quadratic gaussian
LRNN: Layer-recurrent neural network
LTP: Lower target point
LTR: Loop transfer recovery
MEMS: Micro electro-mechanical system
MLP: Multilayer perceptron
MSE: Medium-squared error
NARX: Non-linear Auto-Regressive Network
NLMPC: Non-linear model predictive control
PCL: Prescribed convergence law
PEA: Piezoelectric actuator
PI: Prandtl-Ishlinskii

PID: Proportional-integral-derivative
PSO: Particle Swarm Optimisation
PZT: Lead Zirconate
QCSMC: Cuasi-continous sliding mode control
QCSMC-ANN: Neural cuasi-continous sliding mode control
RMSE: Root-mean-squared error
RRMSE: Relative root-mean-squared-error
RTI: Real-Time Interface
SMC: Sliding mode control
SNPID: Single-neuron proportional-integral-derivative
STA: Super-twisting algorithm
ST-ANN: Neural super-twisting algorithm
TA: Twisting algorithm
TDNN: Time Delayed Neural Network
UTP: Upper target point

Glossary

P_i: Electric displacement vector
i: i-th index notation
j: j-th index notation
k: k-th index notation
σ_{jk}: Stress tensor
d_{ijk}: Matter tensor
d_{33}: Piezoelectric Coefficient
T_c: Curie Temperature [ºC]
α: Displacement Slope[μ/V]
δ: Vertical offset [μ]
e_i: Error of the i-th sample
r_i: Reference value of the i-th sample
N: Total amount of samples
ΔT:Sampling time [s]
W_i: Weight of the i-th neuron at the hidden layer
b_i: Bias of the i-th neuron at the hidden layer
W_j: Weight of the j-th neuron at the hidden layer
b_j: Bias of the j-th neuron at the hidden layer
K_p: Proportional gain
K_i: Integral gain
K_d: Derivative gain
X_i: Error decomposition for neural controller where i = 1…3
η_i: Learning rate for every X_i
K: Neural Proportional-integral-derivative gain
$q^{-}1$: Time shift operator
n_b: Degree of transfer function numerator of a Hammerstein-Wiener block
n_f: Degree of transfer function denominator of a Hammerstein-Wiener block
n_d: Degree of transfer function delay of a Hammerstein-Wiener block
$y_{measured}$: Measured output data for FitPercent calculation

y_{model}: Measured output data from model for FitPercent calculation
$\overline{y_{measured}}$: Mean measured output data for FitPercent calculation
K_E: Error gain of a fuzzy logic controller
K_{ED}: Derivative of error gain of fuzzy logic controller
K_o: Output gain of fuzzy logic controller
PB:Positive big
PM: Positive medium
PS: Positive small
Z: Zero
NS: Negative small
NM: Negative medium
NB: Negative big
μ_a: Input membership function distribution of a fuzzy logic controller
ΔU: Change in the control signal generated
μ_d: Output membership function distribution of a fuzzy logic controller
V: Lyapunov Function
E: Normalized error
$\dot{E}$: Normalized error derivative
u_{sw}: Control signal of super-twisting algorithm
K_1: Gain of the first term of super-twisting algorithm expression
K_2: Gain of the second term of super-twisting algorithm expression
S: Sliding surface of a sliding controller
λ: Gain of the error term in a derivative sliding surface
u_{ann}: Compensation signal from an artificial neural network
T_i: Target output data from an artificial neural network
U_i: Prediction data from an artificial neural network
u: Input voltage [V]
m: Mass [kg]
b: Damping [$\frac{Ns}{m}$]
k: Stiffness [$\frac{N}{m}$]
f_h: Hysteresis [$\frac{N}{V}$]
P: Perturbations [N]
x: Position [m]
ε: Approximation error of a neural network for hysteresis fitting
γ: Gain of a cuasi-continous sliding controller
$\tilde{A}$: Fuzzy set type-2
K_c: Gain of a conventional sliding mode controller
k_3: Gain of the first term of a twisting algorithm

k_4: Gain of the second term of a twisting algorithm
K_{PCL}: Gain of a prescribed convergence control law
β: Gain of the function from a prescribed convergence law

1

Introduction

1.1 Motivation

Throughout the last decades, precision engineering have had an important role as a cutting-edge technology where the downsizing trend of industrial tools began to be required [1]. Industrial processes began to demand accuracy is in the range of few nanometers to micrometers. Despite that conventional actuators may not be able to be reduced or achieve such exactitude, piezoelectric actuators (PEAs) are still a new technology and their performance is still under

scrutiny in the research community.

Piezoelectric actuators are commonly used in micro and nano-mechatronics (also known as micro electro-mechanical systems or MEMS) for positioning applications due to their high resolution and strength (above 100 Newtons) in comparison to their size. All these features can also be combined with a fast actuation and stiffness, depending on the application requirements. Therefore, with these features, PEAs can grant a wide variety of industrial applications.

Negative effects such as as creep, vibration dynamics and hysteresis, are commonly studied to enhance the performance when high accuracy is required. Nevertheless, one of the most studied effects that reduces the performance on PEAs is hysteresis. Specially when tracking is the role of the PEA, this phenomenon can induce errors which can reach a value of 22% [2]. According to Bashash et al. [3], hysteresis can be defined as input/output effect combined of mechanical and electrical actions that depends on the memory or previous states. Hence, this implies that future outputs may be predicted based on the formerly record. Hysteresis can be reduced mainly by means of two strategies: material re-design or closed loop control algorithms [4]. Due to several downsides which will be explained in further sections, the latter option is a suitable choice which will be the major motivation of this thesis.

1.2 Objectives

The main objective of this thesis is the development of advanced control strategies which could improve the tracking accuracy of commercial piezoelectric actuators. Although that a commercial PEA was selected for the experiments, all the control strategies developed are aimed to be used in similar actuators with hysteresis. These control proposals had to accomplish not only a suitable control signal but also had to be reliable for the workbench hardware so that the numerical calculation complexity could be limited. Therefore, in each layout, the common and remarkable points were taken into account as:

- Development of advanced control strategies aimed to reduce the hysteresis of commercial piezoelectric actuator.
- Theoretical and experimental implementation and validation of the control algorithms.

- Evaluation of tracking measurement through performance metrics.
- Design of each controller with reliable control signals and comparison of the computing requirements.

1.3 Structure

This thesis is arranged in a comprehensive way to guide the readers to implement different control algorithms at PEAs. Several control approaches are proposed and the results of the experiments are discussed. A total of 6 subchapters were developed to show the outcomes gathered during the period of research.

Chapter 2 introduces the PEAs from historical facts since the discovery of the piezo-electricity and important events that derived in nowadays configurations. Then, a brief explanation about the working principle is detailed with a link to the hysteresis phenomena. Well-known and up-to-date applications are also reviewed to show how important this devices are for industries and the research community. At the end, an explanation about the PEA model used in this research is explained.

Chapter 3 explains the hardware that was used for the experiments. Since this thesis focuses mainly in a PEA, an in-depth analysis of the commercial PEA is provided within a study of the acquired hysteresis. Also, an explanation of the reference design is specified. Additionally, the peripheral used hardware is also described with its details.

Chapter 4 provides a summary of the control structures used in the research. Further details about the compensation strategies were also explained, such as artificial neural networks and Hammerstein-Wiener for instance. The obtained results from the testing in real time were explained in-depth in case that researchers would like to replicate the analysed strategies. At the end of each research, a conclusion was supplied to highlight the main outcomes gathered from each.

Finally, Chapter 5 concludes with a summary of the most important outcomes gathered along the research period. Moreover, future lines or gaps for research are present based on the analysis provided.

Everything is theoretically impossible, until it is done.

R. Heinlein

2 Piezoelectric Actuators

2.1 Introduction

This chapter provides an introduction to the basics of piezoelectric actuators. A brief history of the piezoelectric actuators since the discovery of the effect is introduced. Also, the working principle is explained and the hysteresis concern is developed. Because it is one of major topics of this thesis,alternative options to reduce phenomenon are explained. Since piezoelectric actuators are available in different geometries, the types of actuators available in the market are

described.

2.2 A historical overview: from pyroelectricy to piezoelectric actuators

Piezoelectricity was discovered by Jaques and Pierre Curie in 1880 where they found that if a pressure was applied to asymmetric crystals (they examined tourmaline, zinc blende, boracite, topaz, calamine and quartz), then a electrical polarization was produced and a mirrored effect with a negative voltage was measured [5]. In this case, the crystal symmetry property is related to the third dimensional relation between stress and electric excitation such that:

$$P_i = d_{ijk}\sigma_{jk} \tag{2.1}$$

Where P_i is the electric displacement vector, d_{ijk} is the piezoelectric matter tensor and σ_{jk} is the stress tensor [6]. Certainly, Equation 2.1 is an extension of the Hooke's law to piezoelectric materials; these are considered as a *non-centrosymmetric* material as it lacks of an inversion center in d_{ijk}, which is considered as a fundamental property [7].

At that time, they defined this effect as *pyroelectricity* (conjunction of with the greek word *pyro* that means fire) since they also measured a temperature change in the poles. Nevertheless, piezoelectricity (where *piezo* means pressure in greek) is mostly related to the generated voltage from a strain in the material. Likewise, piezoelectricity can be produced with a voltage applied to these crystals which will outcome a displacement.

In the following 20 years since the discovery, the foundations of theoretical and experimental investigations were carried but with unpractical applications for the industry. However, during the first world war, piezoelectricity took its first important role as it began to be employed as a sensor by the french forces to detect german submarines: the physicist Paul Langevin (former student of Pierre Curie) developed a sonar which uses reflected sound waves to generate a voltage [8]. Further important applications had been developed during the 1940's when the Austrian neurologists Karl and Friederich Dussik used ultrasound waves to detect brain tumors based on piezoelectric sensors [9].

On the other side, PEAs have a relatively young history. These devices use the inverse phenomenon to produce a mechanical displacement from an

electrical excitation which allows micro- and nanopositioning being adequate at high precision operations. It was not until the beginning of 1980 when research team of the Tokio Institute of Technology in cooperation with Penn University, produced an high-precision deformable mirror for light focus based on a PEA [10]. Almost 10 years later, the Cymbal transducer was patented by Newnham et al. [11]; this consisted of a piezoelectric disk ensemble between metal caps (similar to ring benders which will be explained in the following paragraphs). The usage of these actuators allowed an explosion of applications in the market in fields of photography, automotive, printing and computing [12].

2.3 Working principles of piezoelectrical actuators

A piezoelectric material works as an actuator when a voltage that is applied is transformed in mechanical displacement [13]. A schematic description is provided in Figure 2.1. Not only a precise displacement can be generated but also it can handle high static or dynamic forces [14]. Additional capabilities are related to vibrations control as they are able to handle high frequencies due to their quick switching [15]. Nevertheless, the hysteresis is a major downside of these actuators when they are required in high precision applications.

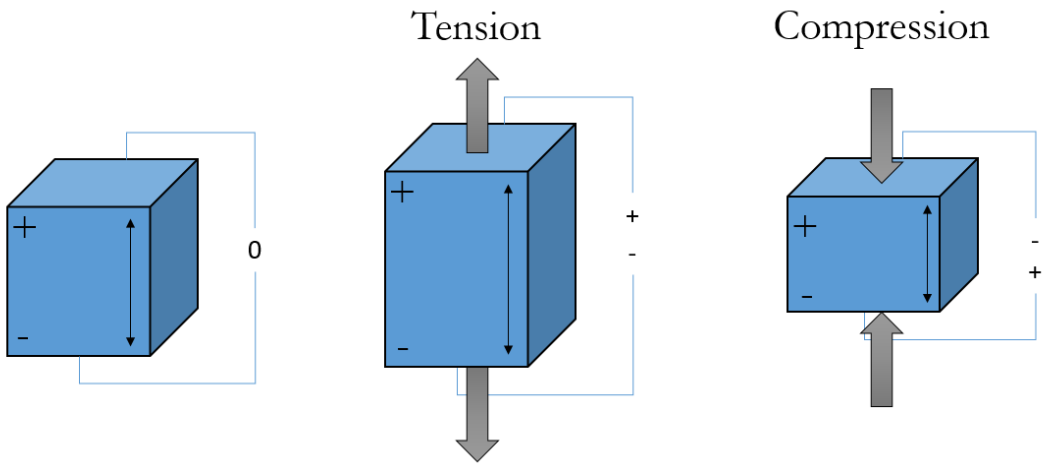

Figure 2.1: Schematic description of PEA working principle.

From a material level perspective, Anastasia Muliana provides an explanation about the hysteresis generated in piezoelectric actuators on her study [16]:

the polarization alignment of the crystals has an electro-mechanical coupling which implies that when an electric field is applied, these are straighten and the material extends its dimension (material polarization). Once that the electric excitation is released, a residual polarization leaves the crystals in a polar position that is different to the one from the beginning [17]. A graphical explanation of this, is provided in Figure 2.2 where (a) shows a piezoelectric material without electrical excitation. Then, (b) is when an electric field is applied and the poles are aligned; finally, (c) is when the field is released and the poles have the residual polarization.

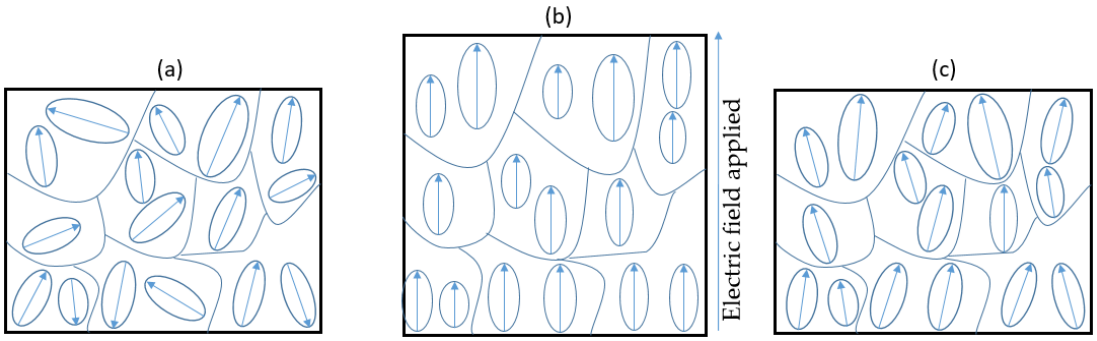

Figure 2.2: Material perspective description of the hysteresis in PEAs.

The first option is perhaps the most complex one since many limitations need to be taken into account. An example of this is the piezoelectric coefficient (also known as d_{33}), which determines the degree of induced strain at a particular electrical field; furthermore, it is one of the main parameters that describes a PEA performance [18]. Thus, a piezoelectric material will show less hysteresis but at the expense of decreasing d_{33} since the material should be harder as Figure 2.3 shows.

Despite that the usage of soft piezoelectric materials increases the piezoelectric coefficient, also it has a temperature dependant effect which implies that the design of a piezoelectric material requires a complex design in several areas. Figure 2.4 shows the effect of piezoelectric coefficient against the Curie temperature (T_c which value decreases exponentially within d_{33}) [18]. T_c is a temperature that is usually 10ºC below the Curie point, which represents the temperature in which the piezoelectric material properties start to be lost [19].

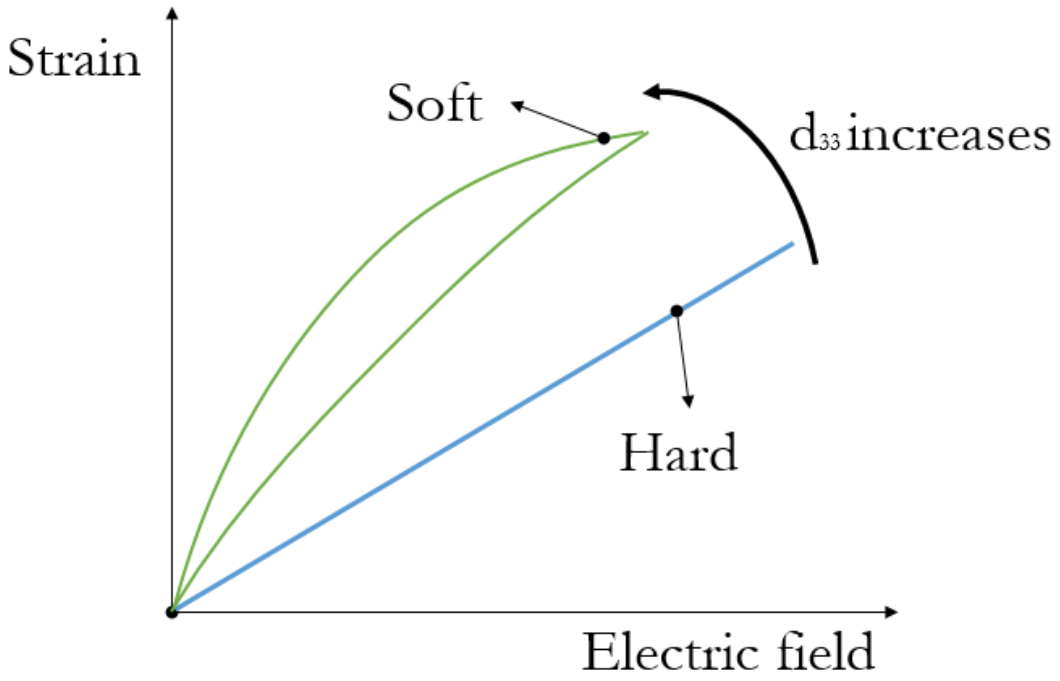

Figure 2.3: Creep effect for a constant reference following.

2.4 Types of piezoelectric actuators

Nowadays, the main types of PEAs that are being used in industry are stack, bending and ring bending. These can be combined in different modes and mechanical structures for different purposes. Based on the explanation of [20], the classification can be made as follows:

- **Stack (Figure 2.5):** These are produced through a stack of piezoelectric disks that are electronically linked. This arrangement allows a linear motion when a voltage is applied because the thickness of the layers increases. In comparison to other options, the assets are related to support a high longitudinal mechanical load. Nevertheless, high impact forces can induce a device break due to its high stiffness. Common applications of these are active vibration control [15], high precision machine tools [21] and optical microsurgery [22].
- **Bending (Figure 2.6):** Also known as *multi-layer actuators*, in this case

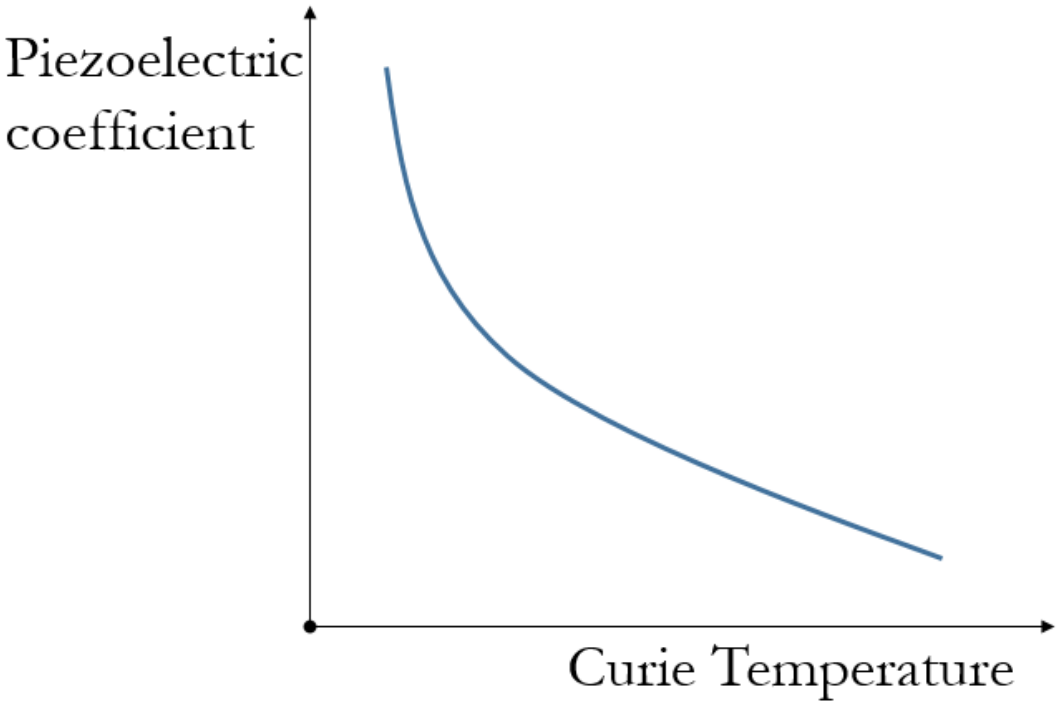

Figure 2.4: Curie temperature contrasted with the piezoelectric coefficient.

the movement is generated by an electric excitation that generates an internal piezoelectric motion which deforms the actuator as a deflection [23]. The advantages are associated with a simple structure, a low production cost and the mechanical quality tends to be high; a main downside is the poor resistance at high impact forces. These devices can be frequently find in manipulation and imaging of atomic force microscopes (AFM) [24], energy harvesting [25], micro-gripers [13], etc.

- **Ring Bender(Figure 2.7):** In this case, the actuator is a rounded disk composed of thin layers of piezoelectric material that are placed in a side. A bending motion is produced due to a deformation of the piezoelectric ring that is attached to the laterals of the ring [26]. Also, since there is a hole in the center of the device, it introduces flexibility at pressure mode operations in high precision valves [27], micro-robotics [28], energy harvesting [29], etc.

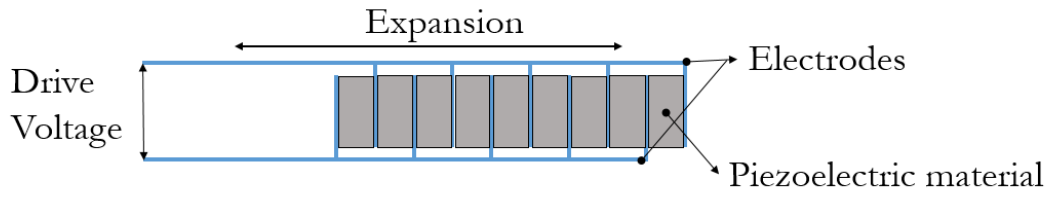

Figure 2.5: Schematic description of an Stack PEA.

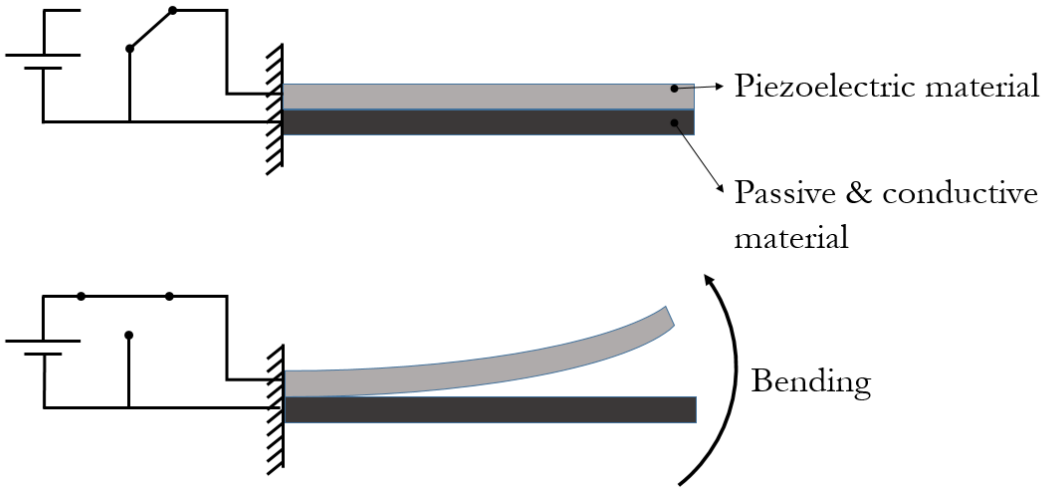

Figure 2.6: Schematic description of a bending PEA.

2.5 Applications

Even-though that the previous mentioned PEAs geometrical configuration can concede different types of applications, the following uses deserve to be highlighted as main technologies that are under research currently.

- **Atomic force microscopy:** An AFM is a device that helps to investigate the mechanical interaction of cells with their environment [30]. This mechanical system combined with the usage of a laser beam and its reflection, allows the development of high resolution images of surfaces.
- **Energy Harvesting:** The discovery of piezoelectricity allowed the generation of voltage and therefore a current trend related to clean energies is

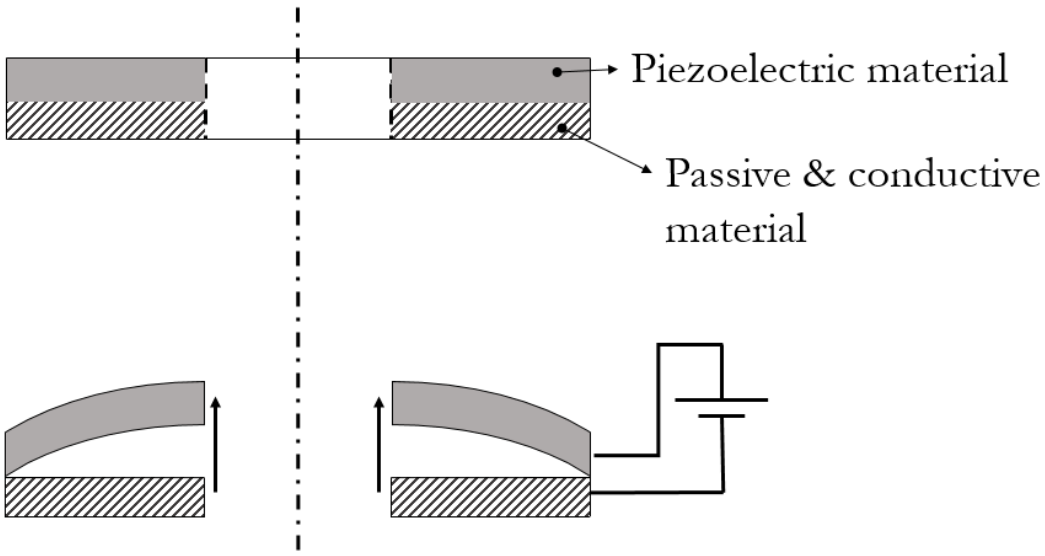

Figure 2.7: Schematic description of an ring bender PEA.

based on this principle. Energy generation from piezoelectrics is related to applying forces and obtain a voltage over time [31]. Cantilever configurations are used for these applications due to their efficiency in vibrational sources such as bridges, human motion or vehicle vibration [32].

- **Piezoelectric motor:** These devices are made from an arrangement of PEAs which induce capabilities as high power-to-weight ratio in a compact size, high precision and fast response time without any backlash [33]. The shape change of the material allows a linear motion that is transformed in rotational [34]. These are widely used in autofocus and optical stabilization operation at cameras [35].

- **Machine tools:** Due to the high-precision features of PEAs, machine tools can improve their precision which allows to be a trend topic in research and industry of manufacturers [36]. The application had been tested in diamond machining [37], vibration assisted polishing machines [38] and ultrasonic processes [39].

- **Micro-grippers:** The downsizing characteristics of PEAs induced the miniaturization of common tools for micro-manipulation. In this case, the in-

troduction of PEA improves the power, force and precision of grippers in comparison to alternative solutions such as electromagnetic, thermal, shape memory alloy [40].

- **Micro-drones:** In 2013, researchers from Harvard University developed a paperclip size microdrone which used a PEA to move the wings, called RoboBee [41]. Later in 2019, they developed one of the lightest wireless flying machine (based on bees) with a weight of 259mg, which was fed through a small photo-voltaic array attached to the device [42].

- **Spinal Injection devices:** Spinal cord injection is a complex task where high positioning accuracy is required in tasks such as open surgery or magnetic resonance imaging. Meinhold et al. [43] provided a research where they used a linear piezoelectric motor for a high accuracy position mechanism which helped to improve the procedure of this complex injection.

- **Drug delivery system:** A drug delivery system helps patients with a medical specific schedule. PEAs helped the downsizing of micropumps which are commonly used in these procedures [44]. Current technologies of PEAs also have to be considered due to bio-compatibility in terms of materials.

Nevertheless, piezoelectric actuators have several downsides which tend to degrade their performance when precise tracking needs to be improved. The major non-linearities identified at PEAs are creep, vibration dynamics and hysteresis. Regarding the latter mentioned, it is known that it can lead to an error of 20%, which is a significant value when precision is required. Despite that it is recommended to use conventional proportional-integral controllers to improve the tracking, along this thesis, we developed different combinations of advanced control strategies. The performance of the proposed control approaches was compared with PID (proportional-derivative-integral) controllers in terms of tracking accuracy. Also, this aim has been considered with the control signal developed so that the robustness and actuator life-time can be increased.

It doesn't matter how beautiful your theory is, it doesn't matter how you smart you are. If it doesn't agree with experiment, it's wrong.

R. Feynmann

3

Experimental setup

This chapter describes the hardware architecture used. The proposed control approaches tried to mitigate the hysteresis effect, the main issue to be reduced and thus, it was measured during experiments. An in-depth analysis for the hysteresis curve is summarized at the most important spots to be considered at the control design stage. Because the PEA operated with high voltage values, the manufacturer provided peripheral devices which helped to conduct experiments with signals that are more suitable for acquisition devices.

3.1 Commercial piezoelectric actuator

The research made in this thesis has been carried with a commercial PEA to generate the experiments with the analysed solutions. As the main actuator, we used a Thorlabs PK4FYC2 which is a stack actuator manufactured with piezoelectric chips made of lead zirconate (PZT) layers that are glued with epoxy and glass beads. The maximum displacement is 38.5μm at 150V. Since the displacement is micrometric and precision is required, the manufacturer included four strain gauges that are configured in a Wheatstone bridge so that the measurement could be obtained from resistance variation, which provided a better resolution [45]. According to the manufacturer, the maximum error due to hysteresis phenomenon is 15%, which can be reduced through the usage of a PID (this will be explained in the further sections)..

	Values	Units
Nominal Displacement	38.5	μm
Actuator Dimensions	7.3 x 7.3.36	mm
Force at maximum displacement	400	N
Blocking force	1000	N
Resonant frequency	34	kHz
Curie Temperature	230	°C

Table 3.1: PK4FYC2 Specifications from the manufacturer

3.2 Hysteresis of the commercial piezoelectric actuator

The mechanics of the hysteresis curve of the selected PEA is shown in Figure 3.2 which was produced by using 2 triangle cycles as input voltage. The sequence starts at the initial point called *lower target point* (LTP) where the PEA undertakes its operation. Thus, a first ascending curve *(a)* climbs until the *upper target point* (UTP), which is the point where the actuator reaches the maximum displacement. An important feature prior to continue with the description is that in case of a new experiment and unless that the PEA is re-calibrated to start from a null displacement, *(a)* will only appear once.

Thereafter, the fall is through an asymmetric path along the first descending curve *b* until the *lower converging point* (LCP). This last-mentioned particular

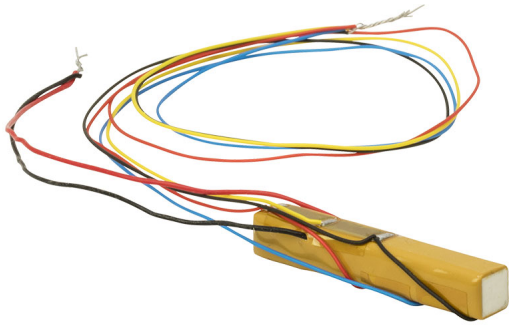

Figure 3.1: Thorlabs PK4FYC2 piezoelectric actuator [46]

point tends to be a convergence mark for all the following cycles except the first one. Subsequently, the second operative cycle rises through the second ascending curve *(c)* till reaches UTP, which is another convergence point. The final driving for the two cycles input voltage ends at along *d* which is equivalent with curve (b).

3.3 Reference design

Typically, triangular and sine waves are used at PEA actuators [47, 48]. Certainly, the sine represents a soft signal which generates an ellipse kind hysteresis graph where the alternative option provides a sharp form due to the slope changes at the maximum driving voltage. In this research, both signals were used for reference following although the hysteresis was envisioned through a triangle wave. The latter mentioned includes high-frequency harmonics, striking slope changes and it is well used in industry like for atomic force microscopes [49]. Therefore, the tracking control performance needs to be robust enough. Several amplitudes were selected but taking into account the upper voltage in order to avoid over-voltage issues and actuator life-span reduction; the period were also different but above 1s.

Because the PEA was operated between 0-150V, this voltage range had to

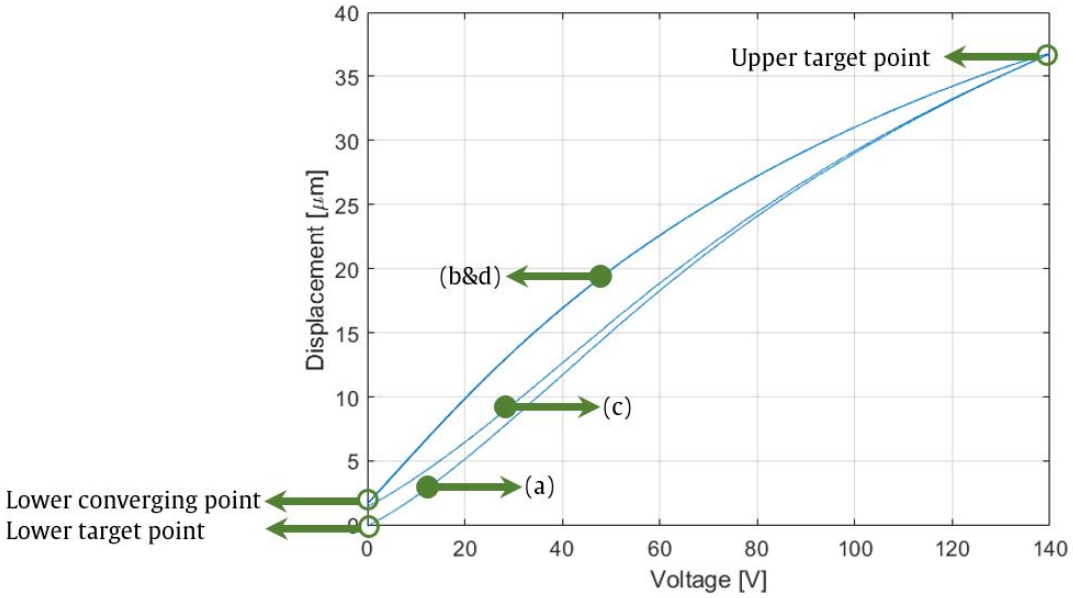

Figure 3.2: Experimental hysteresis graph of a PEA.

be transformed into a displacement reference. A proportional relation is deficient since the LTP is merely for the first cycle, thus a linear transformation can be traced between LCP and UTP with a the linear Equation (3.1) where the slope α is among the two converging points and δ corresponds to the vertical offset at the LCP.

$$Displacement[\mu m] = \alpha \cdot Voltage[V] + \delta \tag{3.1}$$

3.4 Peripheral devices

The 0-150V was generated by a single channel driver cube Thorlabs KPZ101 recommended for the PEA selected, which is flexible for a broad range of actuators. This device allows a convenient way of operation based on open loop mode without the necessity of using a peripheral computer. Additionally, it is also capable to work in close loop with an external signal of 0-10VCC up to a maximum allowed bandwidth of 1kHz.

Since the measurement is based on a Wheatstone bridge, the elongation is a resistance change which can be difficult to read due to the minor values, thus

the manufacturer recommended to use the pre-amplifier AMP002. This device is operated to extend the small differences on a 0-2VCC signal that is fed into a cube reader Thorlabs KSG101. This instrument provides the PEA extension in an embedded LED viewer and an output signal between 0-10VCC.

As previously mentioned, the driving and measurement signals were in the range of 0-10VCC; thus, a dSPACE DS1104 board was used for acquisition and control. This hardware also has the ability to operate in Real-Time Interface (RTI), which is a framework link between dSPACE hardware and MATLAB. This helps to reduce the compilation time for driving algorithms. This board was connected through a PCI bus in a Dell Precision Workstation T3500 with an Intel 64 2.4GHz microprocessor and 18Gb of available memory.

The control architectures were designed in Simulink, by Mathworks, and implemented through dSPACE RTI. The schemes were developed with flexibility for real-time which allowed gain tuning and performance metric calculation. The visualized data in real time was acquired and recorded in ControlDesk. The information gathered was processed and visualized in Matlab by Mathworks. The sampling time for all the experiments was established at 1kHz since it suits the relation between data acquisition and hardware physical limitation. A schematic description of the flow between the hardware and the software is shown in Figure 3.3.

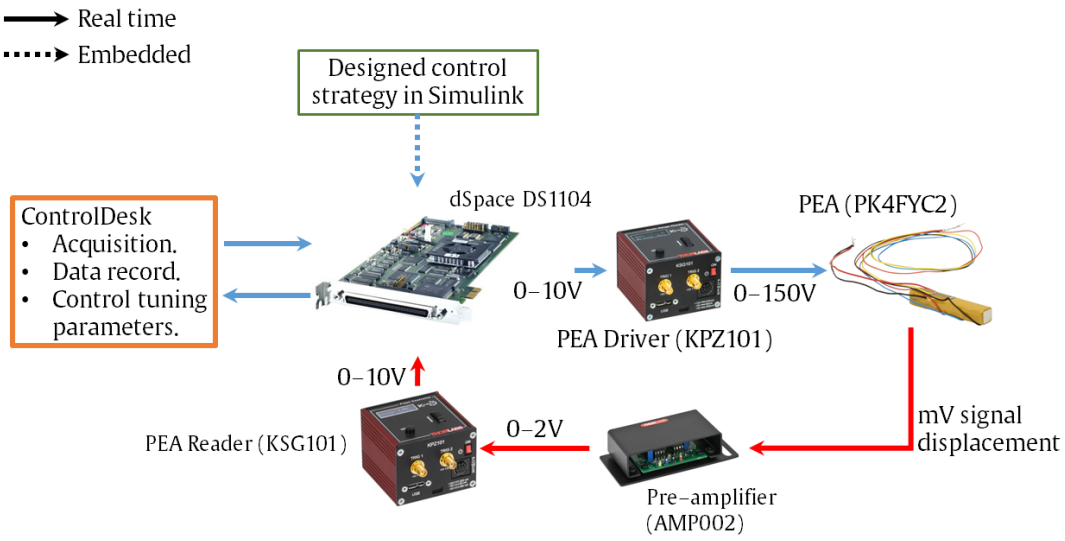

Figure 3.3: Hardware and software flow of the PEA experimental rig.

The important thing is to never stop questioning.

A. Einstein

4

Advanced Control Strategies for PEAs

This chapter presents and compares diverse advanced control strategies as applied to PEA actuators. These strategies have been implemented over a commercial PEA, a Thorlabs PK4FYC2. The choice of controllers was based on fast compensation of error and its reduction as well. Additionally, the control signal was analysed to avoid hardware damage. Performance metrics related

to accuracy such as integral of the absolute error, root-mean-squared error and relative root-mean-squared error were calculated in each case to establish a final comparison of each implemented algorithm in terms of error reduction.

4.1 Performance Metrics

In this research, the control architectures were implemented in experiments to verify and compare their performance. The tuning of the control parameters was executed through Integral of the Absolute Error (IAE) reduction which has the expression present in Equation 4.1 with the intention of reducing the error to zero. The parameter N is an observation data length time for the calculation, where in this case it was chosen to be equivalent to the period of the triangle signal used.

Although the IAE indicates the guidance performance, which is one of the essential goals of this research, other metrics were used so as to reflect the improvements as authors from [49] did in their work: the root-mean-square error (RMSE) and the relative root-mean-square-error (RRMSE). The last two terms of Equation 4.1 are the numerical definitions where e_i and r_i are the error and the reference in the i-th sample, respectively. Additionally, the generated control signal was also inspected in order to avoid actuator damaging.

$$\begin{cases} IAE = \sum_{i=1}^{N} |e_i| \Delta t \\ RMSE = \sqrt{\frac{1}{N} \sum_{i=1}^{N} (e_i)^2} \\ RRMSE = \sqrt{\sum_{i=1}^{N} (e_i)^2 / \sum_{i=1}^{N} (r_i)} x100 \end{cases} \tag{4.1}$$

4.2 PID compared with Neural PID for feedback and feedforward structures.

4.2.1 Contributions

The main contributions of this section are:

- An analysis of different feed-forward (FF) blocks such as linear and neural for a combination with feedback structures.
- Contrasts of FF with conventional PIDs in order to evaluate each performance.
- The inclusion of a novel combination based on a neural PID with the best obtained FF to check the demeanour with advance structures.
- Experimental data which has been analysed in terms of previous mentioned metrics.

4.2.2 State of the art

Hysteresis origins in PEAs are complex since can be related to material properties and electric field combined with mechanical strain [4] which can induce a severe open-loop position error (up to 22% of travel range) [2]. Even though the hysteresis is an effect that cannot be excluded, a control strategy should be designed and implemented so that the position error can be diminished and the PEA can be used in a high precision application. State observers or FF control combined with feedback approach is often used to achieve the best precision in tracking [50]. Usually, compensation is provided with an inverse hysteresis model where the most common ones are Prandtl-Ishlinskii (PI) [51, 52] or Bouc-Wen (BW) [53, 54]; however, these models have certain limitations like complexity to be inverse. For example, since the PI is a combination of several parameters, hence it cannot be analytically inverted so there are approximations like direct identification or iterative algorithms based methods [55]. Other models such as BW are efficient although the performance lowers when the device has enough non-linear asymmetry [56].

Despite the complexity or the low performance of the inverse model compensation, another approach is artificial neural networks (ANN) as system identification which is widely used for clustering, recognition, pattern classification,

optimization and prediction [57–59]. In this case, a FF ANN type works with one or more hidden layers which are linked between the input and output and internally, these nodes are fully connected by weights. A common approach of ANN BB identification is with non-linear auto-regressive networks (NARX) [60]. In this research, an alternative NARX framework was used for prediction, which is a time-delayed neural network (TDNN) where the inputs are added as specified delays for prediction [61, 62]. Even though this approach might reduce the ANN performance but still, the architecture complexity can be simpler and the self-learning ability is sufficiently powerful. Nonetheless, the accuracy of the prediction also depends on the amount and quality of data, which was obtained from the real device for this research.

On the other hand, a fully connected control architecture needs to have a feedback controller to reduce errors during the guidance. As a first approach, a PID without FF was tested and as the system had a strong non-linearity, the performance needed to be improved. Cutting-edge research from recent years in terms of new PID techniques for PEAs have provided a growth in the guidance efficiency such as the single-neuron proportional-integral-derivative (SNPID) [49, 63]. This framework acts with a single neuron system which uses Hebbs self-learning law to update its weights. The combination provided satisfactory results in comparison with the PID controller.

4.2.3 Hysteresis fitting with NN

The PEA non-linearity hysteresis can be considered as a mapping problem since there can be two values for input, thus ANNs have many advantages such as self-learning and simplicity, which is suitable to learn one hysteresis curve. The ANN architecture used to fit the hysteresis loop was TDNN which is a variance of a NARX but where the input weights have tap delays associated. Hence, the output prediction *y(t)* depends on past values of the input and is combined with a non-linear function *f*. In this case, the number of delays chosen was 5, due to the default configuration of Matlab Deep Learning Toolbox.

$$y(t) = f(u(t-1), ..., u(t-5)) \tag{4.2}$$

The function *f* is approximated to a combination of a hidden and an output layer where each has its weights and activation functions. Regarding the

training information, a triangle wave with the previously mentioned features was used to obtain information for 10 seconds such as the displacement. In terms of the training algorithm, due to the fast back-propagation the Levenberg-Marquardt (LM) was chosen. This updates the weights and bias in terms of a back-propagation and optimization where the main metric is the medium squared error (MSE). Boussaada et al. [60] provided a deep analysis of different training algorithms where it was found that LM supplied efficient results. Since the FF compensation was expected in terms of voltage, an inverse model was needed; then, the input voltage used to obtained the hysteresis was the ANN target and the displacement as the input.

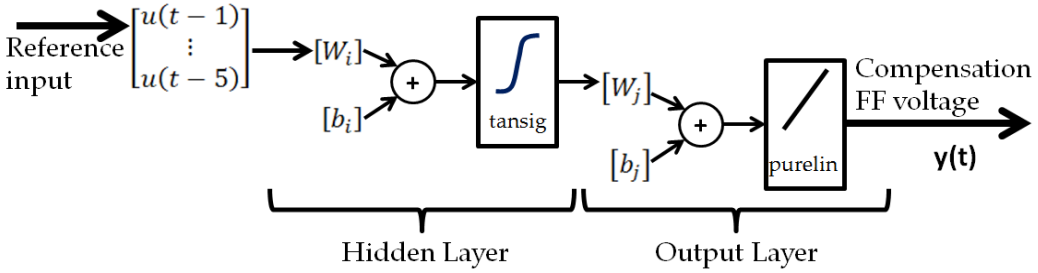

Figure 4.1: TDNN Architecture in terms of delay inputs

Figure 4.1 displays the architecture of the TDNN where the weights and bias are different of in each layer in terms of the subscripts *i* and *j* respectively. The hidden layer uses a *Tansig* activation function whereas the output operates with a *Purelin*. Based on a trial and error, the amounts of neurons was determined on a range which was tested were from 5 to 30 and the optimal one was found to be 22 in which the MSE was 0.004031. The convergence development was found to be optimal since the following curves showed up that model over-fitting is not an issue as Figure 4.2.

Figure 4.3 is a comparison with piezoelectric hysteresis loop and the ANN fitting with the error on the right-hand side. Even-though that the MSE was sufficiently small, the error in the comparison is around 0,5μm which is acceptable, but even more interesting the ANN could manage the asymmetrical shape that belongs to the device. The error compensation was expected to be done by the feedback controllers which were implemented.

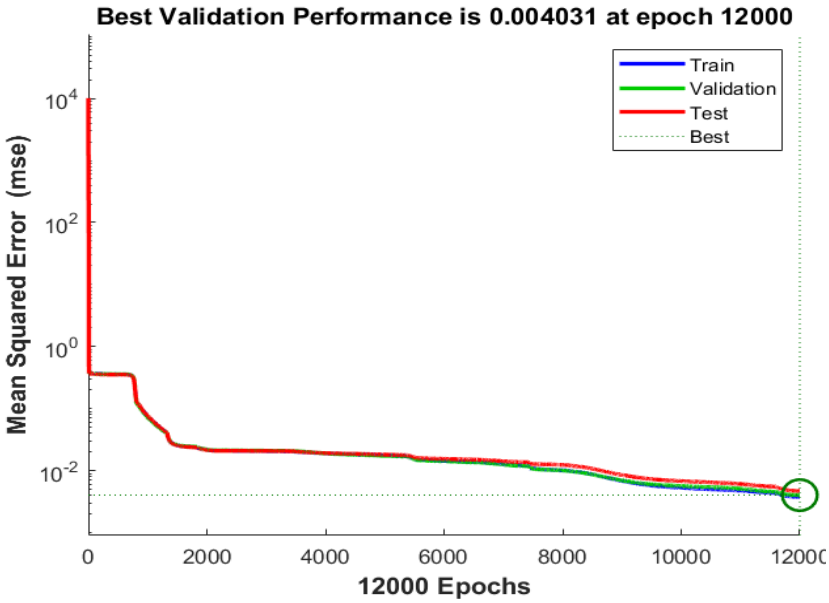

Figure 4.2: MSE vs trained epochs

4.2.4 Control structures used

At the beginning of the experiments, simple and classical algorithms were tested but increasingly complex algorithms were analyzed in order to improve the performance of the controllers. As all solutions were based on real tests, the controllers were tuned in real-time to achieve the best performance. As previously mentioned, there were 4 structures which were evaluated:

- PID without FF compensation
- PID with Linear FF compensation
- PID with ANN FF compensation
- SNPID with ANN FF compensation

The comparison was done with the first three systems which included the same PID tuning values (K_p, K_i and K_d). In every structure, it was considered that the hysteresis loop curve was not the initial trajectory, as previously shown, the initial rise is completely different from the following ones. The best result

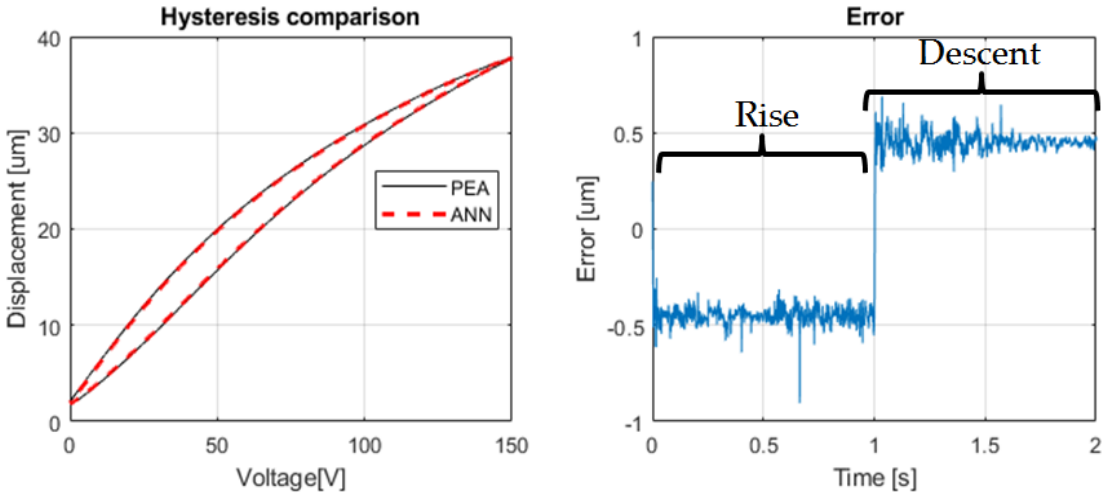

Figure 4.3: Hysteresis fitting with ANN and the associated error

of these three architectures was contrasted with the fourth one, which is an ANN FF compensation with SNPID since the performance was expected to be superior to others.

4.2.5 Proportional-integral-derivative

Although a PID is a classic controller, it is still a competitive approach nowadays [64]. The expression is divided in three parts: a proportional, an integral and a derivative; each term corresponds respectively to speed response, steady-state error reduction and dynamics improvement [65]. Although there are several techniques for tuning such as Ziegler-Nichols as a conventional option, the method of *min*{IAE} was unified for both control strategies. The structure defined by Equation (4.3) is defined by *e(k)* is the error, Δt is the sampling time and the gains K_p, K_i and K_d correspond to the proportional, integral and derivative term, respectively. These were tuned based on IAE reduction in real time.

$$u(k) = K_p e(k) + K_i \sum_{i=1}^{k} e(i)\Delta t + \frac{K_d[e(k) - e(k-1)]}{\Delta t} \tag{4.3}$$

4.2.6 PID With Linear FF Compensation

The second approach proposed was a linear compensation with the previous PID (same constants). Surely, in this case, the linear FF block assumes that the PEA behaves linearly as well. Consequently, this was reflected as Figure 4.4 displays where the maximum and minimum displacement were used to generate a straight line that could resemble the linearity. In this circumstance, the feedback controller was expected to produce more compensation due to the hypothesis previously mentioned as the errors increased.

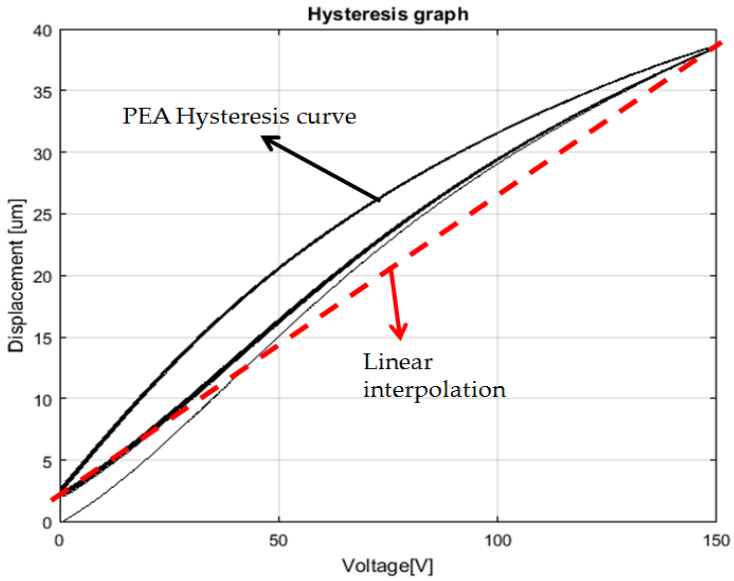

Figure 4.4: Linear interpolation

Since the hysteresis has a different shape during the first cycle in which the PEA starts at zero displacement and the following periods tend to a convergence where the initial displacement is not zero anymore due to the device properties and therefore, the curves are in a path to a common shape. During this research, a linear compensation was taken into account and hence, a straight line was interpolated between the initial offset and maximum value since the PEA was not expected to work only during the first cycle.

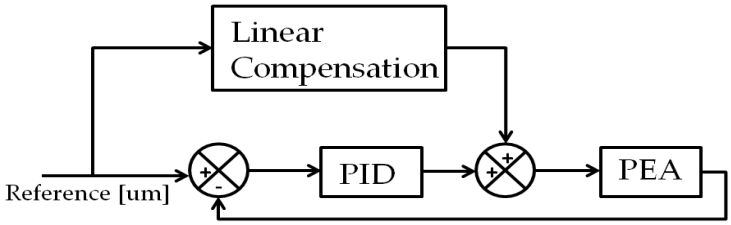

Figure 4.5: PID on feedback and linear compensation on FF

4.2.7 Neural proportional-integral-derivative controller

A major disadvantage of PID controllers are the constants which must be modified to compensate the system nonlinearities. The avoidance of manual tuning was found to be possible with a self-adaptive PID [49]. The error input to the controller was discomposed into three variables (X_1 , X_2 and X_3) in a similar way to a conventional PID but there will be three associated weights (W_1 , W_2 and W_3) which are adjusted by normalization and a learning rate. Therefore, the Hebb supervised learning rule is used to self-tune the weights and the whole controller behaves like a ”single neuron”; this is a non-linear process unit which is helped by the mentioned rule to adapt for a control process.

The error that went through decomposition or also called ”transducer”, complied with Equation (4.4), which is an expression that is related to a conventional PID controller as well. The three new variables were fed into the single neuron with the learning where the algorithm corresponds with the Equations (4.5). Afterwards, the output of the SNPID is the Δu_e which is finally added with the delayed signal like in Figure 4.6.

$$X_i = \begin{cases} X_1 = \Delta e(k) \\ X_2 = e(k) \\ X_3 = \Delta e(k) - \Delta e(k-1) \end{cases} \tag{4.4}$$

Based on [49], the weight that is more important due to environment is mainly akin with X_1 and X_2 and then, a simplification of the previously presented equation can be achieved where the main control structure is related to a weight update with the following normalization for calculation cut down and final control law.

$$\begin{cases} w_i(k) = w_i(k-1) \; + \; \eta_i \left[e(k) \; + \; \Delta e(k) \right] u(k-1) \; e(k) \\ w_i'(k) = \frac{w_i(k)}{\sum_{i=1}^{3} |w_i(k)|} \\ u(k) = u(k-1) \; + \; K \sum_{i=1}^{3} w_i'(k) \; x_i(k) \end{cases} \tag{4.5}$$

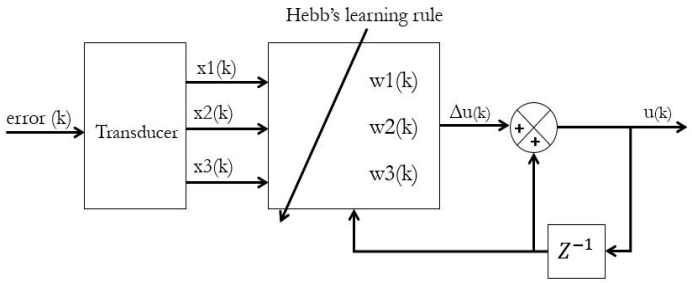

Figure 4.6: Single neuron PID

Results

The experiments were conducted over the hardware described in Chapter 3, where the four architectures were tested. The first try was with a conventional PID (no FF compensation); the following comparisons were merged to show up the performance improvement as the complexity increases. Finally, the last contrast is made with two most sophisticated ones since the guidance, error and control signal are more suitable to compare.

The PID gains were obtained in real-time during the first three experiments, where the values are displayed in the following Table 4.1. Furthermore, K_p and K_i were increased respectively to limits where the input voltage was not critical for the device. On the other hand, the SNPID constants such as K was switched in real-time as well on the same way whereas the learning rates η_1, η_2 and η_3 were assumed as less than 0.5 as the references suggested [49], in this manner was set to 0.4.

The first experiment was the close feedback loop with a PID as a controller. Figure 4.7 displays the guidance embedded with the error where it can be seen that the peaks of the signal had reduced the control performance since there

Table 4.1: PID parameter value

Constant	Value
K_p	10.6
K_i	1000
K_d	0

Table 4.2: SNPID constants value

Constant	Value
K	8.5
η_1	0.4
η_2	0.4
η_3	0.4

was a sign change in the behaviour. In the following sections, this feature will be analysed in depth. The IAE had a value of 0.578 during the period that is shown and it will be compared with the following results.

The second experiment was contrasted with the previous showed result but now with a linear FF compensation. The new architecture increased the performance since the error was worthy reduced as the Figure 4.7 shows due to the FF addition. For this reason, the guidance efficiency had increased substantially although the values are still unreliable for a precision device. The IAE values had significantly decreased to 0.1659, which is 3.48 times less due to the improved framework.

Certainly, the addition of a sophisticated FF compensation such as an ANN was expected to improve the performance and this was reflected in Figures 4.9 where the tracking had improved adequately. The error is fairly reduced compared to the previously presented architectures and for this reason, it will be analysed in-depth during the following subsection with the most advance framework. As it was also expected, the IAE was reduced to 0.0683 with this approach and this results on a 2.42 times less than the previous framework.

Finally, the last architecture tested was the SNPID. Since the results be-

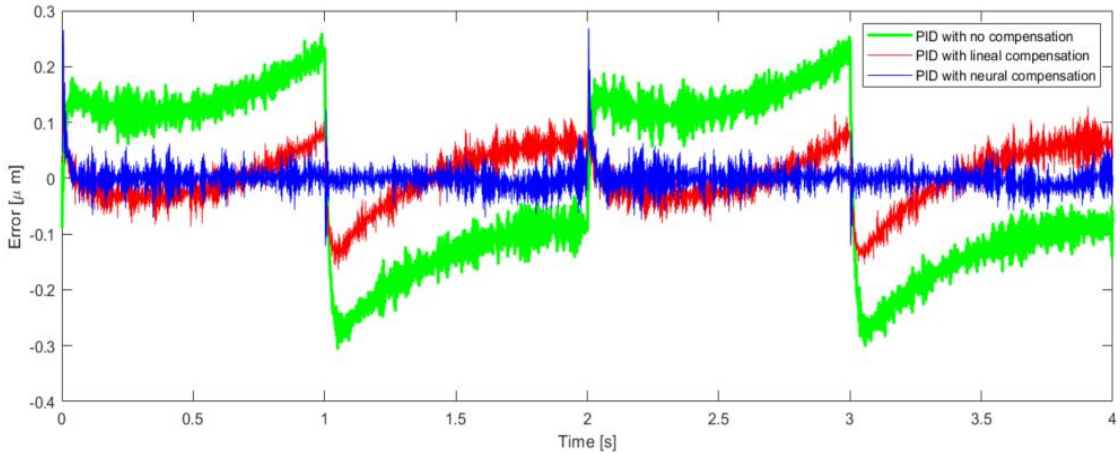

Figure 4.7: Comparison of guidance and error with a PID as a controller in the close loop and feedforward compensations.

haved similarly, an in-depth analysis regarding to error and control signal was performed. Figure 4.10 reveals the error progression along with two triangle reference as previously shown. The performance had undoubtedly increased since the mean error value tends to be very near to zero in both cases. However, the perception of the SNPID had increased essentially the efficiency around peaks (where the top values are in 1 and 3 seconds whereas the lower one is in 2 seconds). The FF with ANN compensation merged with the PID on feedback shows that after the lower peaks, the error increased its amplitude extensively and takes several fractions of a second to reduce it. Nevertheless, the framework with a SNPID corrects these effects with a small perception which resembles in a brief error increment which has less amplitude than the contrasted method; another advantage that can be appreciated is the fast error correction since the PID architecture had a slow demeanour to correct the error, the SNPID had the ability to avoid this situation.

On the other hand, Figure 4.11 shows the control signal which is the sum of the feedback controller and the FF compensation. It can be seen that both signals are almost equal although there were not any drastic changes or significant saturation which could reduce the lifespan of the actuator or make the system unstable.

As the analysis showed, this control structure had the best performance and this was reflected in the IAE. In this state, the value was 0.0499 which means

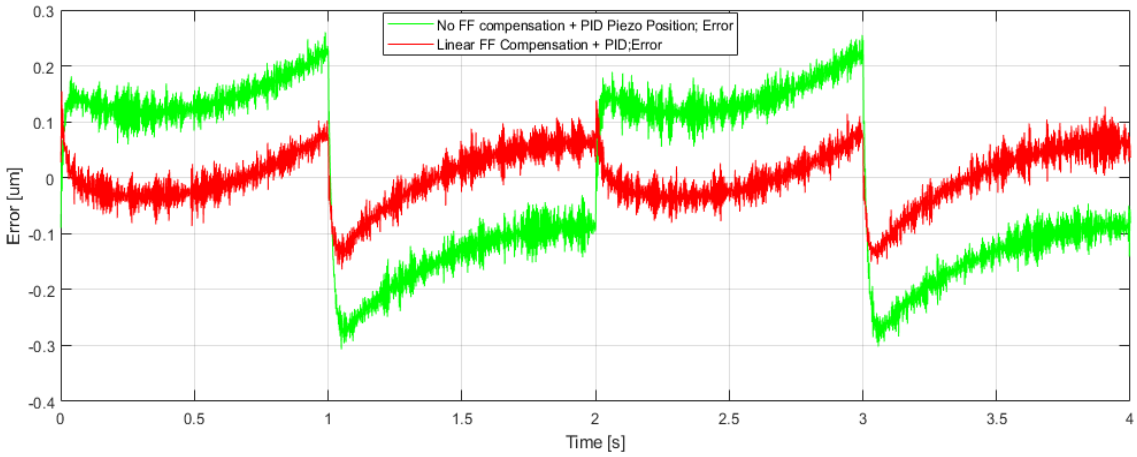

Figure 4.8: Comparison of error with a PID as a controller in the close loop contrasted with a linear FF compensation

that it has been reduced 1.36 times in contrast with the previous structures. The Table 4.3 compares all the IAE values that were exposed.

Table 4.3: IAEs comparison

Controller	IAE
PID	0.578
PID + Linear FF	0.1659
PID + Neural FF	0.0683
SNPID + Neural FF	0.0499

4.2.8 Conclusions

This research has made a deep analysis of to compensate the hysteresis effect. This analysis started with elementary approaches until advanced feedback control algorithms. Also in the feed-forward, there was the inclusion of advanced compensators. All of these structures were experimentally tested with real devices. Furthermore, the controllers were tuned under a rapid control prototyping type since most of the parameters were set in real-time to achieve the best performance for a genuine operation.

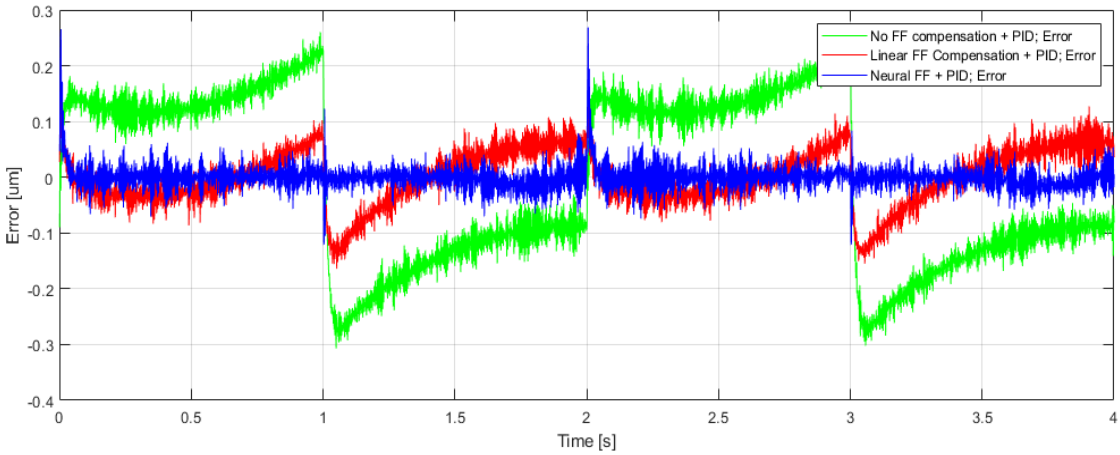

Figure 4.9: Comparison of error with a PID as a controller in the close loop contrasted with linear and ANN FF compensation

The analysis began with the device inspection in terms of frequency and different amplitudes where parameters were chosen to persist with the control design and especially, the ANN design. The FF neural compensation was first contrasted with real data in terms of the hysteresis. The result was acceptable since the interpolation had a small error which could be sufficient for the following compensation. The crucial improvement was the fitting along with the asymmetrical shape of the non-linearity since it was found in the references that this is a problematic feature to model with analytical techniques.

The first control architecture used was a simple one with a PID on the feedback where the results were as expected due to the high non-linearity presence of the device. The errors obtained were not acceptable since the position guidance was the main achievement to be improved. The following contrast was against a linear-compensation and certainly, it was found that even an inaccurate compensation could improve the performance since the IAE had a value of which was 3.48 times less than the first basic control architecture. Although the performance was improved, the value was still not sufficient because the linear interpolation was between two points of the hysteresis curve and this might not be the best solution, due to the asymmetric effect explained.

The last two approaches, which are the most complex ones, provided better outcomes than the previous ones. The addition of an ANN compensation surely was expected to provide better results since the fitting efficiency was higher due

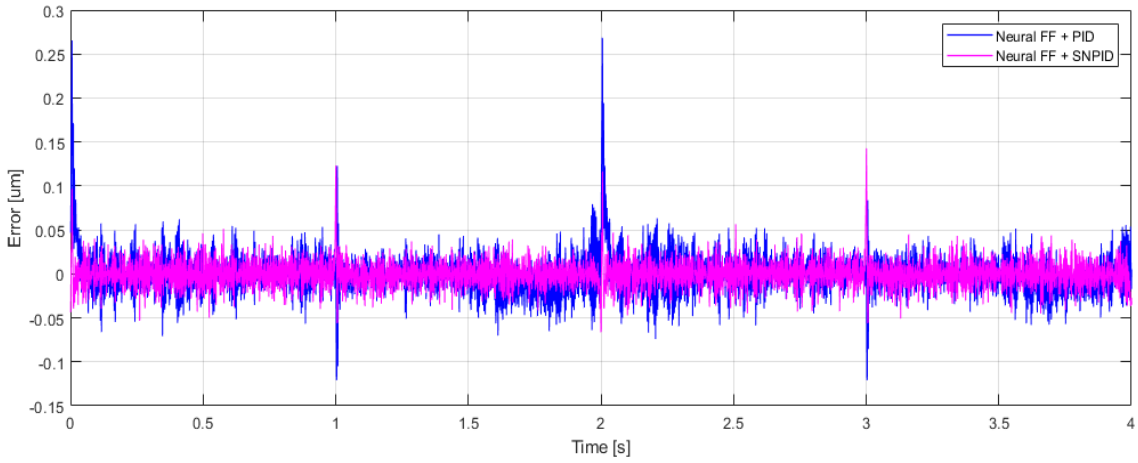

Figure 4.10: Error comparison with a Neural FF compensation with a conventional PID and a SNPID

to the flexibility of the ANNs. As a result, the IAE decreased reasonably in comparison with the linear compensation and it resembled on the performance as it was showed (2.42 times less than the previous). Since this approach was found to be the best one until that point it was chosen for a final comparison with a SNPID which was already known for its high performance. The FF compensation with SNPID improved the process where the conventional PID had a weak response like after a peak. It was found that the SNPID neglects and corrects the errors during these violent slope changes. The IAE for the last framework result in dramatic decrease since the value was 1.36 times less than the third approach; for this reason, this method is considered to be the best of the ones that were tested.

Since the last two methods were found to have a satisfactory response, the control signal was studied. It was found that the control signals for both schemes were acceptable since there were no significant or fast action which can compromise the hardware due to input signal generated. For this reason, it is expected that both approaches can have a valuable (and probably much better) performance for a smoother curve like a sine wave since a triangular was chosen for its high complexity representation and requirement.

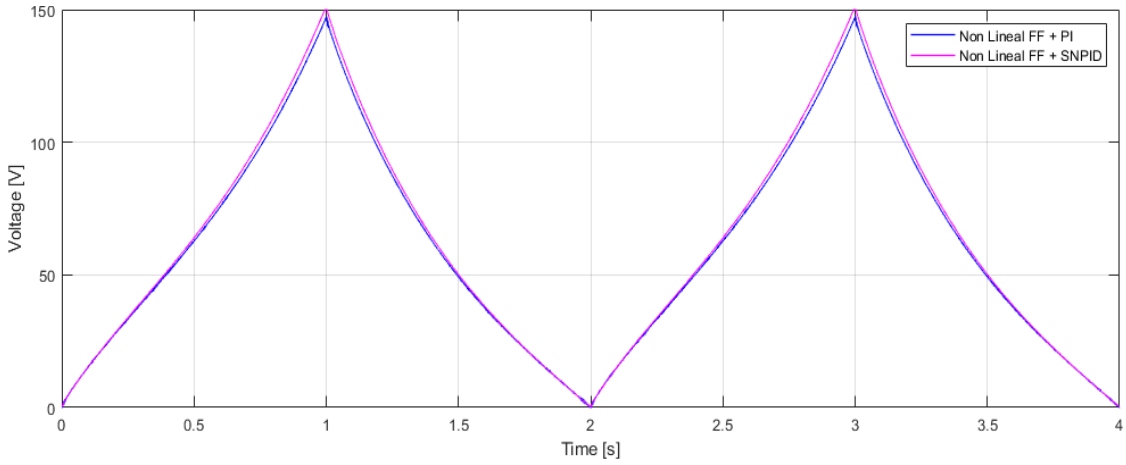

Figure 4.11: Control signal of a Neural FF compensation with a conventional PID and a SNPID

4.3 Fuzzy logic combined with Hammerstein Wiener feedforward compensation.

4.3.1 Contributions

Main contributions and novelties of this section are:

- An analysis of a system identification tool known as Hammerstein-Wiener (HW) to be used as a FF block.
- A novel strategy of fuzzy logic control (FLC) combined with HW that provided good trajectory tracking.
- A practical stability proof of the FLC used.
- A contrast of the FLC proposed with a PID controller in order to check the feedback behaviour.
- To show the enhancement of the HW combined with FLC, this was contrasted with the FLC as a feedback controller alone.
- All controllers were embedded in a experimental platform and evaluated in terms of accuracy and generated control signal.

4.3.2 State of the art

The hysteresis not only has been studied in electromagnetic materials [66] but also in PEAs positioning due to adverse causes in the accuracy and margins of stability [67]; usually, the error inaccuracy can be up to 22% in an open-loop configuration [2]. The microscopic origin and theory of hysteresis in PEAs are complex, although an explanation in [68] shows that this feature is associated to the irreversible restoration of the unit cells when the electric field is reduced; on the other hand, [4] encompass the theory with the movement of the domain walls. Certainly, for these reasons, the hysteresis not only depends on the presently applied input but also in the previous input schedule [69]. Despite the natural origin of hysteresis, which elimination is inconceivable, it can be diminished using a suitable control strategy to achieve an ultra-precision in the guidance.

The decline of hysteresis can be done via an advanced control strategy. FF compensation aims to map the non-linearity of the device to compensate for the phenomena; it has been demonstrated that when the PEA is unloaded, FF is effective [70]. However, the error reduction, dynamic changes and unknown effects are properties in which FF fails to compensate but where a feedback strategy can deal with. The latter mentioned offers a solution that can increase the precision, although the close-loop can result in a low gain margin which narrows the usage of high-gain controllers [71].

Despite the drawbacks of the mentioned strategies, a combination of both frameworks can be a suitable option to analyse. Feedforward-feedback controllers can increase the control accuracy of PEAs through the advantages that both techniques can provide separately [72]; furthermore, this strategy can produce multiple structure combinations. In [73], the hysteresis was compensated with a linear and ANN combined with a conventional PID and a neural type; results shown that the combination of ANN with the neural PID has been the most precise one since the IAE was reduced to 0.049. Authors of [74], described the FF compensation by a PI hysteresis model merged with sliding mode control (SMC) as feedback; results unveiled an error less than 1%. Another solution was presented by [47], where a polynomial based approach mapped the hysteresis curve for FF and combined with a PID control; results have shown a precision increment although the deviation was significant as well. Another ad-

vance strategy was used in [75], where the authors employed a mathematical based model such as Dhal merged with μ_∞ which provided an error of 0.51%. However, these structures have certain drawbacks as computational requirements in the case of ANNs training, time-consumption to achieve a suitable model when a FF was used or complexity implementation as the preceding explained example.

FLC is a structure that mimics human knowledge or action based on linguistic rules which are tuned according to the designer [76–78]; these type of controllers have been used in applications for maximum power point tracking such as fuel cells and photo-voltaic systems [79, 80], electrical drivers [81], etc. The author of [82] indicated that FLC based on PID grants a high accuracy for PEAs guidance but also it can provide other advantages over alternative control structures. The authors of [83] compared an H_∞, which is a robust controller already used in PEAs [84], with a FLC for a tracking problem; results displayed a superior performance in terms of the steady-state error and overshoot. On the other hand, SMC is another well-used framework for PEAs [85]; however, researchers from [86] encourage the usage of FLC over SMC due to its practicality and no chattering effect.

In this research, a type-1 FLC (FLC-T1) based on PID was used; according to [87], this kind of structure tends to perform better than a conventional PID since it handles uncertainties related to the controller input and output, operational changes and disturbances through rules and the fuzzifier. In combination with the FLC and to improve the uncertainty, analytic methods could have been used although certain disadvantages were taken into account. BW is an efficient hysteresis model which could be merged as FF, however, its performance decreases when the non-linearity shows asymmetry [88]. Another option is PI model which is widely used; however, its inversion is complex ,and it could increase the error compensation [89].

Black-box (BB) models are a block based approach that provide a mapping between the input and the output but without taking into account the physical relations of the system [90]. HW is an advance BB which shape consists of a linear representation followed and preceded by non-linear blocks. This identification tool is widely used in non-linear systems such as chemical reactors [48], voltage distortion of batteries [91] and motion precision of electro-mechanical systems [39].

4.3.3 Hysteresis fitting with Hammerstein-Wiener

Hysteresis is highly non-linear not only because there are two different values for a voltage but also an asymmetry is present which can be difficult to represent with an analytical method. Hence, a mapping strategy should be designed to trim the phenomena because there can be two values of voltage for a single reference point. According to [92], Hammerstein blocks are used when the input behaves with significant non-linearity; thus, the input $u(t)$ is transformed by a non-linear function *f* which is then multiplied by a linear transfer function B/F. Conversely, the Wiener block uses a non-linear function *h* which arguments are the input signal multiplied by the linear transfer function and results in an output y(t). The conjunction between both theories (Hammerstein-Wiener) results in a three-block step which maps systems with strong non-linearities in the inputs as in the outputs. The fringes of HW which correspond to the non-linear functions *f* and *h* can be approximated with different methods such as piece-wise linear functions, sigmoid, dead-band, wavelet and polynomial. A summary of these theories is mathematically expressed in Equation 4.6.

Equation 4.7 is the linear subsystem B/F where n_b, n_f and n_d denote, respectively, the degree of B, F and the associated delay. This transfer function is expressed in the time shift operator q^{-1}, which represents $q^{-1}u(t) = u(t-T)$ where u(t) is the system input and T is the sample time. The coefficients which correspond with the three functions can be obtained by using real the data of the PEA.

$$\begin{cases} \text{Hammerstein block} \Rightarrow y(t) = f\Big(u(t)\Big)x(q^{-1}) \\ \text{Wiener block} \Rightarrow y(t) = h\Big(x(q^{-1})\Big) \\ \text{HW} \Rightarrow y(t) = h\Bigg(f\Big(u(t)\Big)x(q^{-1})\Bigg) \end{cases} \tag{4.6}$$

$$x(q^{-1}) = q^{-n_d}\frac{B}{F} = q^{-n_d}\frac{\sum_{i=1}^{n_b} b_i q^{-i+1}}{1+\sum_{j=1}^{n_f} b_j q^{-j}} \tag{4.7}$$

The MATLAB System Identification Toolbox was used to estimate the parameters of HW block; the software approximates the input and output nonlinearities by using a loss function as a first metric to reduce the error between the model output and response measured. The iteration algorithm was set into au-

tomatic choice so that the software can search the adequate one. The second metric that was taken into account was the *Fit Percent* which is related to *"how good the model fits the experimental data"* and it varies from -∞ to 100 which represents, respectively, the lowest and highest fitting accuracy. This metric is expressed as Equation 4.8 shows, where $y_{measured}$ is the measured output data, $\overline{y_{measured}}$ is its mean and y_{model} is the predicted response of the model.

$$FitPercent = 100\left(1 - \frac{||y_{measured} - y_{model}||}{||y_{measured} - \overline{y_{measured}}||}\right) \tag{4.8}$$

4.3.4 Type-1 Fuzzy Control

As it was experimentally observed, if the error value is positive and large with a positive increase, then a big control effort needs to be applied considering that its magnitude should shrink as the error is reaching the zero so that overshoots can be avoided. It was considered that with negative values the situation is symmetric.

An improved procedure from the last presented architecture is a type-1, which is a non-linear controller that operates better than a conventional PID, especially for severe nonlinearities [87]. The input to the controller consists of the error and its derivative which are multiplied by the factors K_e and K_d; this results in the variables E and $\dot{E}$, which represent error and its change normalized in the range of [-1 1]. The constant K_o is intended to increase the output of the FLC based on an incremental control action. Figure 4.12 shows an structure of controller configuration within the fundamental steps of fuzzy type-1 sets which are fuzzification, inference engine and defuzzification.

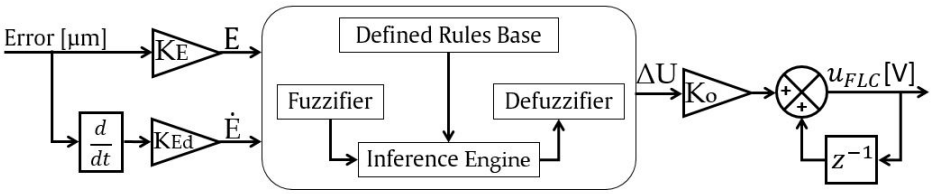

Figure 4.12: Type 1 fuzzy logic control structure.

In regards to the fuzzification, this is the step in which crisp inputs are trans-

formed into linguistic terms by means of membership functions. In this design, a type-1 set was used as input variables; these are defined as a set function on an universe X (that in this case goes in [-1, 1] of the definition of E and $\dot{E}$) through defined membership functions as $\mu_A(x)$. In this case, the membership functions are correspondent on the overlapped triangular configuration of Figure 4.14. In this research, the membership functions for the inputs were uniformly discretized in terms of negative big (NB), negative small (NS), zero (Z), positive small (PS),and positive big (PB); these values were defined in limits of -1, -0.66, -0.33, 0, 0.33, 0.66 and 1, respectively.

$$A = \{(x, \mu_A(x)|x \in X\} \tag{4.9}$$

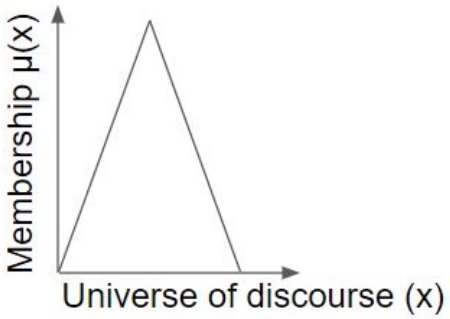

Figure 4.13: Definition of μ(x) vs the universe of discourse.

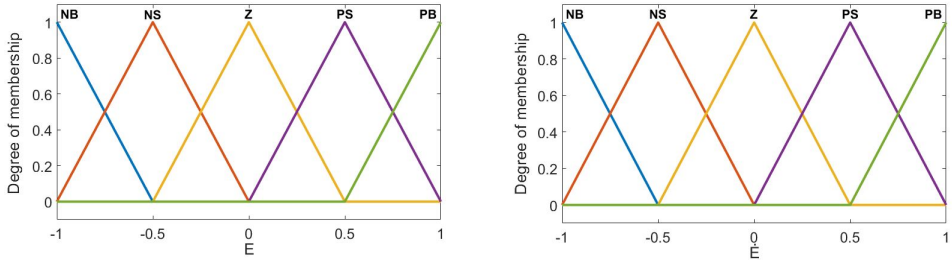

Figure 4.14: Type 1 triangular overlapped membership functions

The inference is exposed mathematically through Equation 4.10 where k and l are the number of membership functions that E and $\dot{E}$ have and were defined in the fuzzification. The discretization is defined as PM,PS, Z, etc. but now with

further terms like negative medium (NM) and positive medium (PM). In this case, the linguistic terms were linked by an AND rule that are expressed in Table 4.4; thus, the outcome of this relation to map into the output membership function is by a MIN relation. Mathematically, this is expressed by input fuzzified values $\mu(E_k)$ and $\mu(\dot{E}_l)$ in which the $min(\mu(E_k), \mu(\dot{E}_k)) = \mu_d$ is the membership value for the output membership function.

$$R_m: \textit{If } E = B_{1k} \textit{ and } \Delta E = B_{2l} \Rightarrow \Delta U = G_m \tag{4.10}$$

ΔU, which is the output of the fuzzy block, is related by the corresponding crisp output set. These were defined as singletons which are constant values discretized between -1 and 1. Therefore, the value of ΔU is expressed by the following Equation where S_i is the value of the defined singleton that is related to μ_d. An schematic description of the previous process is shown in Figure 4.15.

$$\Delta U = \frac{\sum \mu_d(S_i) S_i}{\sum \mu_d(S_i)} \tag{4.11}$$

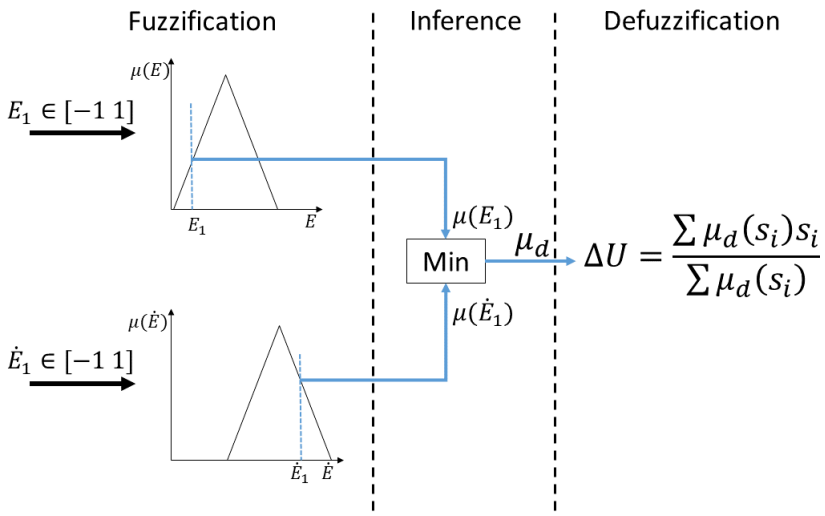

Figure 4.15: Schematic description of FLC-T1 process

This controller was tested under two frameworks: first as a feedback structure and secondly, the HW was added as an FF. The gains had to be different

E \ $\dot{E}$	NB	NS	Z	PS	PB
NB	NB	NM	NM	NS	Z
NS	NM	NM	NS	Z	Z
Z	NM	NS	Z	PS	PM
PS	Z	Z	PS	PM	PM
PB	Z	PS	PM	PM	PB

Table 4.4: FLC linguistic rules.

in both cases since, with the same values, the comparison would have had a significant gap in terms of error. The feedback control with FLC has the role of suppressing errors, alteration of the PEA dynamics and reducing the effects of unknown uncertainties. On the other hand, the same structure but with an HW model as a FF was used as it pretends to compensate the non-linear effects.

4.3.5 Fuzzy logic controller stability proof

Although the scope of the current article is to provide experimental results for PEA tracking performance, a semi-formal stability proof is presented based on the Lyapunov theory of stability [93]: If a dynamical system is asymptotically stable, then, there exists a positive definite Lyapunov function V: $R^n \rightarrow R$ so that $V(x) > 0$, $V(\infty) = \infty$, $V(0) = 0$ & $\dot{V}(x) < 0, \forall x \neq 0$, . Therefore, if the normalized error is defined as $E = X_{ref} - X$, then, a Lyapunov function is defined as Equation (4.12).

$$V = \frac{1}{2}E^2 \tag{4.12}$$

$$\dot{V} = E\dot{E} \tag{4.13}$$

Thus, if the derivative (Equation (4.13)) of the Lyapunov function is negative, it implies that the system is asymptotically stable and it converges to a null error. Considering when the control signal ΔU is positive, then ΔX is positive and ΔE is negative which implies that $\dot{E} < 0$. On the same way, when ΔU is negative, ΔX is negative which yields to a positive ΔE and hence, $\dot{E} > 0$. Therefore, for the dynamic equation of the system it can be concluded that:

- Case 1: If E is PS or PB and ΔE is PB, PS or Z | E is PB and Δ E is NS |

E is Z and ΔE is PB or PS $\Rightarrow U = PS$, PM or PB.

During this situation, the increment of ΔU drives to $\dot{E} < 0$ with a positive E and hence, the error converges to the null value because $\dot{V} < 0$

- Case 2: If E is PS and ΔE is NB | E is NS and ΔE is PB $\Rightarrow U = Z$.

In this condition, the signal ΔU is null and it means that the feedback control signal does not change so that the $\dot{V} < 0$, although the trend stills tends the error to a null value due to the sign of ΔE.

- Case 3: If E is NB or NS and ΔE is NS, NB or Z | E is NB and ΔE is PS | E is Z and ΔE is NB or NS $\Rightarrow U = NS$, NM or NB.

Reciprocally to case 1, when $E < 0$ and $\dot{E} < 0$, which is switched to a positive value since ΔU decreases; thus, this yields the error to converge to a zero value.

For the rest of the linguistic rules, which are the cases of the diagonal of Table4.4, the Lyapunov stability is verified since at each moment, $\dot{V} < 0$ and the error tends to decrease due to the demeanour of E and $\dot{E}$.

4.3.6 Results

Hammerstein-Wiener training results

The different options of approximators for the non-linear blocks were tested to find the best solution in terms of the fit percentage. The results provided a fit percentage that are resumed in Table 4.5. Therefore, the piece-wise had the best fit-percentage, which works as follows: within the chosen inputs and outputs, there are breakpoints associated (x_i, y_i) such that i = 1...n so y_i = R(x_i) where n is the number of breakpoints (input or output), R is the piece-wise function that is approximated through the breakpoints where x_i and y_i are obtained by the algorithm previously explained.

Hysteresis fitting results

A first step before the control evaluation in feedback with FF structure is to test the mapping performance to achieve the tracking persistence. The HW was

Table 4.5: Fit percentage of nonlinear approximators tested for HW compensation

Nonlinear approximator	Fitting percentage [%]
Piecewise	99.58
Sigmoid	93.33
Deadzone	91.02
Wavelet	96
Polynomial	99.57

tested in a hysteresis graph to analyse the fitting of the model although the previous fit percent obtained was suitable. Since the input was expected to be the main reference so that the voltage was the output to be fed into the control system, the comparison was done in terms of the voltage error.

Figure 4.16(a) displays the fitting comparison of the HW model with the real data; Figure 4.16(b) is an associated error graph which displays the development of the fitting along one arbitrary cycle. The comparison shows an acceptable behaviour since HW could manage to fit the hysteresis graph from the lower converging point up to the upper converging point as well as the asymmetry feature that this PEA has. Moreover, the error graph augments the previously described manner where it can be seen that the magnitude fluctuates between -1 and 1 V; a harsh demeanour occurs at 1 second, which is the moment where the input changes its slope to decrease and thus, this was an expected unfolding due to the complex alteration.

Tracking control results

The first was a PID as feedback without FF compensation, the second FLC in feedback and finally, FLC combined with HW-FF. The comparisons were performed in two groups by comparing feedback controllers separately to inspect the performance and emphasize the best feature of each; from this contrast, the best one was analyzed against the complex structure, the FLC with HW-FF.

As previously seen, all the controllers had gains to be tuned which were obtained by reduction of the IAE so to pursue the maximum performance. Regarding the FLC, since the input to the rules block is between [-1 1], this was

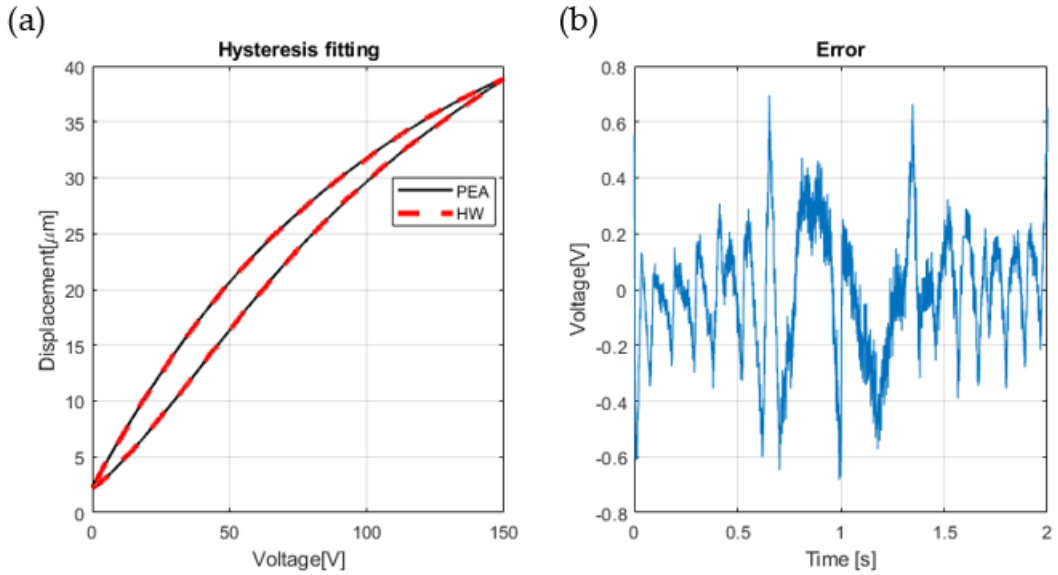

Figure 4.16: Hysteresis graph description where (a) corresponds to the fitting and (b) to the associated error.

PID		FLC close loop		FLC + HW-FF	
Gains	Values	Gains	Values	Gains	Values
K_p	10	K_c	16.2	K_c	4.2
K_i	1000	K_d	0.008	K_d	0.006
K_d	0.001	K_b	0.8	K_b	0.8

Table 4.6: Obtained gains for each control structure during experiments

monitored as well so that the controller behaviour could be suitable. Furthermore, it was taken into account the limits of the PEA input voltage by implementing saturations to prevent critical situations for the device.

The gains obtained for the control structure are summarized in the Table 4.6. These were gathered during the experiments through the minimization of the IAE.

PID vs. FLC

The first contrast was made with a simple PID controller against the FLC. Figure 4.17(a) is the error comparison where it can be seen that the PID has a

maximum value that varies between 0.1 and 0.2 μm during the rising and descending. However, the relevant feature appears during the peaks where the top ones are at 1 and 3 seconds and this yields to a severe behaviour where the error flips its sign into the same absolute value, which is expected due to the slope change. Throughout the lower peak, at 2 seconds, the amplitude of the error was reduced with a smaller value compared to the top one. On the other hand, the FLC behaves similarly although the error magnitude was reduced dramatically since its value is below 0.2μm. Additionally, the sign change feature previously explained is still present but the error was lowered in magnitude during these moments.

As regards the control signal which is shown in Figure 4.17(b), both architectures seemed to behave similarly but at the top peak the FLC increased the performance since the signal is smooth compared to the conventional PID as Figure 4.17(c) shows. In a deep analysis near the lower peak in Figure 4.17(d), it can be seen that in the descending, the FLC provided a better signal with less noise. Along the analyzed area, the FLC reached 0.42V whereas the PID resulted in 0.88V. This means that the FLC supplied a control actuation which has the half of the one provided by the PID. On the other hand, Figure 4.17(e) is a reflection of the analyzed situation but after the lower peak where the variation is higher since the PID generate 0.67V and the FLC 0.18V, which means a difference of around 3.7 times lower for the FLC.

FLC vs. FLC with HW-FF

The previous comparison indicated that the FLC performed better than the PID controller and thus, it was compared with the complex structure with FF since it was expected to increase the performance due to the compensation. Figure 4.18(a) shows the error of the two contrasted structures where the combination of FLC with FF improved the accuracy; although there is a discrepancy during the top peaks, the enhanced framework reduces the error variation and diminishes the issue at highest levels.

Therefore, the peaks can be analysed in-depth since the FLC controller still has a change of error sign every one second as previously was evaluated; the FLC-HW could shrink this difference at the cost of increasing the error amplitude at around 0.1 μm. However, another critical factor is the speed in which the

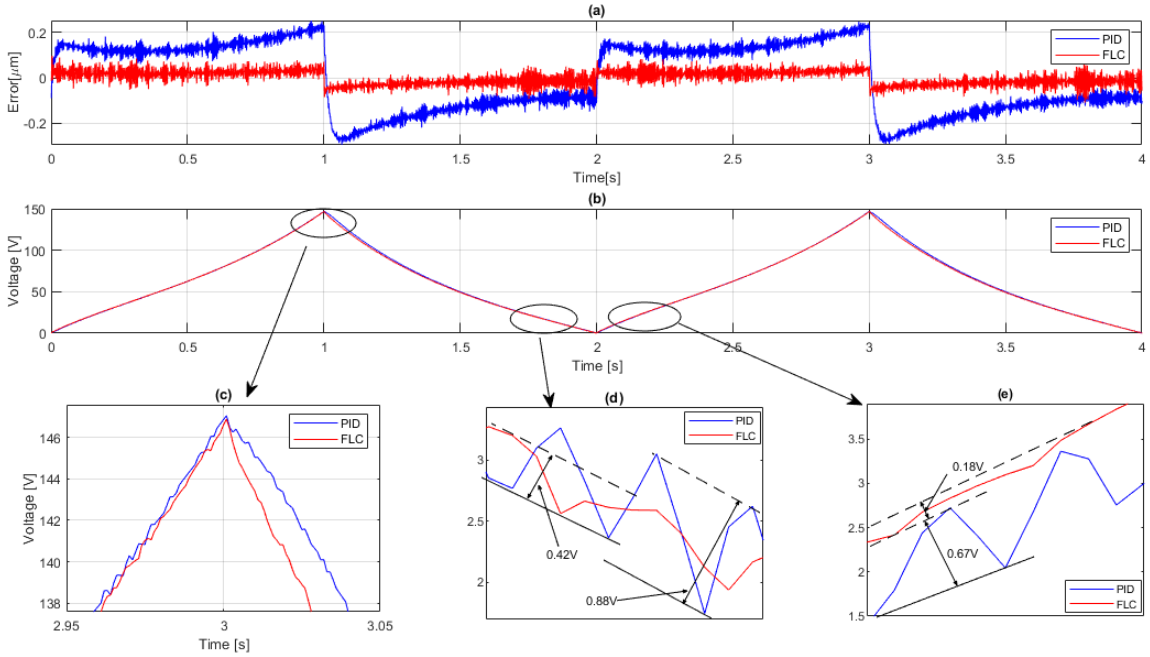

Figure 4.17: Comparison of error and control signal between PID and FLC. (a): Error; (b): Control signal; (c) Control signal at the top peak ; (d): Control signal near the lower peak; (e): Control signal after the lower peak.

controller could reduce the error: The FLC has a slow response to reduce the error after a top peak which has a length of about 0.5 seconds. In opposition, the FLC-HW could counteract with a small perception.

Concerning the control actuation as the Figure 4.18(b) exposes, the manner is similar to the previous case where both behaved similarly. Figure 4.18(c) discloses the mild demeanour described since the signal is acceptable for the complex structure at the top peak. Moreover, the control signal during the lower peak resembles in a similar effort in the FF compensated structure in contrast with the FLC in the feedback alone. For instance, Figure 4.18(d) shows a comparison where the FLC-HW has an amplitude variation of 0.16V and the FLC developed 0.58V, this means that the difference is 3.6 times less. Furthermore, this nature is present during the rising at Figure 4.18(e) since the difference is 3 times less for the FLC-HW which implies that the control signal had improved in comparison with the FLC and the PID.

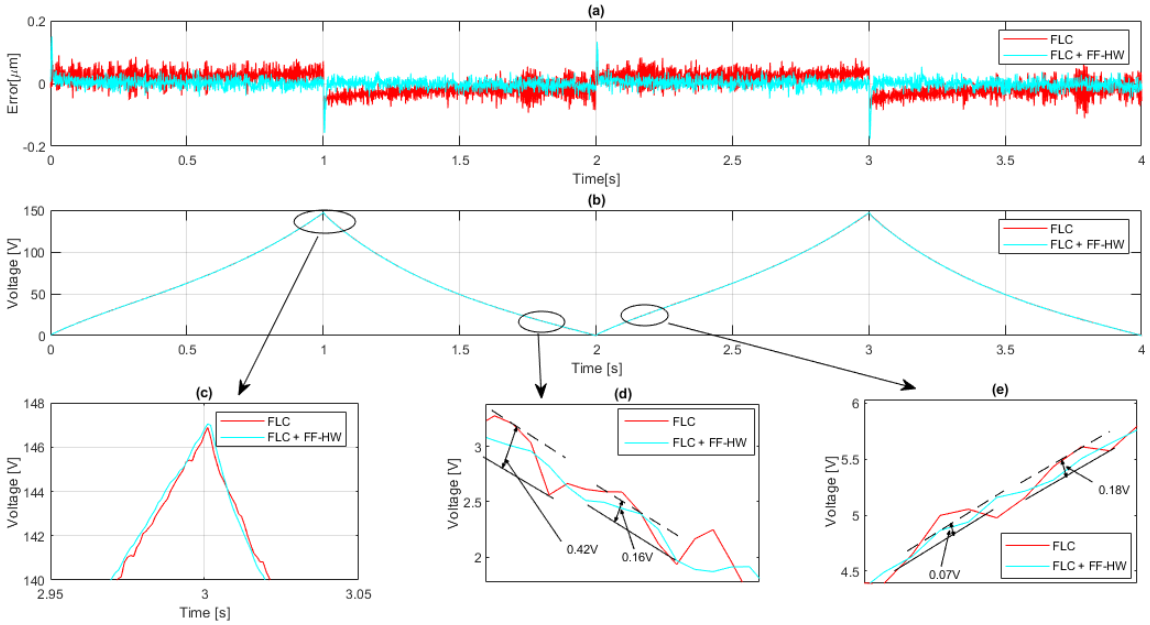

Figure 4.18: Comparison of error and control signal between FLC and FLC with HW. (a): Error; (b): Control signal; (c): Control signal near the lower peak; (d): Control signal after the lower peak.

IAE, RMSE and RRMSE results

The performance evaluation of all displayed structures was based on the IAE values obtained in each experiment which were calculated on a period of 4 seconds for two triangle cycles. Also, another metrics such as RMSE and RRMSE were calculated to compare the performance in depth. All the values obtained are expressed in the Table 4.7 according to the progress of complexity of each architecture.

Regarding the IAE, the PID, FLC and its combination with HW-FF provided, respectively, values of 0.578, 0.111 and 0.048. Undoubtedly, the progression of the complexity of every structure improved the results which are not only reflected in the error and control figures previously presented but also in the IAE. The difference in value for FLC is 5.2 times less than the PID one, although the discrepancy was still enhanced with the FLC combined with HW where the discrepancy was 2.3 times less compared with the FLC alone.

On the other hand, the RMSE and RRMSE had the same disposition as it was expected. The FLC compared with the PID, showed a considerable dif-

ference since the FLC decremented the RMSE to 0.033μm; the RRMSE was reduced to 0.74 %. Finally, the complex feedback with FF structure had a higher performance since the RMSE was trimmed to 0.017 and the RRMSE decreased 0.36% respect to the FLC alone.

Structure	IAE	RMSE [μm]	RRMSE [%]
PID	0.578	0.153	3.42
FLC	0.111	0.033	0.74
FLC + HW-FF	0.017	0.018	0.38

Table 4.7: Results obtained of the IAE, RMSE and RRMSE.

4.3.7 Conclusions

The hysteresis of PEAs represents a problem that can produce a performance reduction when these devices are employed for positioning. In this section, an analysis of structures was attempted to diminish the error with an acceptable control signal so to increase the effectiveness in tracking. All the results were part of experimental tests with a commercial PEA with its respective driver and measurement device.

First, an HW block was used to map the hysteresis where it was found that a piece-wise function reflected the non-linearities with acceptable precision and the errors presented could be compensated by adding a feedback controller. Subsequently, the structures proposed to be tested were: PID, FLC and its combination with HW-FF. The first structure was contrasted with the FLC, where the latter presented an enhancement in regards to the error reduction even at complex situations as peaks of the triangle reference; in terms of the IAE, the improvement resulted in a decline of 5.2 times. The control signal was acceptable since it mirrored a shrink in the noise, during the delicate situation as in top and lower peak, which is favourable for the PEA life-span.

The use of the FLC with HW-FF not only showed that the error was trimmed to lower values but also it was compensated during slope changes where previous frameworks suffered difficulties to overcome these variations. As an overall metric, the IAE dwindled 2.3 times less in comparison with the uncompensated feedback. The control signal raised a significant improvement as the noise was

even lower than in the previously tested structure. Performance growth was also viewed in during the peaks where no saturation or rough changes were observed, which could damage the hardware.

4.4 Super-twisting approach based on artificial neural networks

4.4.1 Contributions

- A novel strategy of a high-order sliding mode control combined with an ANN was designed.
- A stability proof based on Lyapunov's theory was showed in to prove the high performance of the proposal.
- The contrast was against a PID which constants were obtained with the minimization of the IAE.
- Experimental results reported that the novel structure is stable as it was proved theoretically, and the experiments provided a significant error reduction in contrast with the PID.

4.4.2 State of the art

The hysteresis is reflected as non-linearity where the present input depends on the past values and usually is also defined as an effect that appears as a combination of mechanical strain and electric field [94, 95]. Figure 4.19 is a figurative description at a material level when an electric field is applied through a piezoelectric material. In a neutral state without any electric action, the poles are in a arbitrary direction but when it gets exited, the poles begin to be aligned with the field and an elongation is produced which is associated with the ferroelectric effect [96]. When the electric field decreases its value, the poles intention is to be back to their initial direction but with a certain difference compared to the one when the electric field started to increase its value and this produces the hysteresis [68].

According to [4], there are two paths for hysteresis reduction: in terms of the raw matter, the piezoelectric material can be conceived up to an atomic level, which represents a complex task; at a practical level, a control strategy can be designed to drive the position to the desired one by controlling the voltage input signal.

As a first approach, linear controllers can be a suitable option to control the trajectory. In the early 1980s, authors of [97] suggested to implement linear

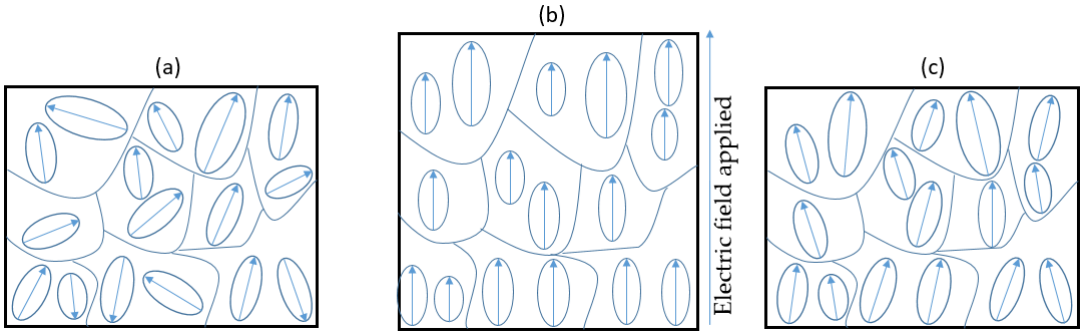

Figure 4.19: Piezoelectric material polarization with an electric field where: (a) is in a neutral state, (b) is with an applied field and (c) is after the electric field action.

strategies to diminish hysteresis from PEAs. Although PID is a classic and simple integration tool for most applications, widely attractive works had been done along the recent years [98–100]. Other PID variants had shown the inclusion of feedback linearization [101], grey relational [102], semiautomatic tuning [103], fractional PID [104] or gain-scheduling in a fuzzy-PID structure [105]. Besides other authors had employed linear quadratic regulators for similar actuator in terms of structural control [106]. However, the hysteresis is a strong non-linear effect where common structures need to have an advanced design so as to diminish [107]. Moreover, with critical uncertainties like modelling and external loads, these linear approaches are limited in a certain bandwidth [108].

The significant presence of nonlinearities in PEAs aims to implement controllers which can deal with these features. Feedback linearization with uncertainties control has been employed recently with the addition of a BW model for hysteresis where the researchers achieved good accuracy although the BW is limited for asymmetric hysteresis response [40, 88]. An advanced approach has equally been used with model predictive control based on an adaptive algorithm that was tested in a real system that provided an error of around 1%, which is acceptable although tests were performed with low amplitude signals [109]. Robust controllers had also been investigated with adequate results; authors from [68] implemented a robust control with its stability analysis of a scheme based on inverse models that produced decent outcomes as an error around 0.5 μm. Also other robust techniques as SMC had captured the interest due to its capability to reject the uncertainties [79, 110]. Several approaches of first order

SMC had been designed and used for PEAs even though that the chattering is an important drawback [85, 111, 112].

In the recent years, many methods have been designed to overcome the chattering phenomenon [113–116]. Thus, the authors of [113, 114] implemented the boundary layer technique which changes the discontinuous term of SMC by a smooth approximation when the states are about to reach the limits of a defined bound; however, the main drawback of this method is the decline of anti-disturbance capabilities [117]. In [115], a multi-surfaces SMC for approximation of unknown perturbations was proposed; despite the novelty of the framework, only simulation results were presented, and the algorithm has a broad number of gains for tuning. Integral Sliding Mode Control (ISMC) represents another employed structure for static-error reduction as it was developed in [116]; nevertheless, when a saturation function is used, the practicality is reduced because the boundaries are complex to obtain and the control accuracy is diminished [118].

Another advanced method for chattering reduction is High Order Sliding Mode Control (HOSMC) which was introduced by [119], which intention is to influence the high order derivatives of the system for the chattering alleviation. This technique is well known for its usage in MPPT control [120, 121], active vehicle suspension [122] but it is also employed for high performance guidance in aircrafts [123] as in PEAs [124, 125]. Super twisting algorithm (STA) belongs to the group of HOSMC and it is well known for its robustness and chattering decrease due to the inclusion of an integral term [121]. Although the implementation of STA is simple, as any other SMC controller, it has a discontinuous and a continuous term; traditionally, for the design of the latter mentioned, the model knowledge is required to construct the control law [126]. However, the hysteresis models have certain drawbacks which can produce difficulties for implementations and design [73].

There are two different approaches for hysteresis modelling: mathematical and physics based [127]. The first kind contemplates the most used ones like Preisach, PI and Krasnosel'skii-Pokrovkii models [128–130], which are based on hysteron operators. This function has the capability to depend on current and past inputs so as to reflect the hysteresis effect [131]. Although these frameworks can be adopted as observers with reasonable accuracy, the inverse calculation for feed-forward control can result intricate [132]. Despite its

complexity, recent cutting edge uni-axial phenomenological models have been developed which are rate and material independent and they only require a history variable [133, 134]. The physics based ones are known as the Domain Wall and the Jiles-Atherton model; these are acknowledged for their description of hysteresis present in magnetic materials and might be unsuitable since they are material dependant models [127].

Despite that an SMC drawback is the model-based approach it was described due to the inaccuracies that these yields, this research was based on a neural super-twisting algorithm (ST-ANN) since the usage of ANNs can reduce these effects [73, 73]. A shallow introduction about the background of research done by the scientific community in ANNs for non-linear mapping is presented in the following sections. A PID was used for results comparison as it has been commonly utilized for these correlations in literature [135–137].

4.4.3 Super Twisting algorithm based on artificial neural networks

The main aim of this research is to provide a suited control law for the PEA, so it could track the required references with fast correction and error reduction. STAs are known for their performance and robustness in guidance accuracy as well as chattering attenuation in comparison with first order SMCs as it was analysed in the state of the art section. The control law is established as Equation 4.14, Equation 4.15 and Equation 4.16 show, where u_{sw} is a continuous and discontinuous composition whose intention is to compensate uncertainties and dynamics that u_{ann} is unable to reduce. The surface S was assumed as Equation 4.17 where the error is $x - x_{ref}$ such that x is the measured PEA displacement and x_{ref} is the reference. Regarding the uncertainties and external disturbances, during the experiments several features were observed such as temperature [73, 138] which affected the strain-gauge measurement, sensor noise and other dynamics unconcerned. The constants K_1 and K_2 are design parameters which were tuned by IAE reduction in real time and taking into account the boundaries of the stability proof of Section 4.4.4.

$$u_{sw} = u_1 + u_2 \tag{4.14}$$

$$u_1 = -K_1 \cdot |S|^{\frac{1}{2}} \cdot sign(S) \tag{4.15}$$

$$\dot{u}_2 = -K_2 \cdot sign(S) \tag{4.16}$$

$$S = \dot{e} + \lambda e \tag{4.17}$$

Neural network compensation detailed

As previously mentioned, most of the PEA models have difficulties to map the dynamics of the systems even due to asymmetric effects or complex model implementation which can result in a high computational requirement. Hence, due to these drawbacks, the linearity and hysteresis dynamics are compensated by an ANN contemplated in a voltage term as u_{ann}.

An ANN consists of an algorithmic configuration that has a minimum of three mathematical connected layers known as *input*, *hidden* and *output* [139]. This biological concept is adopted from the brain neurons which can recognize, learn and change based on previous actions (also called *neuroplasticity*) [140]. Thus, these properties based on the mathematical formulation can lead the ability to perform approximations of non-linear dynamic systems [141, 142]. Recently, these types of system identification technique was implemented like TDNN which have shown good results in fitting performance [61, 143].

In this research, the architecture used for dynamic mapping was a Layer Recurrent Neural Network (LRNN) which is a shallow type with a recurrent inner connection and correlated with a tap delay ; this feature allows the usage of previous states and present inputs to produce outputs within hidden states [144]. These ANNs kinds were proved to be efficient for modeling and mapping hysteresis phenomenon [145]. In the following analysis tests were performed employing the Deep Learning Toolbox of Matlab 2020a (which was compatible with the version used of dSPACE), thus the implementation allows only shallow ANNs for code generation in Simulink [146].

The LRNN structure (shown in Figure 4.20) consist of three nodes as conventional ANN but with an outstanding feature of the hidden layer where a recurrent connection is used with the other layers and acts as a feed-forward over the block. The mechanics of this layer are as follows: at each time-step, the reference is processed at the input through an associated weight W_1, the output of the hidden layer *r(t)* recurs by a specified delay *n* and a weight W_i; finally,

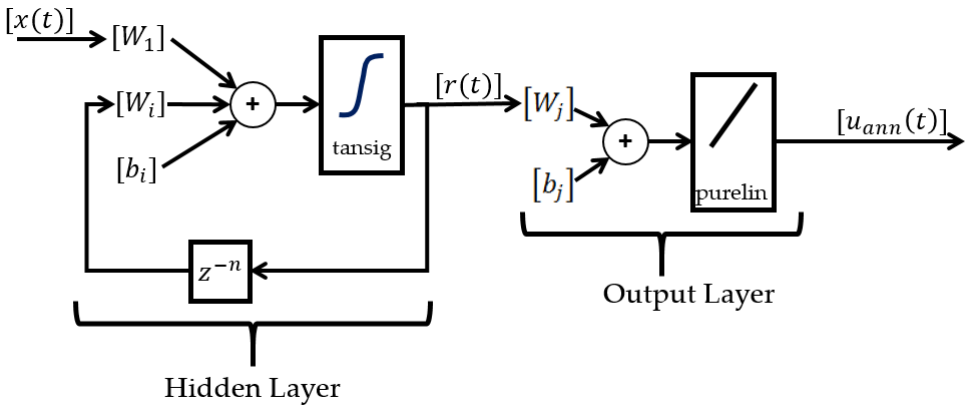

Figure 4.20: Recurrent ANN architecture

a bias vector b_i is added to the operation. The whole sum goes through an activation function that defines the behaviour of the weight associated to the neuron [147]. In this case, the activation function is *tansig* which has limits between -1 and 1 and achieves the output *r(t)*. The mathematical expression is in the Equation 4.18 and Equation 4.19.

$$r(t) = tansig[W_1(x(t)) + b_i + w(r(t-n))] \tag{4.18}$$

$$tansig(x) = \frac{2}{1+e^{-2x}} - 1 \tag{4.19}$$

The operation coming from the hidden layer is then passed as an input in the output layer which has a simple development. The variable *r(t)* is weighted by W_j and a bias b_j is added to be the input of a linear transfer function or also known as *purelin* (defined in Equation 4.21). The output of the entire ANN drives u_{ann} as mathematically is shown in the Equation 4.20.

$$u_{ann} = purelin[W_j(r(t)) + b_j] \tag{4.20}$$

$$purelin(x) = x \tag{4.21}$$

The previous operations have associated weights which were obtained through training algorithms that are calculated based on input and output data from the

real device. It was found as an advice to use LM algorithm as it frequently provides adequately results [148]; however, the obtained data had noise, and the ANN could yield to a low mapping performance. The authors of [149] suggested using the *bayesian regularization*, which is an appropriate training algorithm since it also endorses over-fitting prevention. An iteration in the training consists in the Equation 4.22, where the vector *Wb* contains the current weights and bias, g_k is the current gradient and α is the learning rate. Further details in depth of the bayesian regularization are developed in [150].

$$Wb_{k+1} = Wb_k - \alpha g_k \tag{4.22}$$

The performance of the training algorithm was measured by the mean squared error (MSE) which is defined by Equation 4.23 where T_i is the target output and U_i is the ANN prediction.In the following sections, the LRNN accuracy is proven according to input/output information related to the triangle reference signal due to its complexity compared to a sine wave.

$$MSE = \frac{1}{N}\sum_{i=1}^{N}(T_i - U_i)^2 \tag{4.23}$$

4.4.4 Stability proof of the proposed algorithm

Previous to a formal demonstration, the PEA is assumed as a second order mechanical system as defined in Equation 4.24.

$$m\ddot{x} + b\dot{x} + kx + df_h(x) = du + P \tag{4.24}$$

The expression is defined with *m*, *b*, *k*, *x*, *d*, *u*, *h* and *P* which are the mass, damping constant, stiffness constant, position, piezoelectric coefficient, input voltage, hysteresis and overall perturbations (uncertainties, unmodelled dynamics, etc.), respectively. The term $f_h(x)$ represents the hysteresis which depends on the position *x*. On the other hand, the piezoelectric coefficient *d* is defined as the product between the stiffness and the utmost displacement divided by the maximum driving voltage.

The mechanical values such as *m*, *b*, *k* were obtained with the same data employed for the ANN. The software used was the Parameter Estimator Tool-

box from Simulink based on a Nonlinear least squared with the algorithm Trust-Region-Reflective. The summarize is enlisted in table Table 4.8.

	Values	Units
Mass (m)	0.431	Kg
Damping (b)	1340	$N \cdot s/m$
Stiffness (k)	81263	N/m

Table 4.8: Mechanical properties for the PEA

Considering a control signal defined as in the following Equation 4.25.

$$u = u_{ann} + u_{sw} \tag{4.25}$$

Such that:

$$\begin{cases} u_{ann} = u_{linear} + f_{ann}(x) \\ \\ u_{sw} = -K_1 |S|^{\frac{1}{2}} sign(S) - K_2 \int sign(S) dt \end{cases} \tag{4.26}$$

In previous sections, the u_{ann} was obtained from ANN approximation; moreover, the objective of this term is to compensate the linearity and the hysteresis through a voltage. Additionally, the u_{sw} was previously defined as the STA correction in Equation 4.14 and the intention is to reduce the errors, perturbations and unknown dynamics. This description is summarized in Equation 4.26.

The u_{linear} can be defined as a linear mechanical system without perturbations or hysteresis as in the Equation 4.27. Therefore, by replacing the latter into Equation 4.26, it can be obtained the Equation 4.28.

$$u_{linear} = \frac{1}{d}\left(m\ddot{x}_{ref} + b\dot{x}_{ref} + kx_{ref}\right) \tag{4.27}$$

$$u_{ann} = \frac{1}{d}\left(m\ddot{x}_{ref} + b\dot{x}_{ref} + kx_{ref}\right) + f_{ann}(x) \tag{4.28}$$

With the substitution of Equation 4.28 and the second part of Equation 4.26, a control signal can be achieved as it was defined in Equation 4.25. Thus, when *u* is gathered, it can be replaced in Equation 4.24 to obtain the following Equation 4.29.

$$m\ddot{x} + b\dot{x} + kx + df_b(x) = m\ddot{x}_{ref} + b\dot{x}_{ref} + kx_{ref} + df_{ann}(x) + du_{sw} + P \tag{4.29}$$

This expression can be simplified because the error was defined as $e = x - x_{ref}$. Since the ANN will never provide a perfect fitting, then we define that $f_{ann}(x) - f_b(x) = \varepsilon_{ann}$ as an associated error of approximation. Hence, the preceding expression is redefined as Equation 4.30.

$$m\ddot{e} + b\dot{e} + ke = d\varepsilon_{ann} + P + du_{sw} \tag{4.30}$$

Subsequently, the equation can be solved to obtain the second derivative of the error as in Equation 4.31.

$$\ddot{e} = -\frac{b}{m}\dot{e} - \frac{k}{m}e + \frac{d}{m}\varepsilon_{ann} + \frac{P}{m} + \frac{d}{m}u_{sw} \tag{4.31}$$

Therefore, if the surface defined in Equation 4.17 is derived, the Equation 4.32 is obtained. Thus, the second derivative from Equation 4.31 can be replaced to reach the Equation 4.33.

$$\dot{S} = \ddot{e} + \lambda\dot{e} \tag{4.32}$$

$$\dot{S} = -\frac{b}{m}\dot{e} - \frac{k}{m}e + \frac{d}{m}\varepsilon_{ann} + \frac{P}{m} + \frac{d}{m}u_{sw} + \lambda\dot{e} = \frac{d}{m}u_{sw} + \rho \tag{4.33}$$

Where:

$$\rho = -\frac{b}{m}\dot{e} - \frac{k}{m}e + \frac{d}{m}\varepsilon_{ann} + \frac{P}{m} + \lambda\dot{e} \tag{4.34}$$

In this expression, it is perceived that the intention of the STA is to reduce the errors and its derivatives as well as the perturbations and approximation differences that the ANN could not accomplish. A further development of the expression from Equation 4.33 can yield to the following re-arrangement.

$$\begin{cases} \dot{S} = \dfrac{d}{m}\left(u_1 + u_2\right) + \rho = -\theta_1 |S|^{\frac{1}{2}} sign(S) + u_2 + \rho \\ \\ \dot{u}_2 = -\theta_2 sign(S) \end{cases} \tag{4.35}$$

Where

$$\begin{cases} \theta_1 = \dfrac{K_1 d}{m} \\ \\ \theta_2 = \dfrac{K_2 d}{m} \end{cases} \tag{4.36}$$

A vector transformation can be assumed based on [137, 151–153], with its following derivative in Equation 4.37 and Equation 4.38.

$$\beta = \begin{bmatrix} \beta_1 & \beta_2 \end{bmatrix} = \begin{bmatrix} |S|^{\frac{1}{2}} sign(S) & u_2 \end{bmatrix}^T \tag{4.37}$$

$$\dot{\beta} = \frac{1}{|\beta_1|} \begin{bmatrix} \frac{1}{2}(-\theta_1 \beta_1 + \beta_2 + \rho) & -\theta_2 \beta_1 \end{bmatrix}^T \tag{4.38}$$

The time derivative from Equation 4.38 can be also be expressed in the following Equation 4.39.

$$\dot{\beta} = \frac{1}{|\beta_1|}(A\beta + \sigma) \tag{4.39}$$

Where:

$$A = \begin{bmatrix} -\frac{1}{2}\theta_1 & \frac{1}{2} \\ -\theta_2 & 0 \end{bmatrix} \text{ and } \sigma = \begin{bmatrix} \frac{1}{2}\rho \\ 0 \end{bmatrix}$$

According to the author of [154], a ”practical” approach for the management of ρ can be defined as Equation 4.40. It should be noted that this fact does not limit the applicability of this control scheme as in a real system as the term ρ will have a superior bound. The mechanism for this statement is through the multiplication of a constant $\gamma \in R^+$.

$$|\rho| \leq \gamma |s|^{\frac{1}{2}} \tag{4.40}$$

Hence, the Lyapunov stability proof establishes that a dynamical system is asymptotically stable if there exists a definite Lyapunov function V(S), such that V: $R^n \rightarrow R$ so that $V(\beta) > 0$, $V(\infty) = \infty$, $V(0) = 0$ & $\dot{V}(\beta) < 0, \forall \beta \neq 0$ [93, 155, 156]. Thus, the Lyapunov function chosen is Equation 4.41; the

correspondent time derivative is defined in Equation 4.42.

$$V(\zeta) = \zeta^T D \zeta \tag{4.41}$$

$$D = \frac{1}{2}\begin{bmatrix} 4\theta_2 + \theta_1^2 & -\theta_1 \\ -\theta_1 & 2 \end{bmatrix}$$

$$\dot{V}(\beta) = \frac{1}{|\beta_1|}\beta^T\Big(A^T D + DA\Big)\beta + \frac{2}{|\beta_1|}\beta^T D\sigma \tag{4.42}$$

As previously explained, for this demonstration, the term ρ is bounded; therefore, we define the constrained statement from Equation 4.43.

$$\rho = \gamma|s|^{\frac{1}{2}} sign(s) = \gamma\beta_1 \tag{4.43}$$

The replacement of the bounded condition of Equation 4.43 within the right hand-side term of Equation 4.42, results in the Equation 4.44.

$$\dot{V}(\beta) = -\frac{1}{|\beta_1|}\dot{\beta}^T Q\beta \tag{4.44}$$

Where the *Q* matrix is defined in the follow Equation 4.45.

$$Q = \frac{k_1}{2}\begin{bmatrix} \theta_1^2 + 2\theta_2 - \gamma(\theta_1 + 4\frac{\theta_2}{\theta_1}) & -\theta_1 \\ -(\theta_1 - \gamma) & 1 \end{bmatrix} \tag{4.45}$$

Thus, the stability is conditioned by the gains k_1 and k_2 since it implies that the matrix *Q* should be positive definite. To accomplish this statement, the conditions of Equation 4.46 should be taken into account for the gain tuning at experiments.

$$\begin{cases} \theta_1 < \gamma \\ \theta_2 > \dfrac{1}{4}\dfrac{\theta_1^2(\gamma - \theta_1)}{\theta_1 - 2\gamma} \end{cases} \tag{4.46}$$

4.4.5 Results

LRRN Training Results

The training of the ANN was undertaken with data recorded from the triangle input signal which has an amplitude of 145V and 4s of a period. As data for training, as a compensator, the model had to be inverted which means that the input to the LRNN was the displacement whereas the voltage represents the output. A record of 40s of data was handled and divided in 70/15/15 proportions as for training, evaluation and testing; further details are specified in Table 4.9. In regards to the hardware used for iteration, a Dell Precision 3640 was employed and configured with parallel calculation activated in 7 cores.

	Values
Data points	40.000
Training/ Validation/ Test Sets	70/15/15
Iterations	5300
Performance Metric	MSE
Training Algorithm	Bayesian regularization
Training time[hs]	6

Table 4.9: ANN specifications

The results revealed an acceptable mapping contrasted with the real data of the PEA as it is shown in Figure 4.21. During the first rise between 0 and 2s, the error had a sudden fluctuation up to 0.5s and a following variation with noise around the zero voltage up to less than 2s. At this time value, the change of slope was expected to be sharp although the correction was performed in less than 0.05s with 0.3V of error. During the rise, before 2.7s, the signal showed a leveled average again around 0V. However, after 2.5s the error began to plunge with intensity up to 3.5s with noise until -0.3V. Later, a sudden reply soared up to -0.1V with a following fluctuation and an expected shifting that is mirrored at 0s again due to the slope change.

Despite that the error tends to fluctuate, the response is acceptable. A RMSE of 0.11V was obtained which is tolerable for a signal amplitude of 145V. In addition, even if the achieved output has noise, it is also a replication of the sensor noise which was expected as well. The inclusion of a control is able

to reduce these unexpected features, can manage to diminish the error and increase the accuracy.

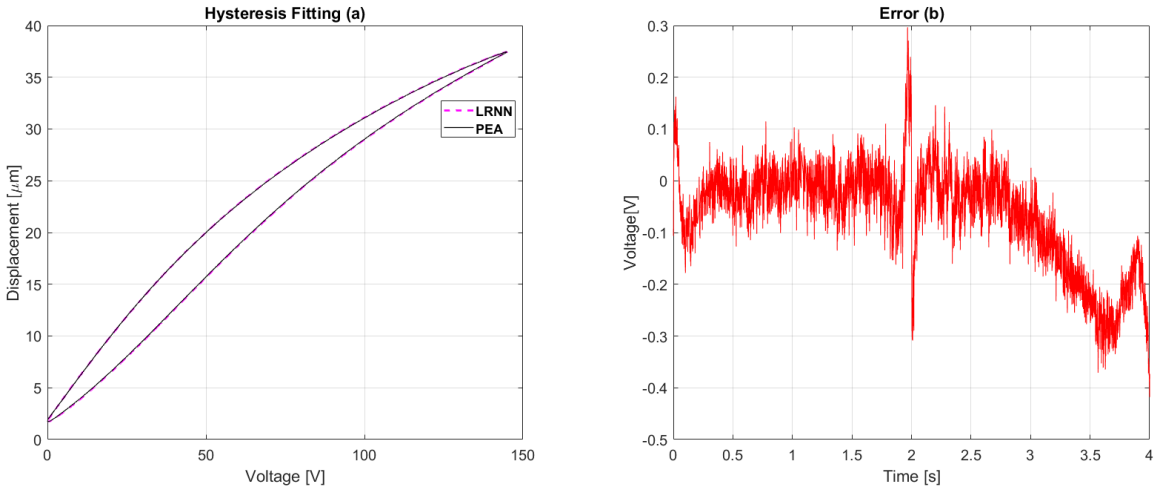

Figure 4.21: Performance of the LRNN where: (a): hysteresis fitting; (b): error approximation.

Tracking control results

The control structures presented were embedded in the dSPACE hardware, where the first one was the PID and the second one was the ST-ANN. The data acquired was produced within the two mentioned references for each controller which outcome in two different comparisons. The performance metric for the controllers tuning in real time was the IAE which had to be reduced so as to obtain outstanding results. Moreover, to secure the equipment, each structure had security blocks like saturations (0-150VCC of input voltage) and antiwind-up for the integral action terms.

Regarding the gains obtained, these were obtained in real-time by the reduction performance of IAE by taking into account the conditions provided by the stability proof. Table 4.10 summarizes the values of the achieved gains.

Triangle reference comparisons

The first comparison was allowed with the main trajectory that was used for the ANN training and also because it was a complex reference to be followed.

PID		ST-ANN	
Gains	Values	Gains	Values
K_p	10	λ	20
K_i	1000	K_1	1.4
K_d	0.001	K_2	118

Table 4.10: Obtained gains of PID and ST-ANN

Figure 4.22 is the error along 8s (2 cycles) of a period and 145V of amplitude. Despite that the PID generates an error between 0.05 and 0.15 μm, this value decreases the performance in a guidance requirement. From the beginning, the first rise between 0 and 2s, the PID had reduced its accuracy due to a gap from zero error which slightly increases its value until the first slope change into negative at 2s. Nonetheless, the ST-ANN shows a stabilized error signal with a mean near the zero and with a variation less than 0.05 μm mostly through the first 2s of analysis.

The following point of interest is at 2s where the trajectory changes promptly its slope. The shifting behaviour of the PID at the upper converging point produces a sudden error correction which lasts a few fractions of a second. The error reverses its sign and value from 0.1 to near -0.15 μm which implies a change of 0.25 μm. In spite of the perceptible slope change that the PID control tried to compensate as fast as it could, the ST-ANN acts with a subtle demeanour as it can be seen in the zoom window where a slight overrun is performed and corrected promptly. This difference showed that the PID overshoots 2.3 more than the ST-ANN.

Between 2 and 4s, the descending occurs and the PID has mirrored manner as previous with during the rise but with less variation. However, the ST-ANN is still in a same performance as previously where the level is around the zero value and with slight error increments between 3 and 4s. At the lower converging point (at 4s), the slope changed back to positive where the PID alternates with lower amplitude in the error switch from -0.05 to near 0.07 μm; the ST-ANN displays imperceptible changes during this moment as it can be seen in the following zoom window. Thereafter, the situation is repeated due to the second triangle cycle achieved each 4s.

During the described error compensation of both architectures, a control

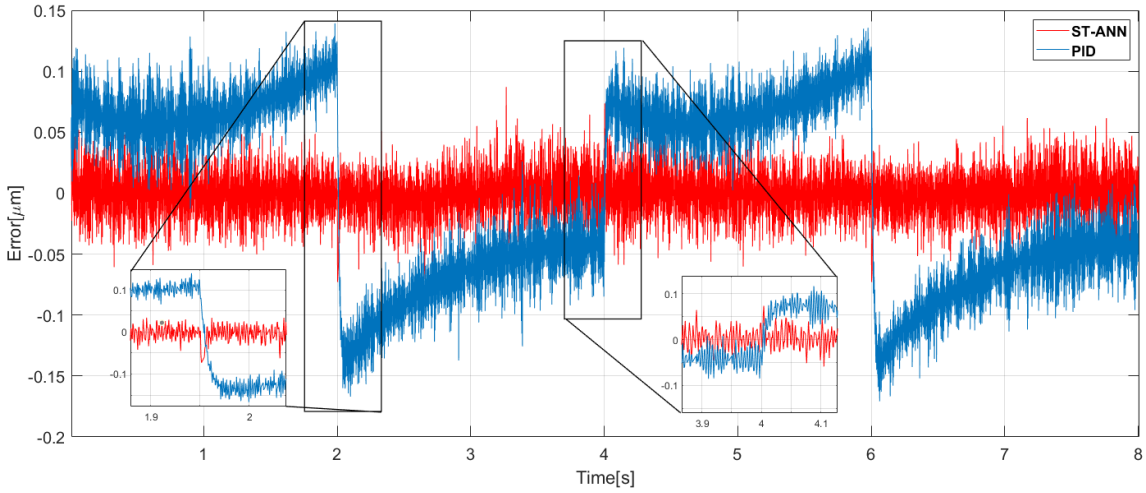

Figure 4.22: Error comparison between the ST-ANN and the PID structures

signal was generated for the PEA and recorded to be displayed in Figure 4.23. Any saturation or sudden changes were exposed which could damage the PEA driver or even reach the instability. Although the complex control framework incorporates a discontinuous term, the generated control signal is acceptable since chattering was unnoticed.

Sine reference comparisons

The triangular trajectories showed a tracking performance suitable and it was expected an increment on the effectiveness for a soft reference with the same features (like amplitude and period) as a sine wave. However, in the Figure 4.24 it can be seen that the PID still has difficulties to follow a soft signal although it could respond with a mild correction compared to previous results. On the other hand, the ST-ANN could manage the error even related to the sharp previous tested signal as the magnitude was around the same values. As the similarity in amplitude (between -0.15 and 0.1 μm between 1 and 3s), the shifting of the slope operates in a similar mien.

Since the current reference signal was soft, it was predicted that the control signal was going to behave the same, in this case, provided that a suitable control was designed. The comparison in Figure 4.25 shows a smooth manner in both architectures with any aggravations that could complicate the life-span

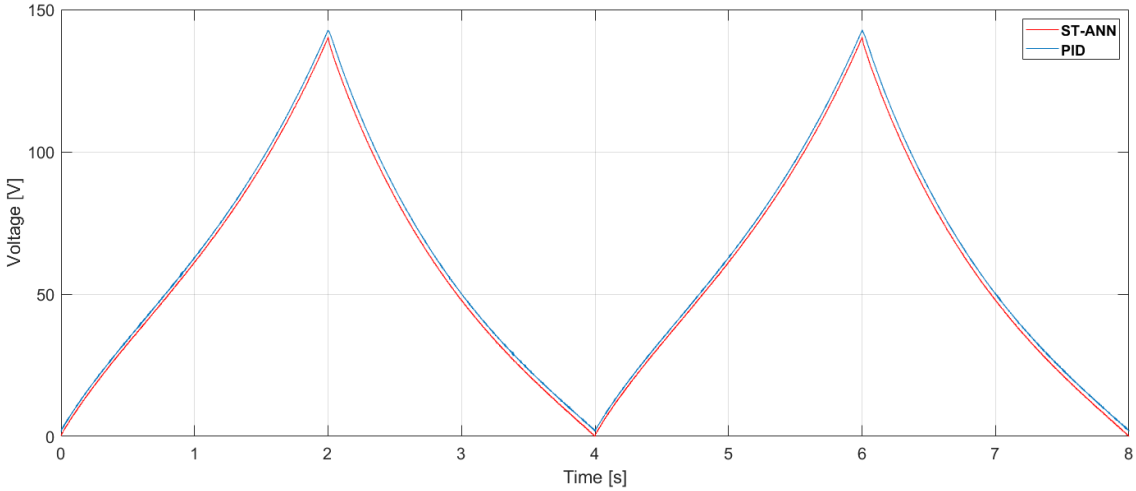

Figure 4.23: Control signals comparison of the ST-ANN and the PID

of the PEA.

Performance metrics comparison

Along this research, the prime objective was to pursuit an error reduction in the mentioned trajectories so as to increase the accuracy. Consequently, the IAE was reduced by tuning of the corresponding gains and thus, the metrics in terms of the error were calculated along a period of the reference signals already used. Table 4.11 shows the results of the IAE, RMSE and RRMSE contrasted in both controllers and signals.

Reference	IAE			RMSE [μm]			RRMSE [%]		
	ST	PID	Difference	ST-ANN	PID	Difference	ST	PID	Difference
Triangle	0.0653	0.28	4.2x	0.0203	0.0756	3.7x	0.45	1.69	3.75x
Sine wave	0.0625	0.28	4.4x	0.0195	0.0795	4x	0.44	1.80	4.09x

Table 4.11: Comparison of the different metrics

The IAE revealed an expected improvement for the ST-ANN where the PID showed 0.28 in both references but the ST-ANN increased the precision with the sine wave by twice (from 0.065 in the triangle up to 0.0625 with the sine wave). This dissimilarity is reflected in both cases where the ST-ANN enhanced 4.2 and 4.4 times in difference.

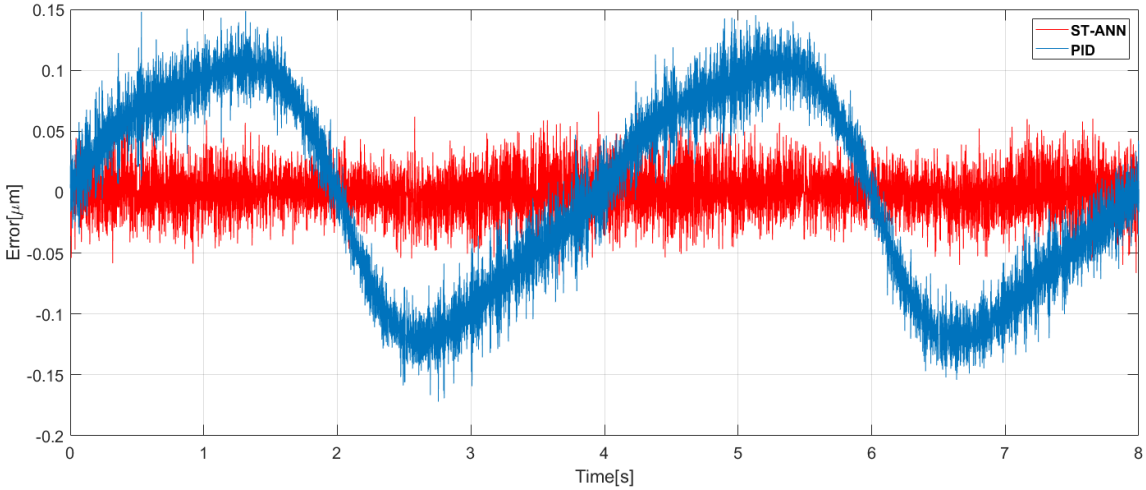

Figure 4.24: Error comparison between the ST-ANN and the PID structures for a sine wave tracking reference

Regarding the RMSE, the reflection is similar with the same magnitude of variation. The ST-ANN yield a RMSE of 0.0203 μm with a triangle trajectory whereas the PID downgraded the performance to 0.0756 μm which implies a difference of 3.7 times. The sine wave was expected to show a similar and even greater disparity which is expressed 4 times higher for the PID.

Finally, the RRMSE endures the previous trend where the ST-ANN overcame the comparisons. The situation was likewise with the triangular reference: the PID showed a value of 1.69% whereas the ST-ANN diminished up to 0.45% and it resembles in 3.75 times of difference. Again, the circumstance is similar in the sine wave trajectory where the magnitudes are alike and the difference is higher as expected.

4.4.6 Conclusions

Along the current research, it was proved that PEA actuators can gather high accuracy in terms of micro-displacement in a way required for special applications, like it was reviewed in the state of the art. Hysteresis is one of the key obstacles, a suitable and advanced control should be designed to accomplish the target of reducing the nonlinearity.

In this study, a commercial PEA from Thorlabs with its peripheral hardware

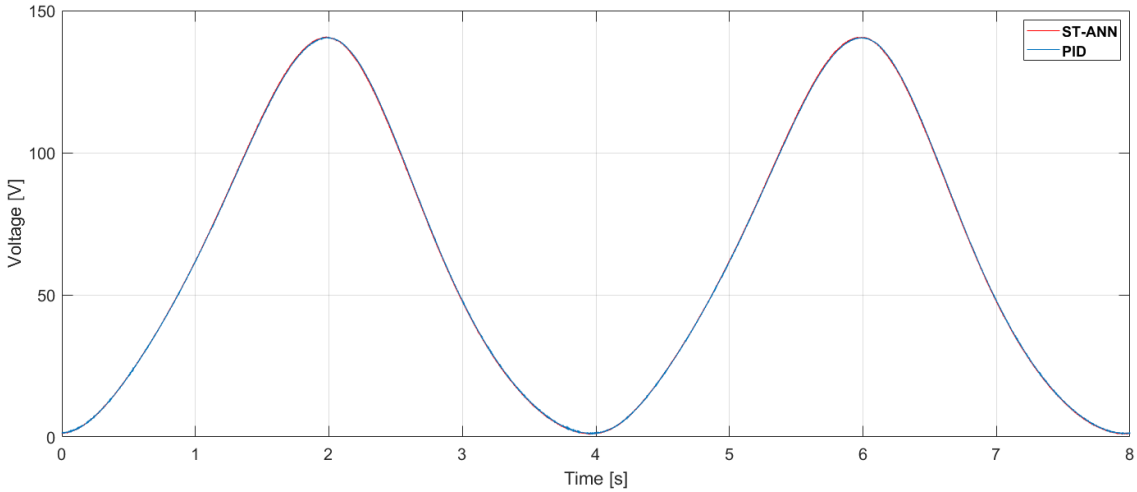

Figure 4.25: Control signal comparison between the ST-ANN and the PID structures for a sine wave tracking reference

was used to test each control structure designed in a dSPACE board. At first, it was shown that the hysteresis provided by the manufacturer can reach up to 15%. A triangular reference of 145VCC of amplitude with a period of 4s was used as the main signal, although a sine wave with the same features was tested for robustness check. It was found that HOSMC controllers are a satisfactory option since the chattering is fairly reduced compared to first order SMC and also due to their robustness. An ANN was used to avoid the issues that the model-based SMC represent and thus, an LRNN trained with bayesian regularization was developed with real data from the PEA.

A Lyapunov stability proof was presented to reveal the theoretical performance of the ST-ANN. It was uncovered that the controller supplies a stable response provided that the STA accomplishes with conditions based on its gains. The following steps were the experiments based on the implementation of the control architectures; the gains of each framework were tuned based on *minIAE*. The stability was also checked and experiments showed instability responses. Regarding the complex reference that the triangle represented, the ST-ANN displayed a remarkable performance in comparison to the PID since the latter had variations specially in the slope changes whereas the advance structure displayed a slight noisy fluctuation (which can be associated to the sensor) around the zero value. The error generated in the sine wave as a reference exhibited

similarities with the ST-ANN whereas the PID could not reduce the error even if the signal was soft. In terms of the control signals, both controllers showed acceptable behaviours even in the triangle as in the sine wave where no saturations or severe changes were appreciated. In general terms, the two controllers revealed soft and adequate signals.

At last, a comparison of metrics was performed where it was shown the advantage of the ST-ANN numerically. Regarding to the IAE, both controllers had almost the same difference but the ST-ANN exposed a higher performance which was between 4.2 and 4.4 times superior to the PID. The other metric compared was the RMSE which resemble a greater discrepancy in the triangle reference, the ST-ANN was 3.7 times higher and in the softer signal it was increased to 4. Finally, the RRMSE behaves similarly since the RMSE magnitudes had closed values.

4.5 Cuasi-continuous sliding mode control based on artificial neural networks

4.5.1 Contributions

- Aiming to enhance the tracking precision of a PEA, a novel strategy of a quasi-continuous sliding mode control combined with an ANN.
- The contrast was against a PID tuned in real-time experiments through the minimization of IAE.
- Experimental results reported that the novel structure is stable as it was proved theoretically, and the experiments provided a significant error reduction in contrast with the PID.

4.5.2 State of the art

Regardless the benefits of PEAs, which are extensive for several uses, downsides have a significant importance in the performance of these appliances. One of the main and most studied one is the hysteresis which is a ferroelectric phenomenon related to the material poles which have arbitrary orientations that align when a voltage is applied but the release of this action yields to a different direction [4, 157]. Thus, for this reason, it is also known as a memory effect as it depends on previous history [128]. In practice, the accuracy can be reduced up to 22% of the nominal displacement as a consequence of this anomaly [2]; another important consequence of this phenomenon is also the instability [158]. Nevertheless, since hysteresis is a natural property, available solutions comprise a material re-design or the implementation of a control algorithm [4].

PID had been widely used in practice as first option. Authors of [159] developed a PID for position which was verified in simulations and later in experiments where the results shown a tracking error reduction of 5%. A main disadvantage of PIDs is the gain scheduling which can vary for different scenarios and or situations; thus, several ways had been suggested to tune these. For instance, authors of [160] proposed the usage of particle swarm optimisation (PSO) in simulation with a suitable PEA model. Obtained gains were used in an experimental platform with a commercial PEA where the results showed an improvement in the position accuracy. However, online tuning algorithms for experimental rigs can require a significant amount of computational resources

and certainly, there are other non-linear controllers which manage the compensation with better performance.

SMC is a non-linear strategy with a discontinuity that drives the system in a sliding surface [161]. A main advantage allowed is the robustness against uncertainties and external disturbances. The classic SMC has been implemented in PEAs for force control by authors of [162], where they found suitable outcomes with sine signals as references. A similar approach was carried in the research of Chouza et al. [114] where SMC based with a PID surface was implemented in a commercial PEA where they tested different reference signals such as ramp, constants and sine wave. In spite of the improvements of error reduction in the ramp and constant references, the sine wave showed an error of around 5%. However, in the analysed background it was shown that the main disadvantage of SMC is the chattering that is generated by the discontinuous property. This is an unwanted effect because not only it increases the energy loss but also the wear in the actuator [163].

Certainly, the chattering can only be reduced and not eliminated because the discontinuity (produced by a sign function) is a main feature of SMC. Thus, in the recent years, many proposals have been published to trim this effect. For instance, authors of [113] changed the discontinuity by a hyperbolic function and in comparison with conventional approaches, the enhancement was acknowledged in the results. Another advance strategy is the usage of HOSMC where high order derivatives are used in the sliding surface and as a result, the chattering is relieve [164, 165]. An example of implementation has been carried by the authors of [166] where they used a HOSMC as an observer for error compensation in a PEA test rig. Results showed significant improvements in comparison with other conventional types of SMC strategies in simulation and experiments. Regardless the enhancement of HOSMC over conventional SMC, the design of sliding controllers establishes that the control law is split into a switching and an equivalent term that are aimed to maintain and compensate the sliding motion [167]. The equivalent is commonly achieved through a mathematical model that describes the system, and this would imply the use of a proper hysteresis description.

Hysteresis models for PEAs are mainly classified in two main categories known as physical and phenomenological [82]. The first mentioned group is a description of the ferromagnetic effect that produces the non-linearity, al-

though the material dependency and complex numerical solutions are the downsides of these theories [127, 168]. In regards to the phenomenological, the sub-classification is related to the ones based on differential equations (Dunhem [169], Backslash [170] and BW [171]), operator models (Preisach [128], PI [172] and Krasnoselskii-Pokrovskii [130]) and polynomial models [47]. Nevertheless, the disadvantages of these approaches are linked with complicated solutions to gather the inverse model, incapability to deal with asymmetric hysteresis, rate dependency and complex implementation [127].

Based on the research about the background that we made, we designed a HOSMC controller known as QC-Continuous (QCSMC) which provided suitable results in terms of chattering reduction in previous works [120]. Due to the drawbacks that we enumerated about hysteresis models, we decided to achieve the equivalent term of the sliding controller through means of an ANN and named as neural QCSMC (or QCSMC-ANN). This is possible since we could conduct experiments to acquire data for the ANN training.

4.5.3 Quasi-continuous sliding mode control

QC-SMC belongs to the HOSMC, known for the robustness and performance in tracking precision; moreover, the chattering reduction is another advantage of this controller over other structures [173]. The control law that we settled as Equation (4.47) comprises the terms u_{ann} and u_{sw} which, respectively, aim to compensate the non-linearities (like the hysteresis) and counteract uncertainties or perturbations The definition of u_{sw} is defined in Equation (4.48) which is dependant on a sliding surface expressed by Equation (4.49) and where parameters λ and γ are positive defined by the designer. The term u_{ann} is dependant on the ANN compensation and further details are given in the following section.

$$u = u_{ann} + u_{sw} \tag{4.47}$$

$$u_{sw} = -\gamma \frac{\dot{s} + |s|^{1/2} sign(\dot{s})}{|\dot{s}| + |s|^{1/2}} \tag{4.48}$$

$$s = e + \lambda \int_0^t e dt \tag{4.49}$$

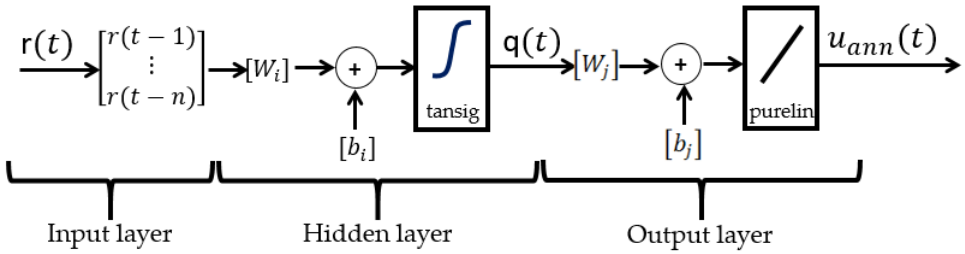

Figure 4.26: ANN

4.5.4 Neural Network Compensation Design

Implementation of conventional SMC methods where the equivalent term has to be through a mathematical model can yield to a insufficient compensation or even increase the computational cost. Nevertheless, in the last years ANNs have been a suitable solution for system identification where the only drawback resides for the time that the training algorithm requires to develop a truthful output. Hence, we used a TDNN due to the efficiency related to training time versus accuracy obtained.

In formerly investigations, we tested TDNN structures to reduce hysteresis which showed proper results in combination with conventional controllers [73]. As the name states, a TDNN is an extension of a classic multilayer perceptron (MLP) that works with time signals. The inclusion of time delays *n* allows the neurons to get further information about the time history of the input; this implies that the ANN will fit to a time set pattern [174]. Mathematically, this is expressed with Equation (4.50) where f is a non-linear function that relates the input/output of the ANN.

$$u_{ann} = f\Big(x(t), x(t-1), x(t-2), ..., x(t-n)\Big) \tag{4.50}$$

A further expansion of the function *f* is as the following Equations (4.51), (4.52), (4.53) and (4.54): the retarded reference inputs $r(t-n)$ are weighted with parameters W_i and bias b_i; later, this operation yields into the activation function called *tansig*. The output *q(t)*, which is the outcome of the described operation, is employed as an input into the output layer. In this case, the procedure is similar as previously but where the activation is done with a linear

transfer function called *purelin*. Subsequently, the output of this layer provides the compensation voltage u_{ann}.

$$q(t) = tansig\left(\sum_{p=0}^{n} W_i \cdot r(t-n) + b_i\right) \tag{4.51}$$

$$tansig(x) = \frac{2}{1+e^{-2x}} - 1. \tag{4.52}$$

$$u_{ann} = purelin[W_j q(t) + b_j], \tag{4.53}$$

$$purelin(x) = x. \tag{4.54}$$

The calculation of the weights and bias, related to the previous explained relations, are achieved with training algorithms. In this case, we used LM which represents a method that guarantees the fitting of the ANN to the experimental data through an adaptive behaviour [175]. This mechanism is generated by the location finding of the minimum of a cost function is declared as the sum of square errors and the real measurements within an iterative updating.

4.5.5 Results

ANN Analysis Results

We recorded experimental data from the PEA where the input was a triangular signal of 145V with 4 seconds of period. Also, the displacement was acquired through the strain gauge reader in a 40 seconds of experiments with a sampling time of 1 kHz. From this data, we used the displacement as an input and the applied voltage as an output because the aim is to achieve an inverse model.

After several tests to achieve the best MSE, we configured the ANN in 22 neurons with 5 input delays. In regards to the data, it was split into 70%, 15% and 15%, respectively, for training, evaluation and testing. Finally, the performance was measured with the mean squared error (MSE) in the validation set were the value obtained was 0.017 in 12.000 iterations made in 4 minutes.

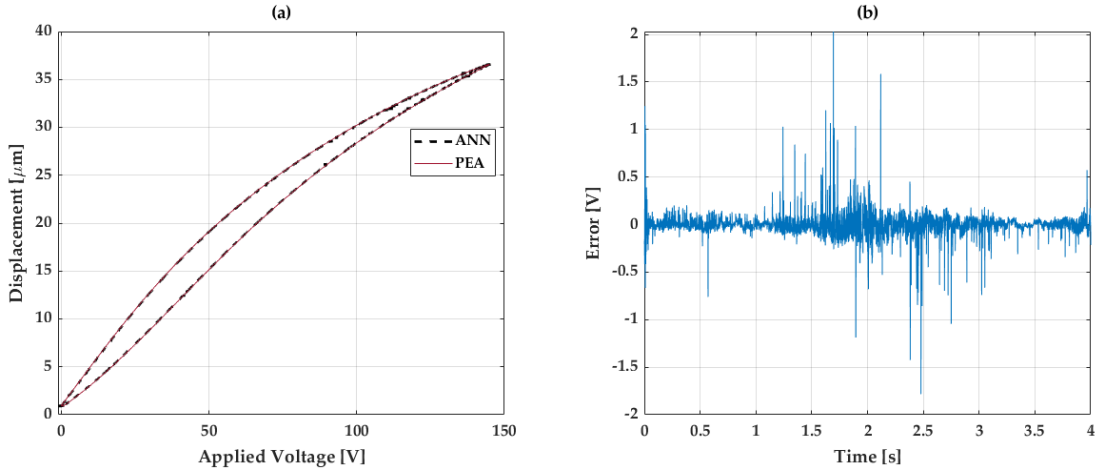

Figure 4.27: Ability of the ANN to fit to the PEA nonlinearity, where: (a) is the hysteresis graph contrast and (b) the error of the fitting .

Figure 4.27 shows the performance of the ANN to fit with the PEA hysteresis in a 4 seconds cycle. Although that Figure 4.27(a) adapts with a decent effectiveness, Figure 4.27(b) exhibits the error where several features can be highlighted. Between 1.5 and 2.5 the error tends to increase with significant peaks; nevertheless, at 2 seconds the deviation increases considerably due to the slope change as it is a complex transition to be projected by the ANN. Still, the calculated RMSE for this case provided 0.041V in comparison to experimental data which was acceptable.

Reference Tracking Results

The control structures were designed in Simulink which was later embedded in dSPACE platform. Despite that the main reference used was a triangle wave, we also used a sine signal (with same period and amplitude) and a variable amplitude triangular signal. The aim of this was to test the flexibility of the proposed structures against different references.

In regards to the parameters of each controller, these were reached through the minimization of the IAE in the experiments. The PID constants K_p, K_i and K_d gathered are, respectively, 1000, 10 and 10^{-4}. The QCSMC-ANN parameters γ and λ acquired are 60 and 8, respectively.

Triangular Tracking Results

The first contract was performed with a triangular wave due to its complexity to be followed. Figure 4.28 presents the error obtained with the QCSMC-ANN and PID in triangular cycles where several points can be highlighted. The PID controller had a variable performance since between 0 and 1 seconds, the error declined; however, in the following second, the error began to rise up until 2 seconds. Despite that in this period the QCSMC-ANN provided a high amplitude in the first second, in the following it was diminished.

Certainly, at 2 seconds, the first critical point appeared since it is where the slope of the triangular reference changes its sign. The PID changed suddenly from 0.1μm to near -0.12μm; although the controller performed an abrupt correction, the QCSMC-ANN generated a similar action but with a faster improvement in time. This is reflected after 2 seconds where the PID had a transitory development without reaching the null value of the error. Nevertheless, the QCSMC-ANN carried with the same demeanour as previously right after the slope change.

The fourth second of this analysis exhibits another crucial point to focus as it is the following slope change at the lower converging point. The PID unveiled a similar situation as previously at 2 seconds but with lower amplitude and a subsequently transitory response. On the other hand, even if the QCSMC-ANN featured a peak that has a value above -0.2μm, the later reaction shows a similar trend as previously described where the controller aims to a mean near the null value. After 4 seconds, since the signal is repeated, the detailed features are mirrored.

Aside from the error development, the control signal is an important feature to analyse as it contributes to the performance of the proposed structures. Figure 4.29 is a contrast of the control signal generated along the analysed error of both frameworks. As main characteristics to take into account at this point, saturations or sudden changes needed to be focus as these can damage the PEA driver cube. Henceforth, it can be perceived that both controllers had a suitable demeanour and any downsides were presented in the experiments.

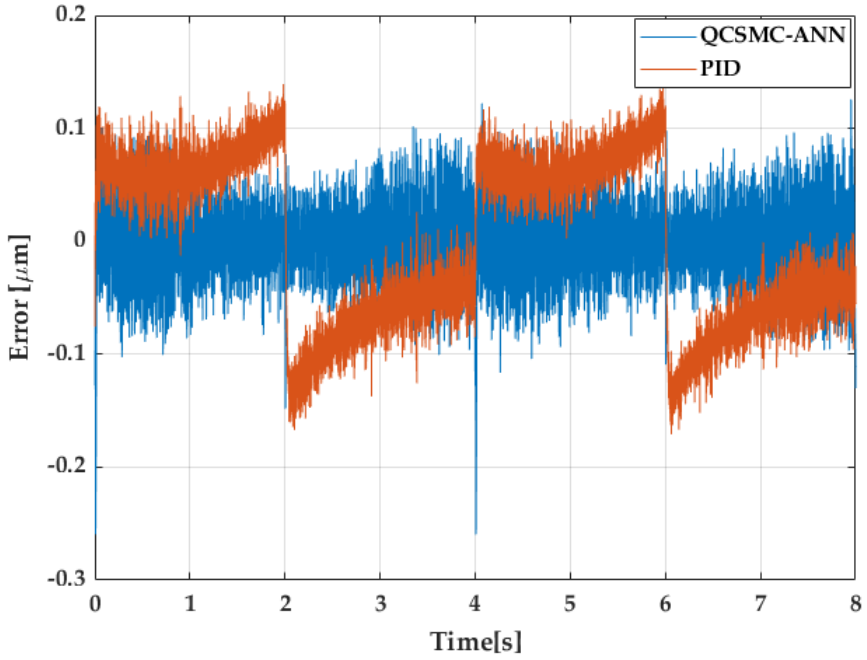

Figure 4.28: Error generated in 2 cycles of a triangular reference.

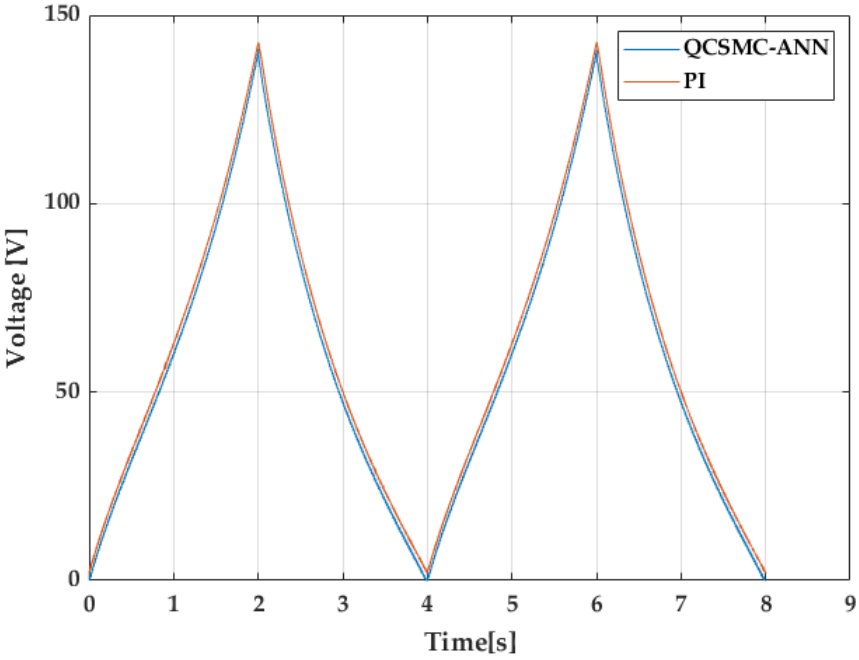

Figure 4.29: Control signal in 2 cycles of a triangular reference.

Sinusoidal Tracking Results

In pursuance of a suitable performance test which can show the docility of the proposed design against similar references, we inspected the development with a sine wave form with the same chosen amplitude and periods as previously. Figure 4.30 shows the error that the PID and the QCSMC-ANN produced in the mentioned reference signal. The PID had a inferior performance in relation to previous test since after 1 second, the amplitude increased with peaks up to 0.15μm. Despite that the slope transition is softer in 2 seconds, the error kept increasing afterwards which resulted in a variation of around 0.3μm. However, the QCSMC-ANN behaved even better than previously since the error was compensated almost equally along the test with an amplitude below 0.05μm which oscillates around the null value.

Finally, the control signal that is presented in Figure 4.31 unveils a better performance than former analysis due to the softness of the signal. It can be seen that any harm changes were developed in the analysed time which can lead to a damage of the involved hardware.

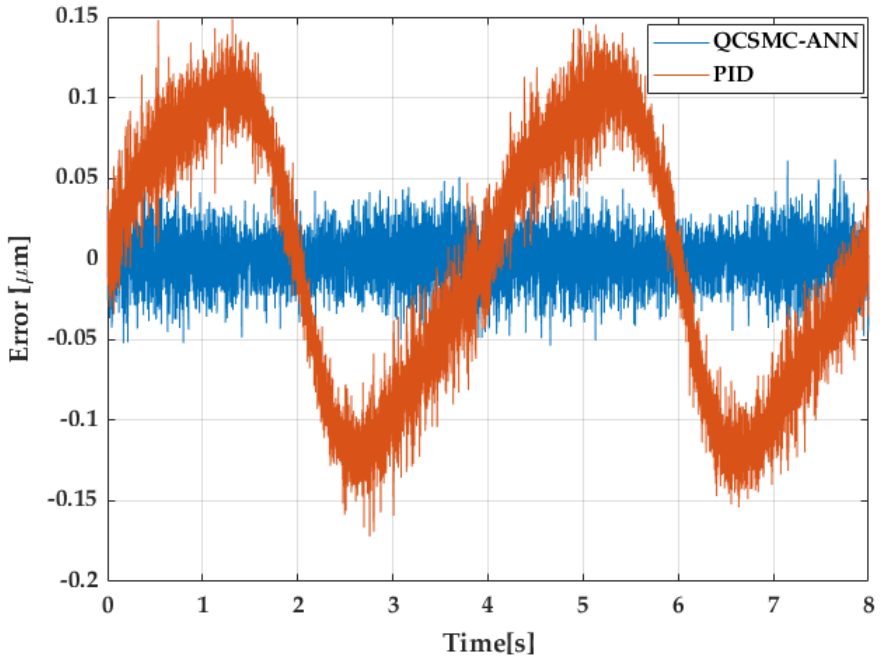

Figure 4.30: Error generated in 2 cycles of a sine wave reference.

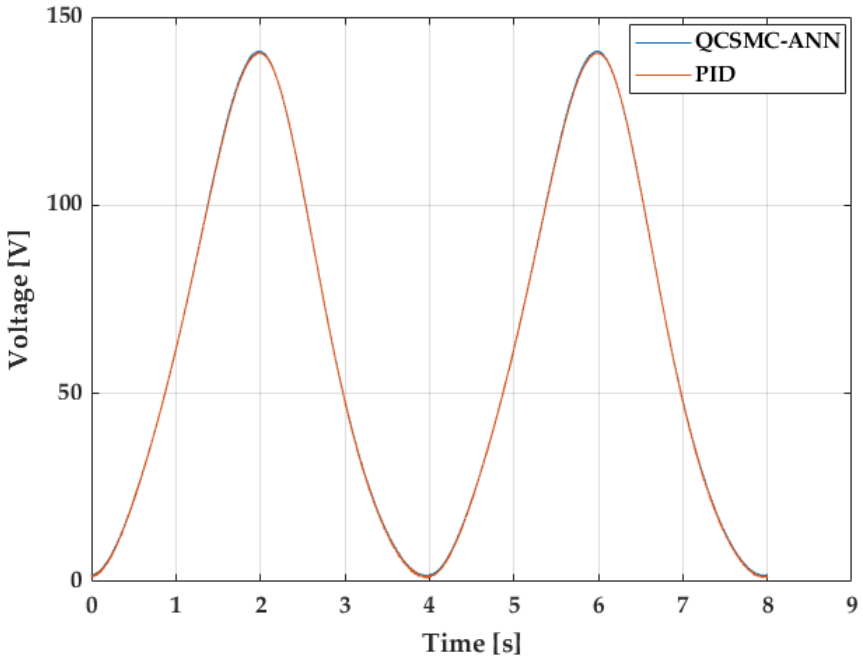

Figure 4.31: Control signal in 2 cycles of a sine wave reference.

Triangular Tracking Results with Variable Amplitude

Another experiment performed is triangular reference signal with variable amplitudes which were settled randomly in 25V and 121V. Figure 4.32 shows the repercussion of the error for the considered reference. During the first 4 seconds where the amplitude was 25V, both controllers had a similar demeanour. The PID shows a perceptible shift at the upper target point in 2 seconds; however, the QCSMC-ANN provided a constant development along this range with the same deviation as the PID. On the other hand, the major difference can be noticeable during 121V where the PID behaves similarly to previous analysed triangular signal where fast corrections occurs during the slope changes of the reference signal. This effect produced a brief increment of the error amplitude in the analysed controllers but the QCSMC-ANN managed to carry this without any transients, a feature produced by the PID.

As previously, another important feature is the control signal which is shown in Figure 4.33. It can be seen that any saturations or sudden corrections that can deteriorate the hardware were developed in the performed experiments.

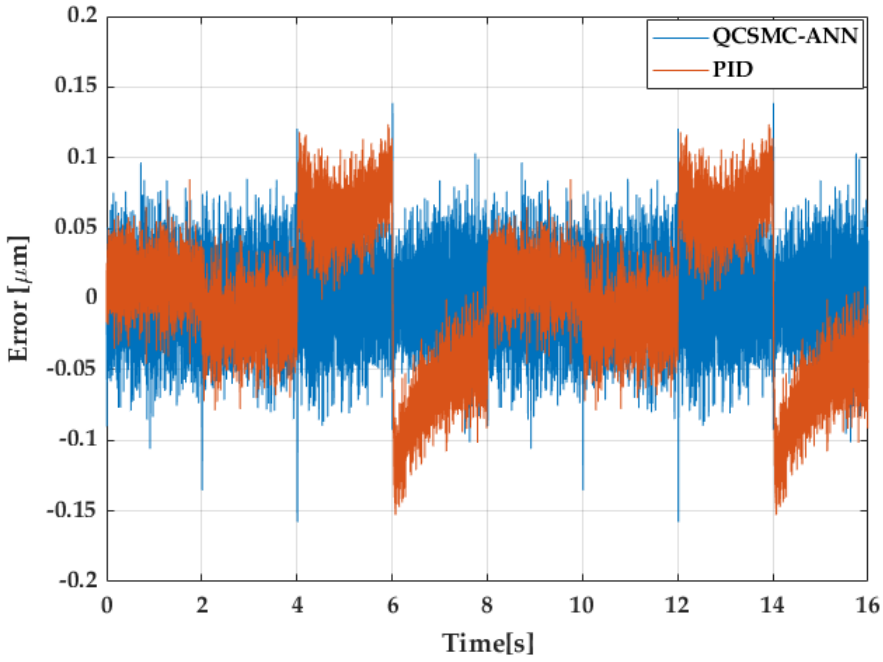

Figure 4.32: Error generated in 2 cycles of a triangular reference with variable amplitude.

Nevertheless, effects about chattering are analysed in further details in the following section.

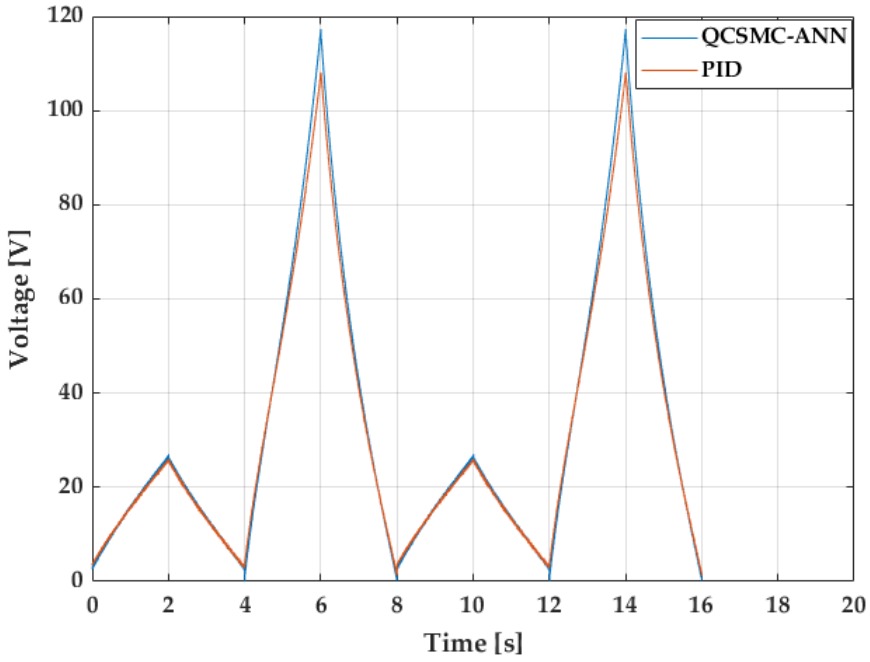

Figure 4.33: Control signal in 2 cycles of a triangular reference with variable amplitude.

Metrics Results

Certainly, for extra precise performance measurement and comparison, we used three tools which aided us to gather more conclusions. As previously explained, the IAE was used to tune the parameters until this value becomes minimum. The RMSE provides the accuracy in terms of the error and because we implemented an SMC based controller (known for the chattering generated in the control signal), we calculated this value based on previous explained method.

In regards to the IAE, the QCSMC-ANN indicated a superior performance in the triangular reference which lead to a 53.07% of difference in comparison with the PID. Nevertheless, in the sine wave test it is shown that this value was augmented as the QCSMC-ANN reached 81.5% more. Additionally, the variable amplitude signal carried with the same trend as the difference achieved was 33.6% favorable for the proposed algorithm. The RMSE showed a similar manner since the QCSMC-ANN kept with the advantage over the PID in both signals granted 46.5%, 79.7% and 38.5% of difference with the triangular, sine and variable amplitude waves, respectively. Lastly, the measured chattering

indicates dominance of the QCSMC-ANN over the PID and even it emblazons through values the suitable performance of the control signal; according to the values of 35.6%, 81.8% and 22% of difference in both signals, it is clear that the QCSMC-ANN had less chattering than the PID controller.

Reference	IAE			RMSE [μm]			Chatt(u) in 4s		
	QCSMC-ANN	PID	Diff [%]	QCSMC-ANN	PID	Diff [%]	QCSMC-ANN	PID	Diff [%]
Triangle	0.1314	0.28	53.07	0.0404	0.0756	46.5	412.75	640.97	35.6
Sine wave	0.0518	0.28	81.5	0.0161	0.0795	79.7	108.8	600.8	81.8
Var. Amp.	0.2067	0.33	33.6	0.0318	0.0519	38.5	514.88	659.4	22

Table 4.12: Comparison of the different metrics

4.5.6 Conclusions

Throughout this research, we developed a control strategy with the aim of increase the accuracy of a commercial PEA. After an analysis of the previous investigations from other authors and based on the study that we made, we found that the hysteresis was the main non-linear phenomenon to be counteracted.

First, we made an analysis of the properties of a commercial PEA PK4FYC2 from Thorlabs. According to the manufacturer, the maximum error is 15% which is a considerable value for applications where high precision is required. As the main reference, we used a triangular wave because it is a complex signal to be tracked due to the high frequency harmonics and sudden slope changes.

Secondly, we proposed a robust sliding controller due to the advantages studied in the related works from the introduction. Thus, we chose to use a QCSMC which belongs to the HOSMC so that the chattering is reduced in comparison to classic SMCs. Commonly, sliding controllers have two terms where one of them is achieved through a mathematical model but instead, a distinctive feature of our controller is the use an ANN. We contrasted the proposed design with a conventional PID in terms of several metrics such as IAE (that was also used to tune the gains of each framework in experiments), MSE and chattering.

In regards to the results, at first, we analysed the performance of the ANN which provided a suitable RMSE and fitting to the hysteresis. Later, we implemented the QCSMC-ANN and the PID in a dSPACE platform for a real-time experiment. The results showed that the QCSMC-ANN generated a lower tracking error which oscillated around the null value. The PID displayed a slow compensation and even with a disparity that had a variation with higher amplitude

that reached the 0.1μm. Nevertheless, both schemes showed suitable control signals in the analysed graphs. Additionally, because we wanted to test the flexibility of both structures against reference changes, we used a sine wave and a triangular reference with variable amplitude. In this case, the first case exhibited a demeanour that was similar in the error and control signal because the reference was softer than the previous one. In regards to the variable amplitude signal, the QCSMC-ANN still provided a superior performance which was verified in graphical and numerical analysis.

Finally, we calculated the mentioned metrics which showed concrete values of performance from the comparisons made. Thus, in terms of the IAE and RMSE, the QCSMC-ANN had a important distinction favorable for the QC-SMC in the proposed reference signals. The calculated chattering also showed a significant difference where the QC-SMC carried with the leading trend.

4.6 Fuzzy Logic Controllers Type-1 and Type-2 combined with Artificial Neural Networks

4.6.1 Contributions

- This work proposes two control algorithms, based on fuzzy logic and neural network compensation, aimed at reducing the error and improving the actuation signal of piezoelectric actuators.
- The proposed control schemes were tested experimentally in a commercial piezoelectric actuator. They were implemented with a dSPACE 1104 device, which was used for signal generation and acquisition purposes.
- The performance of the proposed control schemes was compared against a well tuned PID controller.
- Experimental results show the advantages of the proposed controllers, since they are capable of reducing the error to significant magnitude orders.

4.6.2 State of the art

As previously seen, hysteresis reduction can be handled from two diverse perspectives: tracking control design or material re-engineering [4]. In regards to the latter mentioned option, according to Park and Shrout, [18] there is a property related to the performance called *piezoelectric coefficient* (also known as d_{33}) which determines the degree of induced strain at a particular electrical field. Thus, a piezoelectric material will display a lower hysteresis but at the expense of decreasing d_{33}, which implies that the material will have less stiffness. Therefore, in this case, we pursed the design of a control strategy.

From the perspective of classic control theory, linear controllers can be a suitable first option for a PEA. PID scheme has been implemented several times and it is still being employed for comparisons. An interesting study was produced by authors of [176], where they generated a simulated environment with a BW hysteresis model for the PEA and a PID, tuned by optimisation, was applied. The achieved control parameters were then used in an experimental rig

where the outcomes showed a maximum error percentage of around 5%. Another attractive study was presented by Kaci et al. [177], where they developed a strategy of a PID tuned through a linear quadratic regulator for a resonant plate actuated by a PEA. Despite that the aim was unrelated to tracking, authors attained suitable results in terms of vibration control. On the other hand, a similar approach to vibrations rejection with PEAs was carried by Tang et al. [178], where they used Youla parameterization with a PEA to reduce fluctuations of a telescope and results showed an enhanced performance of the system. Nevertheless, hysteresis is a strong nonlinear and undesired effect which limits the operating range with a linear controller [107]. Furthermore, uncertainties like modelling or external loads are commonly present so that linear strategies are limited in this sense due to the actuation bandwidth [108].

Among the diversity of non-linear strategies, sliding mode controllers ones are one of the most frequently used during the last decades due to their robustness [179]. Different combinations were proposed from various authors for several applications where a PEA had an important role. For example, authors of [180] proposed a conventional SMC for tracking control of a micro-gripper. Despite that the control signal was neglected in the analysis, they obtained errors of around 6%. Another example was developed and implemented by Ling et al. [181], where they used a SMC combined with ANN; tests were carried with soft curve references in which acceptable errors were accomplished. Differently, an approach akin to robust control was developed by Dong & Tan [68], where they established a composed structure of bounded sub-models; experimental results showed acceptable positioning errors. Other alternatives to SMC were analysed by Zhang et al. [40] where they implemented a robust control compensator based on feedback linearization. Outcomes were gathered from simulation and experiments, where they reached a satisfactory accuracy. Nevertheless, most of the robust strategies mentioned have a major downside in practice related to the chattering; this phenomenon is produced by neglected fast dynamics and with finite sampling rate digital controllers [182].

On the other hand, FLC is an easy understanding type of structure because it is expressed through linguistic rules that can be tuned according to the knowledge of a particular system [183]. Actually, Sabarianand et al. [82] established that advantages of FLC for PEAs are related to its capability to deal with non-linearities, uncertainties and innacuracy. Also, according to Sobrinho

& Junior [184], fuzzy sets have better performance in contrast to conventional techniques in embedded systems. For instance, authors of [185] used a fuzzy logic approach for an atomic force microscope (known to have a bending type PEA) and thus, accuracy is an important objective in this case. The simulation outcomes revealed high accuracy and fast corrections. In terms of force control, Kang et al. [186] implemented a FLC in a commercial PEA where they aimed to reduce the hysteresis and they could achieve a fast convergence a suitable force tracking accuracy. Another interesting study was carried out by authors of [187], where they produced a simulated environment for a nanopositioning platform controlled by a PEA through an integral resonant controller based on FLC; results showed improvements up to 1μm in contrast with a conventional technique.

Fuzzy sets that can be described based on classical theoretical techniques are also known as type-1 (previously named as FLC-T1) [188]. Nevertheless, there are at least four sources of uncertainties associated to the disadvantages of T1: (1) uncertain linguistic rules, (2) disagreement of expertise, (3) noise associated to activation and (4) measurement data [189]. Hence, this implies that membership functions are not exact as with FLC-T1 because they can be blurred due to these uncertainties [190]. These issues derived the type-2 (FLC-T2) sets which are capable to handle uncertainties and adapt better when definitions are dubious [191]. As a consequence of these augumented capability mirror uncertaities, FLC-T2 is known to have more robustness than FLC-T1 [192]. Also, it has been showed that FLC-T2 is able to perform better than FLC-T1 systems in control related applications [193–196]. In this research, we implemented FLC-T1 and FLC-T2 control structures.

Nevertheless, based on the background research prior to the development of this study, we found that uncompensated feedback controllers have certain issues in PEA tracking control. These are related to the usage limitation of high gain controllers due to low gain margins of feedback controllers and stability performance [82]. Still, a combination of feedback-feedforward structures is recommended since it fuses the individual advantages of each framework to gather a high-performance controller [50]. A feedforward compensation is commonly based on an inverse system model, which implies that model uncertainties can be reduced provided that the feedback controller is well designed in combination with a suitable hysteresis model, as in this case. For this rea-

son, in this investigation, we proposed two novel combinations of feedback-feedforward structures.

Hysteresis models are divided in 2 groups: mathematical and physics based ones. In regards to the latter mentioned, it is used for ferromagnetic hysteresis description due the complex solutions and material dependency [127, 168]. On the other hand, mathematical models are divided into operator-based (such as PI, Preisach and Kranosel'skii-Pokrovkii [197]) and differential equations-based (like BW, Duhem and Backslash [82]). Despite that these models have certain extensions to deal with asymmetric hysteresis, they introduce two major disadvantages: (1) complex numerical solutions which require multi-steps or (2) Runge-Kutta solvers at each time-step and (3) a higher number of parameters (due to the asymmetry, for example) expands the difficulty to achieve a suitable equivalent model [134]. Among the analysed options for feedforward compensation and based on our prior research from previous sections, we found that ANN are characterised by higher precision and easy implementation over mentioned mathematical models [127]. Therefore, we conclude that ANN are a suitable option to be implemented in this study.

Therefore, this work analyses the applicability of two feedback-feedforward control structures based on FLC-T1 and FLC-T2 strategies, combined with a TDNN to control a commercial PEA. At first, the performance of both FLCs was compared with a conventional PID, commonly used for these correlations [198]. Later, since we had enhanced results, we analysed the two proposed advanced structures. This is an innovative proposal for the tracking control of a PEA since as we reviewed, a FLC-T1 and FLC-T2 combined with a TDNN .

4.6.3 Time delay neural network

A TDNN resides its structure on three nodes based on an ordinary feed-forward ANN as Figure 4.34 shows. The dynamics of the input vector *X(t)* are gathered through n delayed signals and is then linearly transformed with the weight matrix W_k with the bias vector b_k. Later, it is fed into an activation function such as a *tangsig*. The output layer is supplied with the vector *r(t)* and again linearly changed with the weight matrix W_j and a bias b_j and finally, used as an input in *purelin* activation function.

$$r(t) = tansig\left[\sum_{l=0}^{n} W_j\big(x(t-n)\big) + b_k\right] \tag{4.55}$$

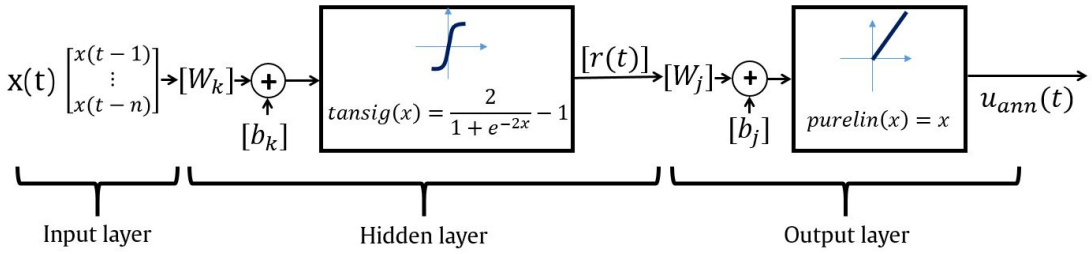

Figure 4.34: Time delay neural network structure

Weights and biases can be defined through a training process gathered from experimental data. In this case, we used MATLAB Deep Learning Toolbox with Bayesian regularization as it is suggested for data with further noise [149]. Usually, in ANN training, a main cost function used for convergence is the mean-squared error through experimental data which is shown in Equation 4.56, where *P* is the number of observations, T_i is the target data and U_i is the ANN output (both at the i-th sample).

$$E_{MSE} = \frac{1}{P}\sum_{i=1}^{P}(T_i - U_i)^2 \tag{4.56}$$

However, if a training is mainly performed using this cost function, it would resemble in an over-fitting. This happens when the ANN fits with the training data but not with the test portion and thus, this would provide an unsuitable overall performance. Thence, bayesian regularization penalizes the Equation 4.56 with a different cost functions where the objective is to penalize large weights and aims to generalization. Further technical details can be found in the research made by the authors of [199–201].

4.6.4 Fuzzy logic controllers

Formerly, details of fuzzy logic type-1 sets were described in Section 4.3.4. However, these type sets lack of capabilities to handle uncertainties, therefore

Zadeh defined the type-2 sets [202]; this concept was later augmented by Mizomoto and Tanaka [203]. This expansion allows efficacy on a fuzzy set in which uncertainties are difficult to measure or determine. Based on Castillo et al. [204], a fuzzy set of type-2 is usually denoted by $\tilde{A}$ but differently to type-1, there is an upper and lower membership function $\underline{\mu}_{\tilde{A}}(x)$ and $\overline{\mu}_{\tilde{A}}(x)$. This is defined in Equation 4.57. These limits are associated with a type-2 feature known as *footprint of uncertainty* (FOU), that is defined in Equation 4.58. In other words, the FOU expresses uncertainty in the definition of type-2 sets membership functions [205–207]; thus, this is an advantage over type-1 sets which require exact values in their membership function definition. For our case, the FOU is graphically expressed in Figure 4.36.

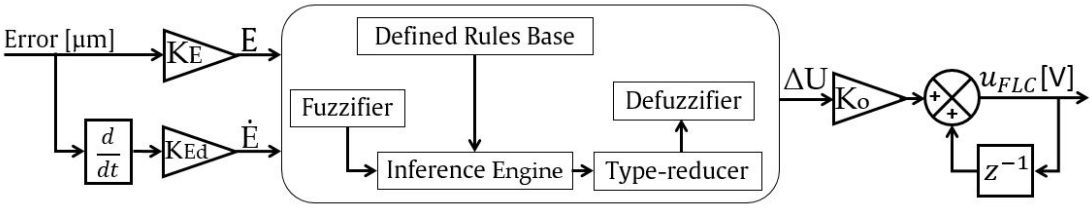

Figure 4.35: Structure of a fuzzy logic controller type-2.

$$\tilde{A} = \left\{ \left((x,u), 1 \right) \middle| \forall x \in X, \forall u \in J_x \subseteq [0,1] \right\} \tag{4.57}$$

$$FOU(\tilde{A}) = \left\{ (x,u) \middle| x \in X \; and \; u \in \left[\underline{\mu}_{\tilde{A}}(x), \overline{\mu}_{\tilde{A}}(x) \right] \right\} \tag{4.58}$$

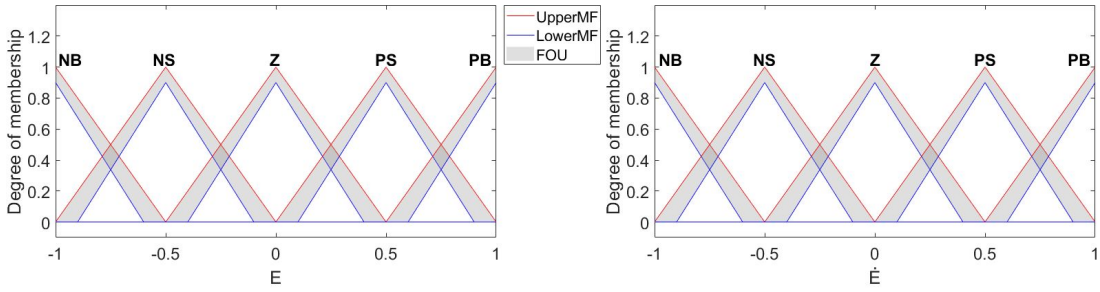

Figure 4.36: FLC-T2 Membership functions

The mechanism of fuzzification of fuzzy sets type-2 is analogue to type-1, although the linguistic form of the inference is defined based on the uncertainties linked to the main feature. Therefore, the rules are expressed in the form of Equation 4.59. Since the FLC-T2 has a range of uncertainties, the defuzzification process has an extension known as the *type-reduction*, which implies the calculation of a centroid. In this case, we used the Karnik-Mendel which is a common used method in fuzzy sets type-2 where the goal is to seek for crucial points that combine the upper and lower membership function limits [208]; further features about this tool can be found in the study of the authors [209]. A schematic resume of the described technique is shown in Figure 4.35.

$$R_m: \ \textit{If}\ E = \tilde{B}_{1k}\ \textit{and}\ \dot{E} = \tilde{B}_{2l} \Rightarrow \Delta U = \tilde{G}_m \tag{4.59}$$

4.6.5 Results

Neural network verification

We trained the ANN with recorded data from experiments were we settled a triangular signal input of 140V with a period of 4s and 1kHz of sampling frequency. Nevertheless, during the ANN configuration, this was reversed to produce the inverse model so that the output is a compensation voltage. The 70% of the total acquired data was used for training, 15% for evaluation and the rest was used in testing. As we previously explained, we used a bayesian regularization for training and implemented through MATLAB in a Dell Precision3640 configured with 7 cores. The training lasted for 16.5 hours with 3927 iterations.

The outcomes are presented in the Figure 4.37 where a 4s cycle is contrasted with a hysteresis fitting with its approximation error. The first rise that is performed between 0 and 2s, where the error has fluctuations which are between $\pm$0.2V. In the first slope change (at 2s), a sharp and expected change appears where the error value switches from 0.25V to -0.25V. Along the voltage descent (last 2s), the error has a negative value in most of the range although it did not exceed -0.2V. Also, for this case, we calculated the RMSE which is equal to 0.0964V and it provides a reasonable accuracy that can be enhanced with feedback controllers.

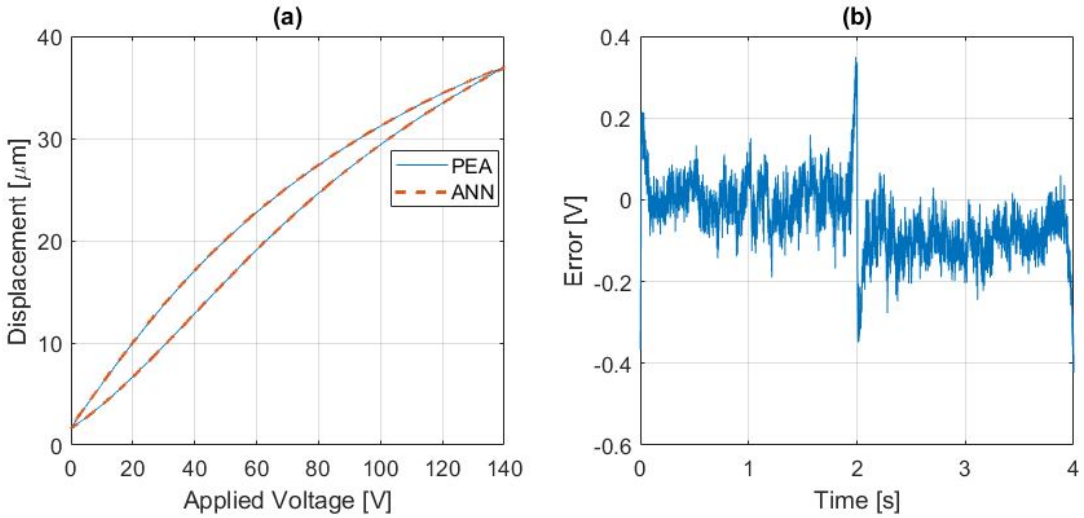

Figure 4.37: ANN capability to fit with the PEA studied nonlinearity where: (a) is the hysteresis graph and (b) is the fitting error

PID		FLC-T1		FLC-T2	
Gains	Values	Gains	Values	Gains	Values
K_p	10	K_e	12	K_e	21
K_i	1000	K_d	0.0006	K_d	0.0002
K_d	0.001	K_b	0.58	K_b	0.14

Table 4.13: Obtained gains for the PID, FLC-T1 and FLC-T2

Experimental comparison of feedback controllers

Feedback control structures such as PID, FLC-T1 and FLC-T2 were implemented in the dSPACE 1104 platform. We recorded the error and the control signal which were overlapped for a suitable contrasted comparison. We tuned the control parameters in real time through the IAE minimization. Additionally, we took into account the limits of the actuator, so we included saturations an limits to avoid damaging the hardware. The achieved gains are summarized in Table 4.13. The FOU was established as 10% and further details of this are explained in following section.

The first experiment outcomes are provided in Figure 4.38 to analyse the error. In this case, we will show 2 cycles (or 8s) in order to interpret the full range behaviour. Therefore, in the first rise (before 2s), the three controllers show a

similar behaviour at different amplitudes. For instance, both FLC types have a lower value than the PID but the curvature trend tends to be similar. Nevertheless, this increases differently after the first second in both FLC controllers and even the FLC-T2 tends to have a better performance that the others since the amplitude lowers its value.

One of the first critical point is at 2s which is were the displacement reaches the UTP and the slope changes its sign. At this moment, the error of the three controllers also changed its sign suddenly due to the sharp variation. Whereas the PID acts with a lower compensation, both FLC have a faster correction in contrast. Also, the FLC-T2 and FLC-T1 performed similarly in the zoomed window in terms of amplitude and time response.

After the first slope change, the reference descents where the error tends to show a reciprocated situation, like in the rise. However, the PID corrected with a higher amplitude difference in comparison to both types of FLC, which again have a similar demeanour. The PID has a curved correction which lasts 1.5s until it can reach levels of the FLC, that is near 3.5s. Moreover, the PID error compensation has higher amplitude values in contrast to the FLC-T1 and FLC-T2 due to the peaks that can be shown near 2.7s and 3.2s.

Finally at the LCP, the circumstance was fairly different to the one from 2s since the controllers behaved more similar. Nonetheless, the PID still reacted worse in terms of amplitude but the correction in time seemed to be faster, specially after 4s where the settling time was faster than before (at 2s). Additionally, the FLC-T2 tended to act better than FLC-T1 after the change; the amplitude was slight lower where certain peaks averaged the null value.

A further precision analysis was carried with the performance metrics that we calculated in Table 4.14. We referred all the values to the PID controller as it showed the lowest effectiveness. The IAE achieved by the PID exhibited 0.5242, which was enhanced by the FLC-T1 with 63.52% and even further by the FLC-T2 with 68.08% of difference. Additionally, this discrepancy it is also shown in the RMSE with a modest 4% extra for the FLC-T2. Finally, the RRMSE displays that the both FLC types had near 3 times higher accuracy than the PID.

In regards to the control signal, Figure 4.39 displays the generated signal of each control framework implemented in a feedback mode. As a first appreciation, it can be seen that there is a lack of saturations which can damage the actuator. Nevertheless, there are certain oscillations which deserve an in-depth

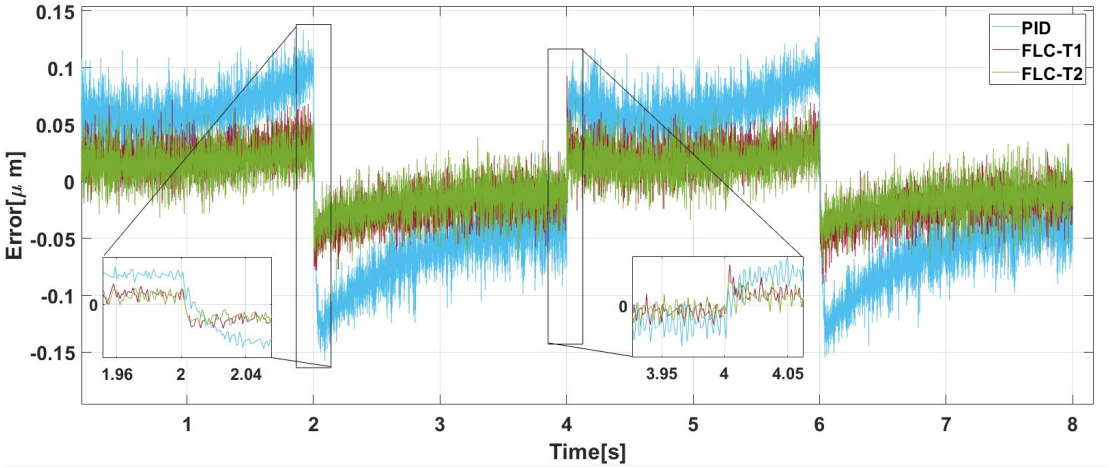

Figure 4.38: Error acquired during the test of the feedback controllers.

Controller	IAE		RMSE		RRMSE
	Value	Diff.[%]	Value[μm]	Diff.[%]	Value[%]
PID	0.5242	-	0.0706	-	0.33
FLC-T1	0.1912	63.52	0.0278	60.62	0.13
FLC-T2	0.1673	68.08	0.0252	64.32	0.12

Table 4.14: Metrics comparison for feedback controllers

analysis: in most of the zoomed windows, we can see quick variations which belong to the PID controller specially in the range of the LCP (around 4s) and in the descent (near 6.7s). This is an important feature to highlight since it not only can lead to an actuator wear but also to extra energy consumption. Nevertheless, FLC-T1 and FLC-T2 behaved similarly in the last mentioned points of interests but with a slight better performance for the FLC-T2 in the rising as it can be seen near 0.5s at the uprising.

Experimental comparison of feedback controllers with neural compensation

After the analysis of feedback structures, we implemented and acquired the outcomes of the advanced proposed controllers. In this case, in order to enhance the proposed algorithms, we made a sweep FOU values in which we could observe a candidate percentage depending on the minimal IAE achieved. This is resumed in Table 4.15 were the values of IAE were calculated in 40s of experi-

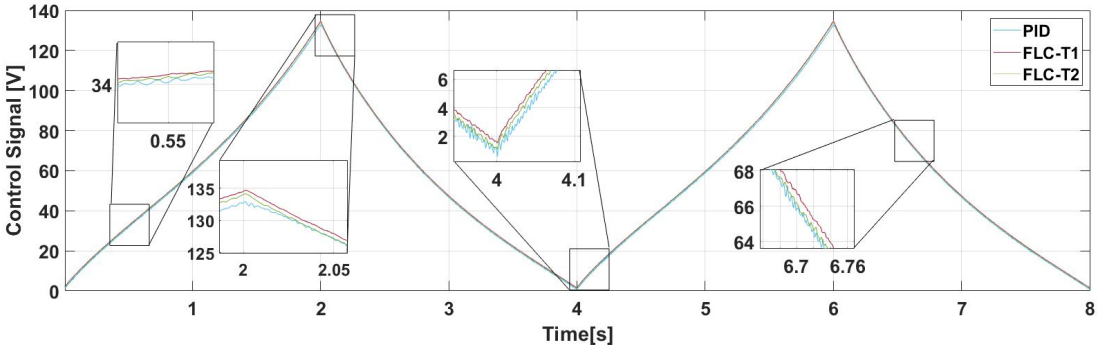

Figure 4.39: Control signal acquired during the test of the feedback controllers.

ment. It can be seen that 10% unveiled the minimum IAE, which we chose for the experiments.

FOU Percentage [%]	IAE Value
5	0.3852
10	0.3850
15	0.3863
20	0.3901
30	0.3896
50	0.3922

Table 4.15: Variation of FOU percentage and the IAE achieved in each case

At the first slope sign shift at 2s, both controllers behaved similarly although the FLC-T1-ANN, seems to have a slightly faster correction. Oppositely, when the slope switches from negative to positive at 4s, the situation has a modest change where the FLC-T2-ANN compensates the error. On the other sides, it can be seen that the FLC-T2-ANN has a suitable performance due to the error amplitude which lower than the alternative option.

In regards to the metrics, Table 4.16 displays the metrics calculated for the advanced controllers. Although the magnitudes are similar, FLC-T1-ANN showed the lower values in overall and thus it was used as a reference for the percentage calculation. The FLC-T2-ANN achieved better outcomes since the difference is 21.32% and 21.34% for the IAE and the RMSE, respectively. On the other hand, the RRMSE shows a meager difference, which is favourable for the FLC-T2-ANN.

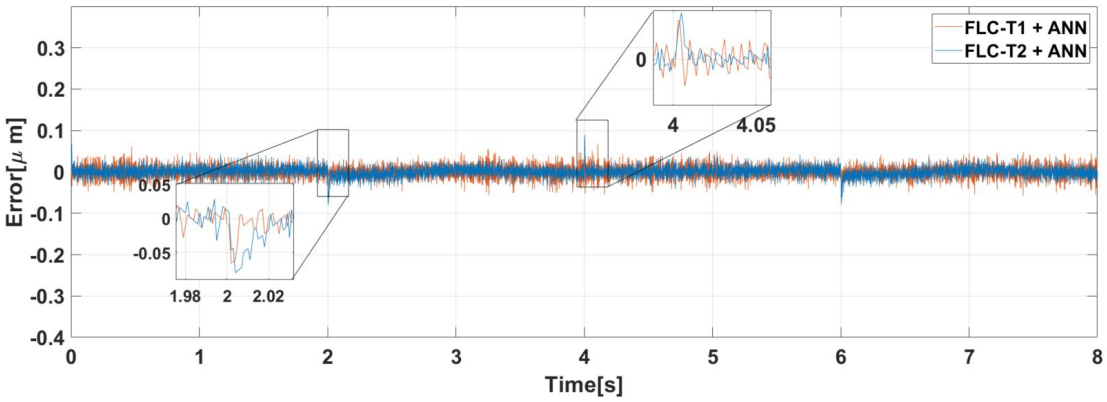

Figure 4.40: Error acquired during the test of the feedback-feedforward controllers.

Controller	IAE		RMSE		RRMSE
	Value	Diff.[%]	Value[μm]	Diff.[%]	Value[%]
FLC-T1-ANN	0.1039	-	0.0164	-	0.078
FLC-T2-ANN	0.0807	22.32	0.0129	21.34	0.061

Table 4.16: Metrics comparison for feedback-feedforward controllers

Finally, the control signal of these proposed architectures is shown in Figure 4.41. In the previous study, saturations or sharp changes are unseen but certain points deserve to be highlighted. During the rise in the first 2s, both controllers have a similar demeanour which can also be seen during the first change at the UTP. Also, a similar situation is seeing during the descent that is pointed near 6.7s. Nevertheless, at the LTP, the FLC-T2-ANN shows a disadvantage because its signal contains further variations in contrast to the alternative.

4.6.6 Conclusions

In this study we analysed the applicability of different feedback-feedforward control structures based on fuzzy logic control strategies, known as FLC-T1 and FLC-T2. We reviewed that the advantage of using FLC-T2 over FLC-T1 is the resolution of the uncertainties by means of the membership functions. These controllers were connected to a trained TDNN in a feedback-feedforward structure which was expected to increase the accuracy of FLC-T1 and FLC-T2 in a feedback configuration. Therefore, the strategies were: (1)PID, (2)FLC-T1, (3)

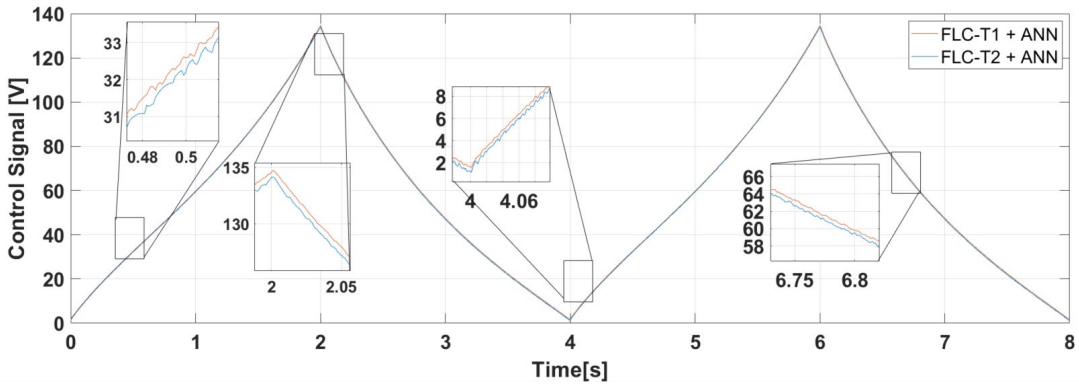

Figure 4.41: Control signal acquired during the test of the feedback-feedforward controllers.

FLC-T2, (4) FLC-T1-ANN and (5) FLC-T2-ANN.

The five control schemes were embedded in an experimental test rig which involved a real PEA. The experimental setup included: a commercial PEA and its peripheral hardware (both provided by Thorlabs) and a dSPACE 1104 platform, which was used for signal generation and acquisition purposes. A triangular signal was chosen as reference, since this is a complex curve to be followed due to the sharp changes and harmonics.

Experiments were carried out with FLC-T1, FLC-T2 and PID control schemes. The latter is a was chosen because is a common approach used for tracking control operations of PEAs. Thus, results showed the superiority of the FLC controllers against PID algorithm in the accuracy and control signal. Actually, the fuzzy schemes displayed an improvement over the PID of around 60% at tracking operations.

Finally, FLC-T1 and FLC-T2 were combined in a feedback-feedforward structure with the TDNN. Experimental results exhibit an evident accuracy enhancement which was reflected in the magnitude order of the error. Nevertheless, FLC-T2-ANN unveils the best performance due to its capability to cope with the uncertainties. This was observed in the graph and numerical error analysis which coexisted with a suitable control signal.

The presented analysis, based on FLC-T2 and FLC-T1 joined with ANN, provided several benefits over conventional algorithms like PID or their feedback structure without the neural compensation. These control schemes achieved considerable improvements in terms of accuracy, paving the way to high preci-

sion applications. In addition, suitable control signals were generated aimed at reducing the efforts at the PEAs.

4.7 Sliding mode controllers combined with ANNs with evaluation of time consumption

4.7.1 Contributions

- Based on our previous works, sliding mode controllers based on ANN compensation as the replacement of the equivalent term, can induce several advantages due to its easiness of implementation. The strategies used are conventional sliding mode control, twisting-algorithm, STA and prescribed convergence law with an ANN as an equivalent model to reach the sliding surface.
- An application analysis of the described techniques for a commercial PEA which has been linked to dSPACE for the implementation of the control algorithms.
- Additionally, an analysis of the time consumption of each algorithm (switching term) which is useful when a designer requires an idea about the hardware to be choose when commercial applications are needed.

4.7.2 State of the art

At macroscopic level, hysteresis is a meaningful effect to be reduced since it induces instabilities and inaccuracies in PEAs [210]. From the point of view of material engineering, the hysteresis can be diminished when a redesign in the structure is performed. This implies that materials need to be harder but at the cost of reducing the Curie temperature, value at which the piezoelectric properties are weak [211]. According to Dragan Damjanovic, hysteresis can also be decreased through an active control system provided that the physical properties of the PEA are well understood [4].

Linear schemes can be an early approach to design a compensation for the hysteresis in PEAs. Mainly, PID controllers had been used widely for innovation and comparison of advance proposals. Han et al. analysed a complex fast steering mirror system that was driven by PEAs where they embedded a PID due to its simplicity [212]. Experiments showed that the rotational precision achieved was in the required design range. On the other hand, another method reviewed has been linear quadratic gaussian (LQG) controller which

has been implemented by authors of [213]. In this research, they studied an active vibration isolation control which is a common application of PEAs due to their fast response. The design was combined with a loop transfer recovery (LTR) in order to retrieve properties like robustness with phase and gain margins [214]. Results showed enhanced features related to vibrations with the proposed structure. However, hysteresis is a strong nonlinear effect and linear techniques can have problems in dealing with modeling uncertainty and external effects which may converge to poor performance and stability [108, 215, 216].

Nonlinear control strategies are able to enhance the performance of a system especially when a design is embedded [217]. In this sense, FLC is an intuitive and simple method which main advantage is the unnecessary model requirement for its design since it has been developed through rules originated from an expert knowledge about a particular system [218]. An implementation of FLC in PEAs has been done by authors of [219] in a precision manipulation mechanism. In their study, they used an adaptive FLC method which was embedded in a control platform. Results showed improvements of 40% in contrast to conventional techniques. Despite that this study showed significant enhancements, the contrasts had been carried against a PID. Another similar study was produced by Luo et al. where they developed an active vibration control with FLC with suitable results in difference to an uncontrolled system [220]. On the other hand, nonlinear model predictive control (NLMPC) is another example to review; this approach is based on a nonlinear mathematical model that predicts the future states for an optimisation of the control law to be applied [221]. Authors of [222] designed a NLMPC based on an ANN for a PEA. This research presented the experimental validation of the proposed controller where results of tracking accuracy showed significant improvements in contrast to a simple PID. Nevertheless, disadvantages of previous mentioned strategies are related to the high computational workload: NLMPC has an optimisation process that requires high computational resources whereas FLC has the same issue when rules are increased [223].

SMC is a robust algorithm frequently used in nonlinear systems where disturbances and uncertainties are meaningful [224]; this is also combined with low computational workload due to its simple calculation [225]. Liang et al. implemented a discrete SMC for a micro-gripper mechanism actuated by a piezoelectric actuator [226]. The objective was to control position and force, which

are both affected by the PEA hysteresis. The researchers were able to achieve errors of 0.2μm during steady reference following while an accurate force control was also accomplished. Authors of [227] embedded an SMC for a medical device aiming to improve the accuracy. Although they studied the system under unknown disturbances and uncertainties, they were able to accomplish a suitable accuracy in terms of the error, the hysteresis was omitted in the study. One of the drawbacks of SMC is the chattering generation which is caused by neglected dynamics and in implementations where the sampling rate is finite, thus it cannot be ignored [182, 228].

Chattering in SMC can be attenuated with different options such as the usage of boundary layer technique [114], replacement of the signum function by sigmoid [229] or asymptotic SMC [230]. Also, the usage of surface derivatives may help to decrease this effect which has been named as HOSMC by Levantovskii [158]. When derivatives are used in the sliding surface, the finite time convergence is guaranteed to the origin while conventional SMC only yields to asymptotic stability [231]. In this sense, Fridman et al. defined that twisting algorithm (TA) is the second generation of SMCs (while conventional SMC belongs to the first one) [232]. Nevertheless, when derivatives are employed, these can induce high noise in a feedback loop [233]. Another tool that could counteract these issues is STA (that also belongs to HOSMC), which has an integral term and avoid the usage of high order derivatives [234]. An unconventional structure that was also found is prescribed convergence law (PCL), that is a second order algorithm known for its convergence rate and tracking capabilities [235]. Implementation of the mentioned algorithms on PEAs were found in the work of Xu et al. from [236], where they made a simulation and experiments in which results were shown for tracking with suitable outcomes. Nevertheless, they used a hysteresis mathematical model based on an uncertainty. Despite that conventional designs of SMCs approaches require the usage of a mathematical description to reach the sliding surface, hysteresis models still have deficiencies for implementation [73].

Classical approaches for hysteresis description are classified in mathematical and physical theories [127]. In this background review, the mathematical models will be surveyed since physical ones like Jill Atherton and domain wall are mainly employed for magnetism description [237]. Ferenc Preisach proposed his theory in 1935 that has been initially used for magnetism and is per-

haps one of the most used in research due to its simplicity [238]. The base of this theory is the *"hysteron operator"* or also called *"relays"*, which sum of several terms can lead to a suitable hysteresis curve [239]. It has also been employed for PEAs as Li et al. performed in their work [240]. Another well known model is PI which is based on a linear combination of hysteron operators [241]. PI model has been also used in the past in works like [242], where they achieved suitable error ranges in the tracking accuracy. Major downsides of hysteron theories is the computational requirement when a high fidelity inverse model is required for control of PEAs [132]. Despite that strategies like vectorial approach can improve the memory consumption, these are still complex tools to implement in real time systems [243]. A model which can tackle these disadvantages due to its easy solution for implementation even its inversion is BW [244]. This has been showed by Yang et al. as a nonlinear equation which can be extended even for asymmetrical hysteresis, a common property of PEAs [245]. However, still this approach main issue is the parameter identification which can vary for each operative condition [246].

4.7.3 Conventional Sliding Mode Control

The first step in the design of an SMC is the choice of a suitable surface. In this sense, the guideline was followed through the criterion of authors from [247] that is expressed in Equation 4.60. The latter has the terms r and λ that are, respectively, the relative degree of the system and a positive constant.

$$S = \left(\frac{d}{dt} + \lambda\right)^{r-1} e \tag{4.60}$$

Based on previous works [248], the relative degree from the system is 2. Therefore, the chosen sliding surface is as Equation 4.61 shows.

$$S = \dot{e} + \lambda e \tag{4.61}$$

The control law of the proposed controllers is established by a neural compensation to reach the sliding surface rather than an equivalent term that comes from a mathematical model, as it was explained in the introduction of this manuscript. Thus, the expression of the control signal for the conventional SMC u_c is defined in Equation 4.62, where u_{ann_c} is the neural compensation (that will be explained

in further sections) and u_{sw_c} is the switching term that provides robustness to the system. As in this case, the conventional SMC is being highlighted, the expression of U_{sw_c} is defined in Equation 4.63. The choice of K should be positive but taking into account that as bigger as it gets, the higher the oscillations are generated [249].

$$u_c = u_{ann} + u_{sw_c} \tag{4.62}$$

$$u_{sw_c} = -K_c \cdot sign(S) \tag{4.63}$$

Based on former explanation, a formal stability proof has been performed using the system and the SMC algorithm. As previously mentioned, the system has a second order properties which implies that mathematically it can be described as Equation 4.64 [114]. The expression is described by *m*, *b*, *k*, *x*, *d*, *u*, *h* and *P* that are, respectively, mass, damping constant, stiffness, position, piezoelectric coefficient, input voltage, hysteresis and general perturbations or unmodeled dynamics.

$$m\ddot{x} + b\dot{x} + kx + df_h(x) = du_c + P \tag{4.64}$$

Therefore, the compensation term of the neural network can be considered as superposition named in Equation 4.65. of a linear term (without perturbations or hysteresis, detailed in Equation 4.66) named as u_{linear} and another which contemplates the nonlinearities that is defined as g_{ann}.

$$u_{ann} = u_{linear} + g_{ann}(x) \tag{4.65}$$

$$u_{linear} = \frac{1}{d}\left(m\ddot{x}_{ref} + b\dot{x}_{ref} + kx_{ref}\right) \tag{4.66}$$

Hence, if the error is defined as the reference minus the measured displacement, a system based on this variable is gathered in Equation 4.67. Also, it is considered that the ANN has an uncertainty in the fitting capabilities, for which reason it is defined an approximation error $g_{ann}(x) - f_h(x) = \varepsilon_{ann}$.

$$m\ddot{e} + b\dot{e} + ke = d\varepsilon_{ann} + P + du_{sw} \tag{4.67}$$

In order to study the stability, the candidate Lyapunov function (based on the sliding surface S) proposed in Equation 4.68 is a quadratic which derived produces Equation 4.69.

$$V = \frac{1}{2}S^2 \tag{4.68}$$

$$\dot{V} = S \cdot \dot{S} \tag{4.69}$$

Previous defined surface in Equation 4.60 can be derivated and combined with the error second derivative from Equation 4.67. Therefore, through replacement, the first derivative of the Lyapunov function results in Equation 4.70.

$$\dot{S} = -\frac{b}{m}\dot{e} - \frac{k}{m}e + \frac{d}{m}\varepsilon_{ann} + \frac{P}{m} + \frac{d}{m}u_{sw} + \lambda\dot{e} = \frac{d}{m}u_{sw} + \rho \tag{4.70}$$

Where:

$$\rho = -\frac{b}{m}\dot{e} - \frac{k}{m}e + \frac{d}{m}\varepsilon_{ann} + \frac{P}{m} + \lambda\dot{e} \tag{4.71}$$

For a practical purpose, the term ρ needs to tend to a constant value since the error is expected to be small in time and the perturbations with the neural network approximation will be finite and constants in overall. Therefore, it can be established an upper and lower bound based on the absolute value of a constant G such that $\rho \leq |G|$ [154]. Thence, with this assumption, Equation 4.72 is generated with the condition of stability according to Lyapunov's theorem.

$$\dot{V} = S \cdot \left(|G| - K_c sign(S)\right) = S|G| - K_c|S| < 0 \tag{4.72}$$

Hence, previous expression can be achieved provided that $K_1 > |G|$ which will allow the second negative term to govern the stability condition of Lyapunov.

4.7.4 Twisting algorithm

Similarly to previous presented technique, the surface will be the same but the control switching term is different as Equation 4.73 shows where the condition of the gains is that both are positive and $k_3 > k_4$ [250].

$$u_{TA} = -k_3 sign(S) - k_4 sign(\dot{S}) \tag{4.73}$$

In this case, a stability proof is fair complex since conventional Lyapunov functions are not suitable for the analysed system. Additionally, alternative proposals might result in a non-asymptotic stability (even using Lasalle's theorem). Thus, the Lyapunov candidate function for this algorithm is meant to be Equation 4.74 which development can be found in the work of Santiesteban et al. [251].

$$V = \alpha S^2 + \gamma |S|^{3/2} sign(S)\dot{S} + \alpha |S|\dot{S}^2 + \frac{1}{4}\dot{S}^4 \tag{4.74}$$

4.7.5 Super Twisting algorithm

STA has been designed to reduce the chattering that TA produced as a first generation algorithm. Thus, the expression in this case corresponds with the one from Equation 4.75 that helps to provide a continuous control signal [252]. In this formula, the necessary conditions are that the constants K4 and K5 should be positive design parameters which will be gathered through minimization of the IAE [253]. Additional details about the Lyapunov demonstration can be found in previous Section 4.4.4.

$$u_{sw} = K_1 |S|^{1/2} sign(S) - K_2 \int sign(S)dt \tag{4.75}$$

4.7.6 Prescribed Convergence Law

PCL is a second order SMC that ensures that the surface and its derivatives (full dynamical collapse) will be null along the time and therefore, that the errors will converge to zero [254, 255]. The minimum conditions that guarantee this statement is when K_5 and β are positive numbers whereas more related stability conditions can be found in the works from [119, 256].

$$u_{PCL} = -K_{PCL} sign\left(\dot{S} + g(S)\right) \tag{4.76}$$

$$g(S) = \beta |S|^{1/2} sign(S) \tag{4.77}$$

4.7.7 Results

All four described strategies had been embedded in dSPACE platform which provided information that was processed for graphical and numerical analysis. The used ANN is the one described in Section 4.6.3. Following figures present the collected information achieved during the tracking of a triangular signal with an amplitude of 140V and a period of 4s. All controllers showed different performance and control signal, which are both analysed as follows. Figure 4.42 demonstrates the acquired error during 8s, which is 2 triangular wave cycles. Graphically, main spots to be analysed are the slope changes (2s, 4s and 6s) and a general conclusion can be achieved through numerical tools to grant a better verdict.

Figure 4.42(a) displays the error in the first slope switch from rising to decreasing voltage in a short time range. It can be seen that all the controllers behave similarly in the change since an overshoot is generated. In this sense, the strategy that provided the higher overshoot has been TA(0.17V) whereas the lowest one was STA (0.12V), which also gave the best settling time (near 0.018s). It can also be seen that after 2s, TA showed more variation in the amplitude than the conventional SMC, expected to be the algorithm with more chattering.

At the lower converging point in 4s (showed in Figure 4.42(b)), the performance of the controllers is rather different though the TA still has enough variation. The PCL algorithm seems to provide the highest undershoot because the amplitude was around 0.25V in contrast to the 0.08V from STA, that specified the lowest value. The settling time has also achieved the best value with STA, which has been of around 0.016s.

Despite that it was expected a similar behaviour at 6s, SMC and TA behaved differently. Figure 4.42(c) sights a higher error value in generated amplitude of SMC with a slower settling time in comparison to the other controllers. Additionally, it also shows higher chattering along the time than TA until 6.03s which is when the situation changes and TA generates even more.

Numerical results were achieved based on the data gathered from Figure 4.42, which are mirrored in Table 4.17 by tools explained in Section 4.1. The values of IAE and RMSE had been referenced to the SMC which showed the highest in both metrics. TA exhibited a similar value in both metrics with a difference

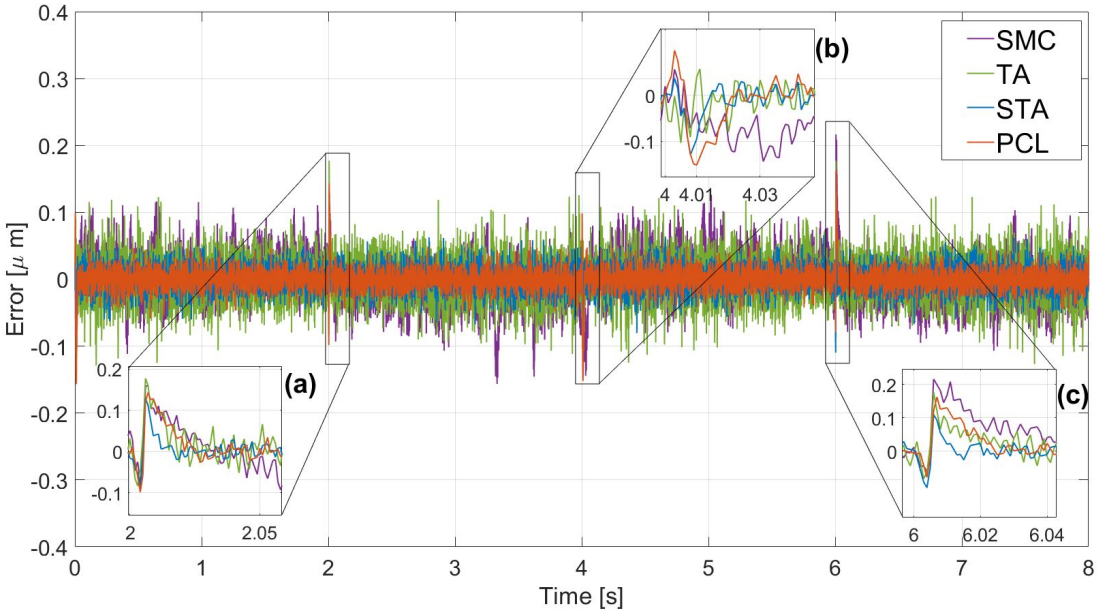

Figure 4.42: Tracking error comparison of the embedded controllers

below 10%. Nevertheless, STA boosted the difference as it reached almost 50% of dissimilarity with SMC. Thus, PCL algorithm prevails over the rest of options as it showed significant enhancement of above 55% in IAE and RMSE. The RRMSE expressed the same trend since the difference between SMC and PCL was progressive, were the latter has more than the half of improvement.

Controller	**IAE**		**RMSE**		**RRMSE**
	Value	Diff.[%]	Value[μm]	Diff.[%]	Value[%]
SMC	0.2456	-	0.0387	-	0.18
TA	0.2272	7.5	0.0355	8.35	0.16
STA	0.12	48.63	0.0199	48.56	0.09
PCL	0.1013	57.94	0.0177	54.29	0.08

Table 4.17: Metrics comparison for the tested controllers

Figure 4.43 represents the acquired control signal which was produced by the algorithms along the error compensation that has been previously analysed. Despite that saturations that can damage the actuator were unseen during experiments, several zoomed windows were pictured to provided a better analysis

in each part. For instance, Figure 4.43(a) shows an expected scenario during the beginning where the TA generated a considerable variable signal in contrast to the other algorithms. Actually, it can be seen that PCL was able to provide a softer response indeed; these phenomena can be seen either in Figure 4.43(e). Later in Figure 4.43(c), previous trend is still the same as the TA provided more chattering than other options. It is also possible to see that all the controllers made a necessary sharp switch due to the slope change but PCL had the lowest amplitude change. Nevertheless, in Figure 4.43(c), the switch was softer with slight overshoots in all the frameworks.

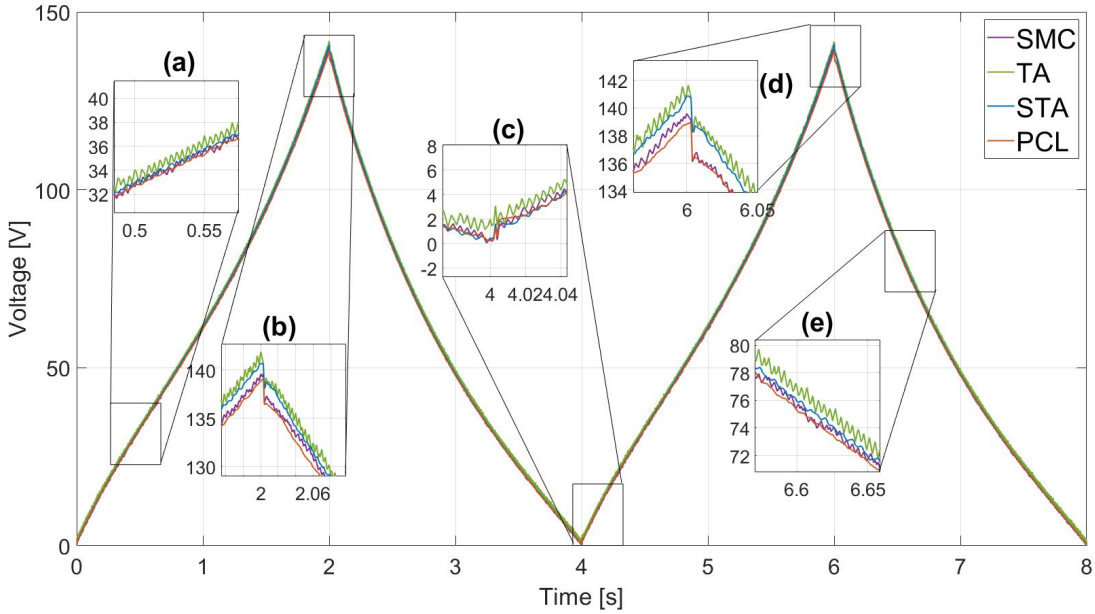

Figure 4.43: Control signal comparison of the embedded controllers

Lastly, Figure 4.44 provides the required computational time with its mean and standard deviation for each control strategy. This data is an important feature because it provides an idea for a designer about the choice required of a hardware control board. At first, it can be seen that the SMC requires the lowest time (which mean is 1.07μs) due to its simplicity. TA uses a derivative term which makes sense that the value increment is 1.42μs, which is 32% of increase in comparison to SMC. However, TA provided a lower standard deviation in comparison. On the other hand, STA shows an almost similar computational time like TA since its value is 1.53μm, which is 42% more than SMC. Finally,

PCL gave the highest value which has been almost 2μs with the highest standard deviation in comparison with all the other algorithms. This implies that PCL has 86% higher time consumption than conventional SMC.

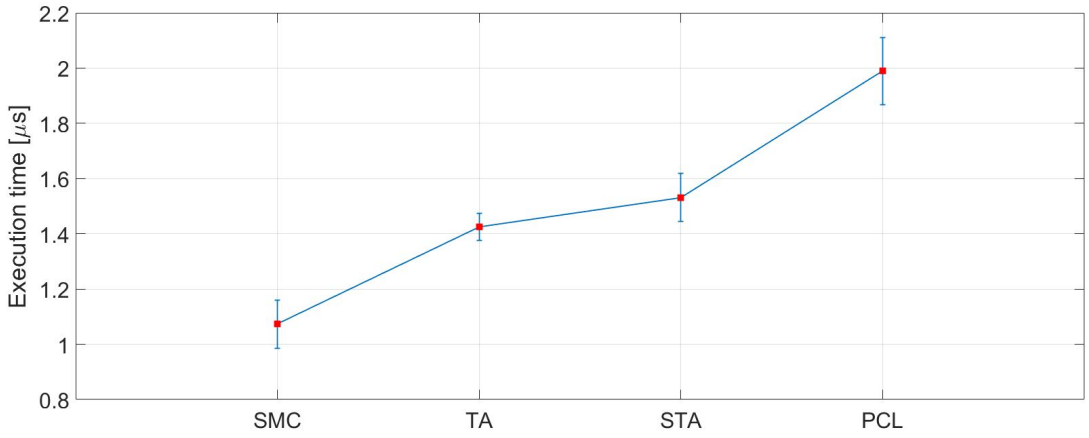

Figure 4.44: Computational time comparison of the embedded controllers

4.7.8 Conclusions

In this research, four sliding controllers with a neural combination for tracking reference following were analysed and embedded in a PEA. Traditional methods like conventional SMC and TA were contrasted with advanced ones as STA or PCL; the outcomes were correlated to define the best performance of each in a complex reference to be followed like a triangular wave.

An experimental rig was developed with a commercial PEA with peripheral devices from Thorlabs that has been hooked with a dSPACE. The PEA PK4FYC2 properties related to the hysteresis were acquired experimentally and analysed in details where interesting features were emphasized. Major gathered conclusions were different obtained curves between the first cycle and the following ones (provided that there is more than one period experiment), which is linked to the creep effect of PEAs.

As formerly mentioned, four SMC controllers were chosen but with a different approach from classic method to gather a control law. Commonly, mathematical models are used to achieve a term that could guide the system to a sliding surface but due to the disadvantages named in the introduction (like

computational requirements or parameter identification), an ANN replaced this approach. Hence, a TDNN was trained with gathered experimental data which performance was contrasted against the PEA hysteresis in terms of fitting, which allowed a suitable performance to be used in a control structure.

The implementation of the sliding controllers showed different behaviours which were evaluated at first within the graphic results of error and control signal generated. In this stage, the slope sign changes were analysed where the STA developed the best response due to the lowest under-/overshoot and settling time. Therefore, the STA combined with an ANN is established as the most robust tested algorithm as it was observed graphically.

Additionally, numerical metrics were calculated to discover an overall behaviour of the proposed schemes. The calculation of the IAE, RMSE and RRMSE showed that PCL achieved a better performance over the rest of the algorithms since it showed generous enhancement of tracking performance due to the low value gathered. Behind the PCL, STA also provided a suitable demeanour which implies that not only has delivered the most robust development but also it generated one of the best numerical results.

Another important metric gathered has been the consumed time of each algorithm. This is also an important value to be known as it provides a notion of the computational requirements that each structure requires and therefore, the choice of a control board hardware for industrial purposes. The simplest conventional SMC gave the lowest time consumed, and PCL provided the highest one in terms of average and standard deviation (due to the high order features).

For the truth of the conclusions of physical science, observation is the supreme Court of Appeal.

A. Eddington

5

Conclusions, Major Contributions and Future Guidelines

5.1 Conclusions and contributions

Along this thesis, the main purpose was to develop advanced control techniques which could manage to enhance a piezoelectric tracking performance based on the reduction of the hysteresis. Major outcomes are resumed as follows.

In chapter 1, an overview of piezoelectric actuators was unveiled. It was seen the development of these devices since the piezoelectric effect discovered by Curie Brothers in 1880 until the current applications. Also, from the material perspective, it was studied the working principle which is related to the polarization alignment of grains and what it causes the hysteresis. The latter, it is known to degrade the performance of PEAs during tracking and its origins known to be induced by residual polarization of crystals. It was studied that the hysteresis can be reduced provided that the material is redesigned but also, a control strategy can cope with it. Additionally, the applications of PEAs were studied from a shape classification which most known ones are stack, bending and ring bender. Most common applications of PEAs are in the fields of atomic force microscopes, energy harvesting, piezoelectric motors for micro-movements, machine tools, micro-grippers, micro-drones, injection devices and drug delivery systems.

Chapter 2 presented the set-up designed for carrying out the experimental validation of the proposed control algorithms. A commercial PEA by Thorlabs, namely PK4FYC2 model, was included in the set-up. According to the manufacturer, the hysteresis of this device could yield up to 15% of error reference tracking. The vendor reccomends using PID controllers to reduce the error in tracking applications. Hence, for this reason, a conventional PID was used in most of the experiments for comparison purposes. Also, an in-depth description of an hysteresis curve (obtained experimentally from the PEA) was analysed in two cycles of a triangular reference. In most of the experiments that had been developed in this thesis, the triangular reference was used not only because it is a complex signal to be followed due to its fast slope changes but also because this signal is represented with high frequency harmonics. Through the end of this chapter, other peripheral devices were described which helped with the implementation of control law designs. A dSPACE 1104 connected to a working computer through Simulink from MATLAB were one of the main tools for control design. However, the dSPACE platform manages input-output signals of 0-10V and the PEA is feed with 0-150V and the displacement is measured by a strain gauge that gives small voltage values. Therefore, an physical input block from Thorlabs (model KPZ101) was employed and it transforms a control signal from dSPACE of 0-10V into a 0-150V. For the measurements, another Thorlabs output block (model KSG101) with a pre-amplifier (AMP002) were used for voltage

transform at 0-10V to be the input reading of the dSPACE.

Chapter 3 is where the main contributions of this thesis had been developed. The main goal of this research is to reduce the uncertainty of a piezoelectric actuator when it has a complex reference that is also affected by the hysteresis. Feedback control algorithms were analysed and evaluated to enhance the precision of PEA for industrial applications. In this sense, the performance of a control design not only need to be measured in terms of control signal but mainly, the metrics should take into account the evolution of the error signal. For this reason, in most of the proposals, the integral of the absolute error, root-mean-squared-error and relative-root-mean-squared-error were calculated with the obtained data. These could give a numerical perspective of the performance achieved in each situation. Additionally, because the minimization of the integral of the absolute error is commonly used as optimisation tool, this was developed for online tuning of all the proposed designs.

In the first proposed design, different strategies based on a PID with feedforward combinations were analysed. In regards to the latter, a linear compensator was used with a conventional PID. It was found that the error and the control signals were enhanced with feedback-feedforward structures instead of conventional feedback controllers like PIDs. For an advanced perspective, a shallow neural network was trained with real data from the piezoelectric actuator that simulates the inverse model for a feedforward compensation. Because of the increment of available computational capacity, some tools like ANN are being used to generate a black-box system which has a combination of inside linear relations which factors (commonly known as weights and bias) can be obtained by training the ANN with real data. Also, it was found through the literature review that single neuron PIDs could cope better than a classic PID. Hence, the final comparison was performed in a feedback-feedforward structure which was an ANN-PID and ANN-SNPID. In terms of error, the value of IAE was significantly reduced when the ANN-SNPID was used and the control signal had a soft demeanour without any significant signals that could affect the actuator lifespan. Hence, the main contribution of this first research was the development of advanced strategies in which the feedforward-feedback strategies were highlighted over conventional feedback ones. In this sense, the usage of an ANN showed that not only in enhances the tracking performance combined with a PID but also with a SNPID in terms of IAE.

The second research explored other alternative feedfoward strategies. Hammerstein Wiener blocks are common structures for system identification which main advantage is the fast convergence. It comprises input-outout nonlinear blocks with a middle linear connection. Like with ANNs, these have factors which need to be tuned in contrast with real data from a given system. On the other hand, a fuzzy logic control was used as it could be used a feedback controller. Main principle of FLC is that it can be tuned from a human expert knowledge of the system. A type-1 set was configured through normalized gains that could handle the error with its derivative to provide the increment of the control signal. A practical stability proof based on Lyapunov's theory was also used in the proposed fuzzy controller. The comparisons were mainly two: (1) PID against the FLC in feedback structures and (2) FLC in combination with Hammerstein-Wiener for a feedback-feedforward arrangement. It was found that the fuzzy controller could handle better the error reduction than a PID controller as well as the control signal. Additionally, a higher improvement was unveiled with the combination of FLC and Hammerstain-Wiener's feedforward combination. This delivered a significant enhancement not only in the error response and control signal but also in metrics like IAE, RMSE and RRMSE. Therefore, the main contribution of this research was the development of a feedforward-feedback strategy in which a Hammerstain-Wiener block was involved with an FLC to improve the PEA tracking performance. This was proved in terms of stability features through an analysis and experiments with graphical analysis and numerical metrics.

The third research was aimed to an alternative usage of sliding mode control, more specifically by means of super-twisting algorithm. Sliding controllers have two terms in which one is called ”equivalent” that drives the system into an stable path and another known as ”switching”, which maintains this state in a robust way. The equivalent term is usually obtained from a physical-mathematical description. However, the available options for hysteresis model compensation have certain issues. Therefore, an ANN was used as an alternative. Super-twisting algorithm is an sliding structure that helps to reduce the chattering (the main downside of sliding mode controllers). Hence, these two strategies were combined in a feedback-feedforward structure to analyse the enhancement provided the tracking capabilities of a PEA. Also in this case, the stability was analysed by means of Lyapunov's theory. The experimental outcomes showed sig-

nificant enhancements to be highlighted not only with triangular refence waves but also with sine ones in order to show the flexibility of the design. Also, a numerical metric was calculated and it was concluded that the proposed combination of super-twisting algorithm with ANN was able to improve the tracking of the PEA. This approach achieved to improve the performance in tracking operations of the PEA. In addition, the stability was demonstrated both analytically and experimentally.

The fourth control scheme was similar to previous one but with certain unrelated features. In this sense, a cuasi-continuous sliding mode control was used. This belongs to the high order sliding mode controllers group, which intention is to reduce the generated chattering. Since the classic design principle is as previously described, where the control law comprises an equivalent and a switching term, the equivalent was again used with a neural network trained with real data. In this research, the experimental outcomes were contrasted against a conventional PID. The experiments were carried out using different references like triangular, sine and variable amplitude triangular waves. In all the cases, the combination of cuasi-continuous with an ANN was able to achieve a much higher performance result not only in tracking behaviour but also in the measured error, which was reduced. Henceforth, the major contribution of this research was the proposed cuasi-continuous control combined with an ANN in a feedback-feedforward structure.

The fifth proposed controller has been an scheme based on fuzzy logic in combination with ANNs. Previously, it was found the suitable capabilities of FLC to handle errors when it was embedded as a controller and specially with its combination in a feedforward-feedback structure. Nevertheless, an ANN was used in this case rather than a Hammerstein-Wiener block. Also, in the previous case, a fuzzy logic type-1 block was used which is known to be defined with relative precise linguistic/numerical rules. However, for cases in which inexact or imprecise information is used or when the expert has certain doubts regarding the definition, type-2 sets are defined. The particularity of these sets is the capability to generate membership functions with certain fuzziness. Eventhough the calculation can be more complex than type-1 sets, it can also allow an overall enhancement in terms of control capabilities. This was shown in the experiments in which feedback-feedforward structures were embedded with configurations of FLC-T1-ANN and FLC-T2-ANN. The outcomes showed meaningful

improvements in terms of error reduction as well as generated control signals. To summarized, the main contribution of this proposal was the contrasts of two advanced feedforward-feedback structures based on fuzzy logic (like type-1 and type-2) with an ANN from which it was found that FLC-T2 with ANN is able to enhance the tracking performance of a PEA.

Finally, the last research comprised a an applicability review for PEAs tracking improvement of sliding mode controllers. In this case, conventional SMC, twisting, super-twisting and prescribed convergence law were analysed. As previously, the structures were combined with an ANN that was already trained with 140V of amplitude and 4s of period. Hence, a particular distinction of these tests was the capability to achieve the computational time that each switching law took. This is an important feature because it can provide capabilities for hardware engineers who need to implement different control schemes over hardware platforms that provide limited processing capabilities. Though that the error and control signals developed a better performance for STA in the graphical analysis, the numerical metrics analysis showed a better performance for the PCL. In regards to the computational time, it was observed that PCL required more time to develop a control signal and it was followed by the STA. Therefore, major contributions of this research was not only the test of several sliding mode control structures combined with ANNs but also the calculation time that took each approach which can be useful for a hardware designer.

5.2 Future guidelines

During the research and reviewed background, came up several research lines that were left for future development.

- In regards to PID controllers, it was tested a neural PID with Hebb's learning rules. Nevertheless, these learning rules are not absolute and other ones could be used such as delta for instance.
- In this research, only shallow neural networks were used. This was mainly as a consequence of dSPACE limitation which only allowed implementing this kind of neural networks. Hence, deep learning structures such as long-short-term-memory neural networks could be a suitable tool for improving the system identification.

- Although an in-depth investigation of the application of fuzzy logic to PEAs was provided, including type-1 and type-2 approaches, are other branches which could open new paradigms. For instance, though that Karnik-Mendel was used as a type-reduction algorithm, there are still other strategies to be tested. In particular, enhanced Karnik-Mendel (EKM) or iterative algorithm with stop condition (IASC); these are known for its low computational requirements.

- On the field of sliding mode controllers, it would be an interesting idea to test other approaches which could be embedded with ANNs such adaptive structures which could be through the usage of fuzzy logic. This would make an smart controller which computational time could be calculated in order to check its efficiency.

- Though that the hysteresis was analysed in-depth in this thesis, PEAs also present other non-linear effects that may influence their behaviour. In particular, the creep effect, which is less significant and appears in sudden actions. It may be worth analysing the reduction of this phenomenon through the employment of the techniques analysed along this whole research.

A

Published & Accepted Articles

Through the development of this thesis, the following publications had been produced where each one corresponds to the main research topic and collaboration in related fields.

1. Napole, C.; Barambones, O.; Calvo, I.; Velasco, J. Feedforward Compensation Analysis of Piezoelectric Actuators Using Artificial Neural Networks

with Conventional PID Controller and Single-Neuron PID Based on Hebb Learning Rules. *Energies* **2020**. Impact factor: 3.004; Category & position: Energy & Fuels 70/114.

2. Napole, C.; Barambones, O.; Calvo, I.; Derbeli, M.; Silaa, M.Y.; Velasco, J. Advances in Tracking Control for Piezoelectric Actuators Using Fuzzy Logic and Hammerstein-Wiener Compensation. *Mathematics* **2020**. Impact factor: 2.165; Category & position: Mathematics 24/330.

3. Napole, C; Barambones, O.; Derbeli, M.; Silaa, M.; Calvo, I.; Velasco, J. Tracking Control for Piezoelectric Actuators with Advanced Feed-Forward Compensation Combined with PI Control. *1st International Electronic Conference on Actuator Technology: Materials, Devices and Applications*, **2020**.

4. Napole, C; Barambones, O.; Derbeli, M.; Calvo, I; Silaa, M.;.; Velasco, J. High Performance Tracking for Piezoelectric Actuators Using Super-Twisting Algorithm Based on Artificial Neural Networks. *Mathematics* **2020**. Impact factor: 2.165; Category & position: Mathematics 24/330.

5. Derbeli, M.; Barambones, O.; Silaa, M.Y.; Napole, C. Real-Time Implementation of a New MPPT Control Method for a DC-DC Boost Converter Used in a PEM Fuel Cell Power System. *Actuators* **2020**. Impact factor: 1.994; Category & position: Engineering, Mechanical 77/135.

6. Velasco, J.; Calvo, I.; Barambones, O.; Venegas, P.; Napole, C. Experimental Validation of a Sliding Mode Control for a Stewart Platform Used

in Aerospace Inspection Applications. *Mathematics* **2020**. Impact factor: 2.165; Category & position: Mathematics 24/330.

7. Silaa, M; Derbeli, M.; Barambones, O.; Napole, C.; Cheknane, A.; Gonzalez de Durana, J.M. An Efficient and Robust Current Control for Polymer Electrolyte Membrane Fuel Cell Power System. *Sustainability* **2021**. Impact factor: 3.251; Category & position: Environmental Sciences 60/125.

8. Derbeli, M.; Charaabi, A.; Barambones, O.; Napole, C. High Performance Tracking for Proton Exchange Membrane Fuel Cell System PEMFC Using Model Predictive Control. *Mathematics* **2021**. Impact factor: 2.258; Category & position: Mathematics 24/330.

9. Napole, C.; Barambones, O.; Derbeli, M.; Cortajarena, J.A.; Calvo, I.; Alcorta, P.; Fernandez Bustamante, P. Double Fed Induction Generator Control Design Based on a Fuzzy Logic Controller for an Oscillating Water Column System. *Energies* **2021**. Impact factor: 3.004; Category & position: Energy & Fuels 70/114.

10. Napole, C.; Derbeli, M.; Barambones, O. Fuzzy Logic Approach for Maximum Power Point Tracking Implemented in a Real Time Photovoltaic System, *Applied Sciences* **2021**. Impact factor: 2.679; Category & position: Engineering, Multidisciplinary 124/274.

11. Napole, C.; Derbeli, M.; Barambones, O.; Calvo, I. Advanced Trajectory Control for Piezoelectric Actuators Based on Robust Control Combined

with Artificial Neural Networks, *Applied Sciences* **2021**. Impact factor: 2.679; Category & position: Engineering, Multidisciplinary 124/274.

12. Derbeli, M; Napole, C.; Barambones, O. Machine Learning Approach for Modeling and Control of a Commercial Heliocentris FC50 PEM Fuel Cell, *Mathematics* **2021**. Impact factor: 2.258; Category & position: Mathematics 24/330.

13. Calvo, I.; Gil-Garcia, J.M.; Villar, E.; Fernández, A.; Velasco, J.; Barambones, O.; Napole, C.; Bustamante, P. Design and Performance of a XBee 900MHz Acquisition System Aimed at Industrial Applications, *Applied Sciences* **2021**. Impact factor: 2.679; Category & position: Engineering, Multidisciplinary 124/274.

14. Fernandez-Bustamante, P.; Barambones, O.; Calvo, I.; Napole, C.; Derbeli, M. Provision of Frequency Response from Wind Farms: A Review, *Energies* **2021**. Impact factor: 3.004; Category & position: Energy & Fuels 70/114.

15. Calvo, I.; Villar, E.; Napole, C.; Fernández, A.; Barambones, O. Reliable Control Applications with Wireless Communication Technologies: Application to Robotic Systems, *Sensors* **2021**. Impact factor: 3.576; Category & position: Instruments & Instrumentation 15/64.

16. Napole, C.; Derbeli, M.; Barambones, O. A Global Integral Terminal Sliding Mode Control Based on a Novel Reaching Law for a Proton Exchange

Membrane Fuel Cell System, *Applied Energy* **2021**. Impact factor: 9.746; Category & position: Engineering & Chemical 6/143.

17. Derbeli, M.; Napole, C.; Barambones, O.; Sanchez, J.; Calvo, I.; Fernandez-Bustamante, P. Maximum Power Point Tracking Techniques for photovoltaic panel: a review and experimental applications, *Energies* **2021**. Impact factor: 3.004; Category & position: Energy & Fuels 70/114.

18. Napole, C.; Derbeli, M. ; Barambones, O. Experimental Analysis of a Fuzzy Scheme against a Robust Controller for a Proton Exchange Membrane Fuel Cell System, *Symmetry* **2022**. Impact factor: 2.713; Category & position: Multidisciplinary Sciences 33/72.

19. Velasco, J.; Barambones, O.; Calvo, I.; Venegas, P.; Napole, C. Validation of a Stewart platform inspection system with an artificial neural network, *Precision Engineering* **2022**. Impact factor: 2.713; Category & position: Engineering Multidisciplinary 29/90.

References

[1] Stuart T. Smith and Richard M. Seugling. Sensor and actuator considerations for precision, small machines. *Precision Engineering*, 30(3):245–264, 2006.

[2] F. Stefanski and B. Minorowicz. Open loop control of piezoelectric tube transducer. *Archives of Mechanical Technology and Materials*, 38:23–28, 2018.

[3] Saeid Bashash and Nader Jalili. Underlying memory-dominant nature of hysteresis in piezoelectric materials. *Journal of Applied Physics*, 100:014103–014103, 07 2006.

[4] D. Damjanovic. Hysteresis in piezoelectric and ferroelectric materials. In *The Science of Hysteresis*, chapter 4, pages 338–452. Academic Press, 2006.

[5] Helge Kragh. The beginnings of piezoelectricity. a study in mundane physics by shaul katzir. *Centaurus*, 49:251 – 252, 12 2007.

[6] David Zou, Tang Alvin, and Evgheni Pan. Symmetry types of the piezoelectric tensor and their identification. *Royal Society of London Proceedings Series A*, 469:20755–, 05 2013.

[7] Susan Trolier-McKinstry. *Crystal Chemistry of Piezoelectric Materials*, pages 39–56. Springer US, Boston, MA, 2008.

[8] Armin Schneider and Hubertus Feussner. Chapter 5 - diagnostic procedures. In Armin Schneider and Hubertus Feussner, editors, *Biomedical Engineering in Gastrointestinal Surgery*, pages 87–220. Academic Press, 2017.

[9] Wagner Coelho de Albuquerque Pereira, Christiano Bittencourt Machado, Carlos Alther Negreira, and Rafael Canetti. *Ultrasonic Techniques for Medical Imaging and Tissue Characterization*, pages 433–465. Springer Berlin Heidelberg, Berlin, Heidelberg, 2008.

[10] Kenji Uchino, Yuzuru Tsuchiya, Shoichiro Nomura, Takuso Sato, Hiromi Ishikawa, and Osamu Ikeda. Deformable mirror using the pmn electrostrictor. *Appl. Opt.*, 20(17):3077–3080, Sep 1981.

[11] Jindong Zhang, W.Jack Hughes, R.J. Meyer, Kenji Uchino, and Robert E. Newnham. Cymbal array: a broad band sound projector. *Ultrasonics*, 37(8):523–529, 2000.

[12] Kenji Uchino. Piezoelectric actuators 2006. *Journal of Electroceramics*, 20:301–311, 08 2008.

[13] Y.Q. Fu, J.K. Luo, A.J. Flewitt, and W.I. Milne. Smart microgrippers for biomems applications. In *MEMS for Biomedical Applications*, pages 291 – 336. Woodhead Publishing, 2012.

[14] Peng Zhang. Chapter 3 - sensors and actuators. In Peng Zhang, editor, *Advanced Industrial Control Technology*, pages 73–116. William Andrew Publishing, Oxford, 2010.

[15] Li Sui, Xin Xiong, and Gengchen Shi. Piezoelectric actuator design and application on active vibration control. *Physics Procedia*, 25:1388–1396, 12 2012.

[16] Anastasia Muliana. Time dependent behavior of ferroelectric materials undergoing changes in their material properties with electric field and temperature. *International Journal of Solids and Structures*, 48(19):2718–2731, 2011.

[17] Dong An, Yixiao Yang, Ying Xu, Meng Shao, Jinyang Shi, and Guodong Yue. Compensation of hysteresis in the piezoelectric nanopositioning stage under reciprocating linear voltage based on a mark-segmented pi model. *Micromachines*, 11(1), 2020.

[18] Seung-Eek Park and Thomas R. Shrout. Ultrahigh strain and piezoelectric behavior in relaxor based ferroelectric single crystals. *Journal of Applied Physics*, 82(4):1804–1811, 1997.

[19] Ahmad Safari, B. JADIDIAN, and Enver Akdogan. *Piezoelectric Composites for Transducer Applications*, pages 533–561. Pergamon, 12 2000.

[20] Peng Zhang. 1 - sensors and actuators for industrial control. In Peng Zhang, editor, *Industrial Control Technology*, pages 1–186. William Andrew Publishing, Norwich, NY, 2008.

[21] F. Aggogeri, F. Al-Bender, B. Brunner, M. Elsaid, M. Mazzola, A. Merlo, D. Ricciardi, M. de la O Rodriguez, and E. Salvi. Design of piezo-based avc system for machine tool applications. *Mechanical Systems and Signal Processing*, 36(1):53–65, 2013. Piezoelectric Technology.

[22] Emmanuel Vander Poorten, Cameron N. Riviere, Jake J. Abbott, Christos Bergeles, M. Ali Nasseri, Jin U. Kang, Raphael Sznitman, Koorosh Faridpooya, and Iulian Iordachita. 36 - robotic retinal surgery. In Mohammad H. Abedin-Nasab, editor, *Handbook of Robotic and Image-Guided Surgery*, pages 627–672. Elsevier, Amsterdam, Netherlands, 2020.

[23] Rüdiger Ballas. *Piezoelectric Multilayer Beam Bending Actuators Static and Dynamic Behavior and Aspects of Sensor Integration*. Springer, 03 2007.

[24] Nahid Hosseini, Adrian Nievergelt, J Adams, Vladimir Stavrov, and Georg Fantner. A monolithic mems position sensor for closed-loop high-speed atomic force microscopy. *Nanotechnology*, 27:135705, 04 2016.

[25] O. Takashi and O. Norikazu. Power-efficient driver circuit for piezo electric actuator with passive charge recovery. *Energies*, 13:2866, 2020.

[26] Dong-Ju Kim, Jung-Doung Yu, and Yong-Hoon Byun. Piezoelectric ring bender for characterization of shear waves in compacted sandy soils. *Sensors*, 21(4), 2021.

[27] Paolo Tamburrano, Riccardo Amirante, Elia Distaso, and Andrew R. Plummer. Full simulation of a piezoelectric double nozzle flapper pilot valve coupled with a main stage spool valve. *Energy Procedia*, 148:487–494, 2018. ATI 2018 - 73rd Conference of the Italian Thermal Machines Engineering Association.

[28] Shannon Rios, Andrew Fleming, and Yuen Kuan Yong. Miniature resonant ambulatory robot. *IEEE Robotics and Automation Letters*, PP:1–1, 10 2016.

[29] Xiangdong Xie, Q. Wang, and Nan Wu. A ring piezoelectric energy harvester excited by magnetic forces. *International Journal of Engineering Science*, 77:71–78, 04 2014.

[30] Kristian Franze. Atomic force microscopy and its contribution to understanding the development of the nervous system. *Current Opinion in Genetics and Development*, 21(5):530–537, 2011.

[31] Andrew J. Lee, Ya Wang, and Daniel J. Inman. Energy Harvesting of Piezoelectric Stack Actuator From a Shock Event. *Journal of Vibration and Acoustics*, 136(1), 11 2013.

[32] Zhengbao Yang, Shengxi Zhou, Jean Zu, and Daniel Inman. High-performance piezoelectric energy harvesters and their applications. *Joule*, 2(4):642–697, 2018.

[33] Richard Crowder. 9 - related motors and actuators. In Richard Crowder, editor, *Electric Drives and Electromechanical Systems (Second Edition)*, pages 227–239. Butterworth-Heinemann, second edition edition, 2020.

[34] Georgios A. Bertos and Evangelos G. Papadopoulos. Chapter six - upper-limb prosthetic devices. In Jacob Segil, editor, *Handbook of Biomechatronics*, pages 177–240. Academic Press, 2019.

[35] Wei Gu. Chapter 116 - tiny dual full-bridge piezo motor driver operates from low input voltage. In Bob Dobkin and John Hamburger, editors, *Analog Circuit Design*, pages 243–244. Newnes, Oxford, 2015.

[36] S. Assarzadeh and Majid Ghoreishi. *The Application of Piezoelectric Materials in Machining Processes*, pages 57–68. IntechOpen, 02 2013.

[37] Hong LU, Deug-Woo LEE, Sang-Min LEE, and Jeong-Woo PARK. Diamond machining of sinusoidal grid surface using fast tool servo system for fabrication of hydrophobic surface. *Transactions of Nonferrous Metals Society of China*, 22:s787–s792, 2012.

[38] Elaijah Islam, Abu Musa Abdullah, Aminur Rashid Chowdhury, Farzana Tasnim, Madelyne Martinez, Carolina Olivares, Karen Lozano, and M. Jasim Uddin. Electromagnetic-triboelectric-hybrid energy tile for biomechanical green energy harvesting. *Nano Energy*, 77:105250, 2020.

[39] Z. Zhang, D. Zhang, H. Zheng, T. Huang, and Y. Xie. Identification of a precision motion stage based on the hammerstein-wiener model. In *2019 Chinese Control Conference (CCC)*, pages 1637–1642, 2019.

[40] Xiaodong Chen, Zilong Deng, Siya Hu, Jinhai Gao, and Xingjun Gao. Design of a flexible piezoelectric microgripper based on combined amplification principles. *Nanotechnology and Precision Engineering*, 2(3):138–143, 2019.

[41] Kevin Y. Ma, Pakpong Chirarattananon, Sawyer B. Fuller, and Robert J. Wood. Controlled flight of a biologically inspired, insect-scale robot. *Science*, 340(6132):603–607, 2013.

[42] Jafferis Noah, Helbling Farrell, Karpelson Michael, and Wood Robert. Untethered flight of an insect-sized flapping-wing microscale aerial vehicle. *Nature*, pages 491–495, 2019.

[43] Waiman Meinhold, Daniel Enrique Martinez, John Oshinski, Ai-Ping Hu, and Jun Ueda. A direct drive parallel plane piezoelectric needle positioning robot for mri guided intraspinal injection. *IEEE Transactions on Biomedical Engineering*, 68(3):807–814, 2021.

[44] Srinivasa Rao Karumuri, Md Hamza, Ashok Puli, and Girija Sravani. Design and optimization of mems based piezoelectric actuator for drug delivery systems. *Microsystem Technologies*, 26, 05 2020.

[45] José Luis Giordano. On the sensitivity, precision and resolution in DC wheatstone bridges. *European Journal of Physics*, 18(1):22–27, jan 1997.

[46] Thorlabs. Pk4fyc2 piezoelectric actuator. Accessed on June 8th 2022.

[47] J. Gan, X. Zhang, and H. Wu. A generalized prandtl-ishlinskii model for characterizing the rate-independent and rate-dependent hysteresis of piezoelectric actuators. *Review of Scientific Instruments*, 87:035002, 03 2016.

[48] W. Li, L. Nie, Y. Liu, and M. Zhou. Rate dependent krasnoselskii-pokrovskii modeling and inverse compensation control of piezoceramic actuated stages. *Sensors*, 20(18), September 2020.

[49] Y. Qin and H. Duan. Single-neuron adaptive hysteresis compensation of piezoelectric actuator based on hebb learning rules. *Micromachines*, 11:84, 2020.

[50] Jingyang Peng and Xiongbiao Chen. A survey of modeling and control of piezoelectric actuators. *Modern Mechanical Engineering*, 03:1–20, 01 2013.

[51] Wei Tech Ang, F.A. Garmon, P.K. Khosla, and C.N. Riviere. Modeling rate-dependent hysteresis in piezoelectric actuators. In *Proceedings 2003 IEEE/RSJ International Conference on Intelligent Robots and Systems (IROS 2003) (Cat. No.03CH37453)*, volume 2, pages 1975–1980 vol.2, 2003.

[52] K. Kuhnen and H. Janocha. Adaptive inverse control of piezoelectric actuators with hysteresis operators. In *1999 European Control Conference (ECC)*, pages 791–796, 1999.

[53] Micky Rakotondrabe. Bouc–wen modeling and inverse multiplicative structure to compensate hysteresis nonlinearity in piezoelectric actuators. *IEEE Transactions on Automation Science and Engineering*, 8(2):428–431, 2011.

[54] D.H. Wang, W. Zhu, and Q. Yang. Linearization of stack piezoelectric ceramic actuators based on bouc-wen model. *Journal of Intelligent Material Systems and Structures*, 22(5):401–413, 2011.

[55] Xiaobo Tan, Ram Iyer, and P Krishnaprasad. Control of hysteresis: Theory and experimental results. *Proc SPIE*, 08 2001.

[56] Junho Song and Armen Der Kiureghian. Generalized bouc–wen model for highly asymmetric hysteresis. *Journal of Engineering Mechanics*, 132(6):610–618, 2006.

[57] Ricardo de A. Araújo, Adriano L.I. Oliveira, and Silvio Meira. A morphological neural network for binary classification problems. *Engineering Applications of Artificial Intelligence*, 65:12–28, 2017.

[58] Tao Gong, Tiantian Fan, Jizheng Guo, and Zixing Cai. Gpu-based parallel optimization of immune convolutional neural network and embedded system. *Engineering Applications of Artificial Intelligence*, 62:384–395, 2017.

[59] Daniela Sánchez, Patricia Melin, and Oscar Castillo. Optimization of modular granular neural networks using a firefly algorithm for human recognition. *Engineering Applications of Artificial Intelligence*, 64:172–186, 2017.

[60] Zina Boussaada, Octavian Curea, Ahmed Remaci, Haritza Camblong, and Najiba Mrabet Bellaaj. A nonlinear autoregressive exogenous (narx) neural network model for the prediction of the daily direct solar radiation. *Energies*, 11(3), 2018.

[61] Alexander Alyukov, Yuri Rozhdestvenskiy, and Sergey Alyukov. Active shock absorber control based on time-delay neural network. *Energies*, 13:1091, 03 2020.

[62] Hang Xie, Hao Tang, and Yu-He Liao. Time series prediction based on narx neural networks: An advanced approach. In *2009 International Conference on Machine Learning and Cybernetics*, volume 3, pages 1275–1279, 2009.

[63] Yuen Liang, Suan Xu, Kaixing Hong, Guirong Wang, and Tao Zeng. Neural network modeling and single-neuron proportional–integral–derivative control for hysteresis in piezoelectric actuators. *Measurement and Control*, 52:002029401986684, 10 2019.

[64] M. Soleimani Amiri, R. Ramli, M.F. Ibrahim, D.A. Wahab, and N. Aliman. Adaptive particle swarm optimization of pid gain tuning for lower-limb human exoskeleton in virtual environment. *Mathematics*, 11 2020.

[65] Y. Zhao, X. Huang, Y. Liu, G. Wang, and K. Hong. Design and control of a piezoelectric-driven microgripper perceiving displacement and gripping force. *Micromachines*, 11:121, 01 2020.

[66] M. Jesenik, M. Marjan, and T. Mladen. Determination of a hysteresis model parameters with the use of different evolutionary methods for an innovative hysteresis model. *Mathematics*, 8:201, 2020.

[67] J. Main and E. Garcia. Piezoelectric stack actuators and control system design: Strategies and pitfalls. *Journal of Guidance Control and Dynamics*, 20:479–485, 1997.

[68] A. Dong, L. Haodong, X. Ying, and Z. Lixiu. Compensation of hysteresis on piezoelectric actuators based on tripartite pi model. *Micromachines*, 9:44, 2018.

[69] K. Kuhnen and H. Janocha. Compensation of creep and hysteresis effects of piezoelectric actuators with inverse systems. In *International conference on new actuators, Actuator 98*, pages 309–312, 1998.

[70] D. Croft, G. Shedd, and S.Devasia. Creep, hysteresis, and vibration compensation for piezoactuators: Atomic force microscopy application. In *Proceedings of the 2000 American Control Conference*, volume 3, pages 2123 – 2128, 2000.

[71] J. Peng and X. Chen. A survey of modeling and control of piezoelectric actuators. *Modern Mechanical Engineering*, 03, 2013.

[72] F. Jiwen, W. Jia, L. Chong, Z. Wei, and L. Zhili. A compound control based on the piezo-actuated stage with bouc–wen model. *Micromachines*, 10:861, 2019.

[73] C. Napole, O. Barambones, I. Calvo, M. Derbeli, M. Silaa, and J. Velasco. Advances in tracking control for piezoelectric actuators using fuzzy logic and hammerstein-wiener compensation. *Mathematics*, 8, 11 2020.

[74] S. Yu, M. Xie, H. Wu, J. Ma, Y. Li, and H. Gu. Composite proportional-integral sliding mode control with feedforward control for cell puncture mechanism with piezoelectric actuation. *ISA Transactions*, 2020.

[75] I. Ahmad, M. A. Ali, and W. Ko. Robust u-synthesis with dahl model based feedforward compensator design for piezo-actuated micropositioning stage. *IEEE Access*, 8:141799–141813, 2020.

[76] Shruti K and D. Paresh. A basic review of fuzzy logic applications in hydrology and water resources. *Applied Water Science*, 10, 2020.

[77] C. Pérez. A proposal of an adaptive neuro-fuzzy inference system for modeling experimental data in manufacturing engineering. *Mathematics*, 8:1390, 2020.

[78] Cheng-Hung C., S.Y. Jeng, and L. Cheng-Jian. Mobile robot wall-following control using fuzzy logic controller with improved differential search and reinforcement learning. *Mathematics*, 8:1254, 2020.

[79] M. Derbeli, L. Sbita, M. Farhat, and O. Barambones. Proton exchange membrane fuel cell — a smart drive algorithm. In *2017 International*

Conference on Green Energy Conversion Systems (GECS), pages 1–5, 2017.

[80] M. Derbeli, I. Mrad, L. Sbita, and O. Barambones. Pem fuel cell efficiency boosting — robust mpp tracking. In *2018 9th International Renewable Energy Congress (IREC)*, pages 1–5, 2018.

[81] R.-E. Precup and S. Preitl. Development of fuzzy controllers with non-homogeneous dynamics for integral-type plants. *Electrical Engineering*, 85:155–168, 2003.

[82] Sabarianand D V, P. Karthikeyan, and T. Muthuramalingam. A review on control strategies for compensation of hysteresis and creep on piezoelectric actuators based micro systems. *Mechanical Systems and Signal Processing*, 140, 2020.

[83] A. M. Mashhad and S. K. M. Mashhadi. H infinity robust controller comparison with pd like fuzzy logic controller for an auv control. In *2015 4th Iranian Joint Congress on Fuzzy and Intelligent Systems (CFIS)*, pages 1–5, 2015.

[84] A. Sebastian and S. M. Salapaka. Design methodologies for robust nano-positioning. *IEEE Transactions on Control Systems Technology*, 13(6):868–876, 2005.

[85] P. Huang, P. Shieh, F. Lin, and H. Shieh. Sliding-mode control for a two-dimensional piezo-positioning stage. *IET Control Theory Applications*, 1(4):1104–1113, 2007.

[86] C. P. Coleman and D. Godbole. A comparison of robustness: fuzzy logic, pid, and sliding mode control. In *Proceedings of 1994 IEEE 3rd International Fuzzy Systems Conference*, pages 1654–1659, 1994.

[87] J. Mendel. *Type-1 Fuzzy Systems: Design Methods and Applications*, chapter 4, pages 229–234. Springer International Publishing, 2003.

[88] J. Song and A.D. Kiureghian. Generalized bouc–wen model for highly asymmetric hysteresis. *Journal of Engineering Mechanics-asce - J ENG MECH-ASCE*, 132, 06 2006.

[89] M. Janaideh, Y. Feng, R. Rakheja, C. Su, and C. Rabbath. Hysteresis compensation for smart actuators using inverse generalized prandtl-ishlinskii model. In *2009 American Control Conference*, pages 307 – 312, 07 2009.

[90] G. Mercère, O. Prot, and J. A. Ramos. Identification of parameterized gray-box state-space systems: From a black-box linear time-invariant representation to a structured one. *IEEE Transactions on Automatic Control*, 59(11):2873–2885, 2014.

[91] Y. Firouz, J. Van Mierlo, P. Van den Bossche, and Y. Katoh. Nonlinear modeling of all-solid-state battery technology based on hammerstein-wiener systems. In *2019 IEEE Electrical Power and Energy Conference (EPEC)*, pages 1–5, 2019.

[92] M. Schoukens and K. Tiels. Identification of nonlinear block-oriented systems starting from linear approximations: a survey. *Automatica*, 85:272–292, 2016.

[93] A. Ramm. Stability of solutions to some evolution problems. *Mathematics*, 1, 2010.

[94] M. Nafea, Z. Mohamed, A. Abdullahi, M.R. Ahmad, and A. Husain. Dynamic hysteresis based modeling of piezoelectric actuators. *J. Teknol.*, 67:9–13, 04 2014.

[95] H. Li, Y. Xu, M. Shao, L. Guo, and D. An. Analysis for hysteresis of piezoelectric actuator based on microscopic mechanism. *IOP Conference Series: Materials Science and Engineering*, 399, 09 2018.

[96] G. Helke and K. Lubitz. *Piezoelectric PZT Ceramics*, pages 89–130. Springer Berlin Heidelberg, Berlin, Heidelberg, 2008.

[97] C. V. Newcomb and I. Flinn. Improving the linearity of piezoelectric ceramic actuators. *Electronics Letters*, 18(11):442–444, 1982.

[98] J. F. Cuttino, A. C. Miller, and D. E. Schinstock. Performance optimization of a fast tool servo for single-point diamond turning machines. *IEEE/ASME Transactions on Mechatronics*, 4(2):169–179, 1999.

[99] P. Ronkanen, P. Kallio, M. Vilkko, and H. N. Koivo. Displacement control of piezoelectric actuators using current and voltage. *IEEE/ASME Transactions on Mechatronics*, 16(1):160–166, 2011.

[100] C. Lin and S. Yang. Precise positioning of piezo-actuated stages using hysteresis-observer based control. *Mechatronics*, 16(7):417 – 426, 2006.

[101] Gi Sang Choi, Yo An Lim, and Gi Heung Choi. Tracking position control of piezoelectric actuators for periodic reference inputs. *Mechatronics*, 12(5):669–684, 2002.

[102] J. Lin, H. Chiang, and C.C. Lin. Tuning pid control parameters for micro-piezo-stage by using grey relational analysis. *Expert Systems with Applications*, 38(11):13924 – 13932, 2011.

[103] D. Abramovitch, S. Hoen, and R. Workman. Semi-automatic tuning of pid gains for atomic force microscopes. *Asian Journal of Control*, 11:188 – 195, 06 2008.

[104] R. Rebai, K. Guesmi, and H. Boualem. Design of an optimized fractional order fuzzy pid controller for a piezoelectric actuator. *Control Engineering and Applied Informatics*, 17:41–49, 09 2015.

[105] E. Applebaum and J. Ben-Asher. Fuzzy gain scheduling using output feedback for flutter suppression in unmanned aerial vehicles with piezoelectric materials. In *IEEE Annual Meeting of the Fuzzy Information, 2004. Processing NAFIPS '04.*, volume 1, pages 242–247 Vol.1, 2004.

[106] M. Ezzraimi, R. Tiberkak, A. Melbous, and S. Rechak. Lqr and pid algorithms for vibration control of piezoelectric composite plates. *Mechanics*, 24, 11 2018.

[107] Ziqiang Chi. Recent advances in the control of piezoelectric actuators. *International Journal of Advanced Robotic Systems*, 11, 11 2014.

[108] William Oates and Ralph Smith. Nonlinear optimal tracking control of a piezoelectric nanopositioning stage. *Proceedings of SPIE - The International Society for Optical Engineering*, 6166, 03 2006.

[109] T. Minh, L. Nguyen, and X. Chen. Tracking control of piezoelectric actuator using adaptive model. *Robotics and Biomimetics*, 3, 12 2016.

[110] B. Draženović, C. Milosavljevi, and B.Veselić. *Comprehensive Approach to Sliding Mode Design and Analysis in Linear Systems*, pages 1–19. Springer Berlin Heidelberg, Berlin, Heidelberg, 2013.

[111] J. Velasco, O. Barambones, I. Calvo, J. Zubia, I. Saez de Ocariz, and A. Chouza. Sliding mode control with dynamical correction for time-delay piezoelectric actuator systems. *Materials*, 13, 2019.

[112] J. Shen, W. Jywe, C. Liu, Y. Jian, and J. Yang. Sliding□mode control of a three□degrees□of□freedom nanopositioner. *Asian Journal of Control*, 10:267 – 276, 05 2008.

[113] J. Velasco, I. Calvo, O. Barambones, P. Venegas, and C. Napole. Experimental validation of a sliding mode control for a stewart platform used in aerospace inspection applications. *Mathematics*, 8:2051, 11 2020.

[114] A. Chouza, O. Barambones, I. Calvo, and J. Velasco. Sliding mode-based robust control for piezoelectric actuators with inverse dynamics estimation. *Energies*, 12:943, 03 2019.

[115] H. Thanh, M.T. Vu, X. Mung, N. P. Nguyen, and N.T. Phuong. Perturbation observer-based robust control using a multiple sliding surfaces for nonlinear systems with influences of matched and unmatched uncertainties. *Mathematics*, 8:1371, 08 2020.

[116] H. Lin, J. Leon, W. Luo, A. Marquez, J. Liu, S. Vazquez, and L. Franquelo. Integral sliding-mode control-based direct power control for three-level npc converters. *Energies*, 13, 01 2020.

[117] M. Zaihidee, S. Mekhilef, and M. Mubin. Robust speed control of pmsm using sliding mode control (smc)—a review. *Energies*, 12:1669, 05 2019.

[118] S. Chen and C. Kuo. Design and implementation of double-integral sliding-mode controller for brushless direct current motor speed control. *Advances in Mechanical Engineering*, 9(11):1687814017737724, 2017.

[119] L. Fridman and A. Levant. *Higher-Order Sliding Modes*, volume 11, pages 53–101. Taylor and Francis Group, 01 2002.

[120] M. Silaa, M. Derbeli, O. Barambones, and A. Cheknane. Design and implementation of high order sliding mode control for pemfc power system. *Energies*, 13:4317, 08 2020.

[121] M. Derbeli, O. Barambones, M. Farhat, J. A. Ramos-Hernanz, and L. Sbita. Robust high order sliding mode control for performance improvement of pem fuel cell power systems. *International Journal of Hydrogen Energy*, 45(53):29222 – 29234, 2020.

[122] Y. Shahid and M. Wei. Comparative analysis of different model-based controllers using active vehicle suspension system. *Algorithms*, 13:10, 12 2019.

[123] R. Huo, X. Liu, X. Zeng, and Z. Lei. Integrated guidance and control based on high-order sliding mode method. In *2017 36th Chinese Control Conference (CCC)*, pages 6073–6078, 2017.

[124] X. Liu and W. Wang. High order sliding mode and its application on the tracking control of piezoelectric systems. *International Journal of Innovative Computing, Information and Control*, 4:697–704, 03 2008.

[125] Y. Wang, H. Su, K. Harrington, and G. Fischer. Sliding mode control of piezoelectric valve regulated pneumatic actuator for mri-compatible robotic intervention. In *ASME 2010 Dynamic Systems and Control Conference, DSCC2010*, volume 2, 09 2010.

[126] Y. Yan and Y. Yu. *Quantization Behaviors in Equivalent-Control Based Sliding-Mode Control Systems*, pages 221–241. Springer Berlin Heidelberg, Berlin, Heidelberg, 2013.

[127] M. Armin, P. N. Roy, and S. K. Das. A survey on modelling and compensation for hysteresis in high speed nanopositioning of afms: Observation and future recommendation. *International Journal of Automation and Computing*, 17:479, 2020.

[128] R. Xiong, X. Liu, and Z. Lai. Modeling of hysteresis in piezoelectric actuator based on segment similarity. *Micromachines*, 6:1805–1824, 11 2015.

[129] L. Huang, Y. Hu, Y. Zhao, and Li X. Modeling and control of ipmc actuators based on lssvm-narx paradigm. *Mathematics*, 7:741, 08 2019.

[130] R. Xu, D. Tian, and Z. Wang. Adaptive tracking control for the piezoelectric actuated stage using the krasnosel'skii-pokrovskii operator. *Micromachines*, 11:537, 05 2020.

[131] F. Carneiro, P. Abreu, and M. Restivo. Hysteresis compensation in a tactile device for arterial pulse reproduction. *Sensors*, 18:1631, 05 2018.

[132] J. Lin and M. Chiang. Tracking control of a magnetic shape memory actuator using an inverse preisach model with modified fuzzy sliding mode control. *Sensors*, 16:1368, 08 2016.

[133] N. Vaiana, S. Sessa, F. Marmo, and L. Rosati. A class of uniaxial phenomenological models for simulating hysteretic phenomena in rate-independent mechanical systems and materials. *Nonlinear Dynamics*, 93, 08 2018.

[134] N. Vaiana, S. Sessa, and L. Rosati. A generalized class of uniaxial rate-independent models for simulating asymmetric mechanical hysteresis phenomena. *Mechanical Systems and Signal Processing*, 146:106984, 01 2021.

[135] F. Valenzuela, R. Reymundo, F. Martínez, A. Onofre, and C. E. Castañeda. Super-twisting algorithm applied to velocity control of dc motor without mechanical sensors dependence. *Energies*, 13(22):1–15, 2020.

[136] R. Khan, L. Khan, S. Ullah, I. Sami, and J. Ro. Backstepping based super-twisting sliding mode mppt control with differential flatness oriented observer design for photovoltaic system. *Electronics*, 9:1543, 09 2020.

[137] P. Gao, G. Zhang, and X. Lv. Model-free hybrid control with intelligent proportional integral and super-twisting sliding mode control of pmsm drives. *Electronics*, 9:1427, 09 2020.

[138] Paolo Cappa, G. Rita, K. McConnell, and L. Zachary. Using strain gages to measure both strain and temperature. *Experimental Mechanics*, 32:230–233, 09 1992.

[139] H. Li, Z. Zhang, and Z. Liu. Application of artificial neural networks for catalysis: A review. *Catalysts*, 7:306, 10 2017.

[140] Z. Allam. Achieving neuroplasticity in artificial neural networks through smart cities. *Smart Cities*, 2:118–134, 04 2019.

[141] V. S. Nguyen. Investigation of a multitasking system for automatic ship berthing in marine practice based on an integrated neural controller. *Mathematics*, 8:1–23, 07 2020.

[142] P. Matrenin, V. Manusov, A. Khalyasmaa, D. Antonenkov, S. Eroshenko, and D. Butusov. Improving accuracy and generalization performance of small-size recurrent neural networks applied to short-term load forecasting. *Mathematics*, 8:2169, 12 2020.

[143] Yanfang Liu, Naiming Qi, and Zhi Li. Modeling and identification of temperature-dependent hysteresis in piezoelectric materials considering parameter sensitivity. *IEEE Access*, PP:1–1, 02 2020.

[144] H. Ahn and N. Park. Deep rnn-based photovoltaic power short-term forecast using power iot sensors. *Energies*, 14:436, 01 2021.

[145] C. Grech, M. Buzio, M. Pentella, and N. Sammut. Dynamic ferromagnetic hysteresis modelling using a preisach-recurrent neural network model. *Materials*, 13:2561, 06 2020.

[146] M. Beale, M. Hagan, and H. Demuth. *Deploy Training of Shallow Neural Networks*, chapter Dynamic Neural Networks, pages 21–22. The Mathworks Inc., 2020.

[147] J. Doubravová, J. Wiszniowski, and J. Horalek. Single layer recurrent neural network for detection of swarm-like earthquakes in w-bohemia/vogtland - the method. *Computers and Geosciences*, 93, 05 2016.

[148] Davut Karayel, Orhan Güngör, and Egidijus Šarauskis. Estimation of optimum vacuum pressure of air-suction seed-metering device of precision seeders using artificial neural network models. *Agronomy*, 12(7), 2022.

[149] B. Negash and A. YAW. Artificial neural network based production forecasting for a hydrocarbon reservoir under water injection. *Petroleum Exploration and Development*, 47:383–392, 04 2020.

[150] H. Okut. *Bayesian Regularized Neural Networks for Small n Big p Data*, chapter 2, pages 28–48. Intech, 10 2016.

[151] O. Morfin, C. Castaneda, A. Valderrabano-Gonzalez, M. Hernandez-Gonzalez, and F. Valenzuela. A real-time sosm super-twisting technique for a compound dc motor velocity controller. *Energies*, 10:1286, 08 2017.

[152] J. Moreno. *Lyapunov Approach for Analysis and Design of Second Order Sliding Mode Algorithms*, volume 412, pages 113–149. Springer, 09 2011.

[153] M. Alhato, S. Bouallègue, and H. Rezk. Modeling and performance improvement of direct power control of doubly-fed induction generator based wind turbine through second-order sliding mode control approach. *Mathematics*, 8:1–31, 11 2020.

[154] J. A. Moreno and M. Osorio. Strict lyapunov functions for the super-twisting algorithm. *IEEE Transactions on Automatic Control*, 57(4):1035–1040, 2012.

[155] G. Stamov, I. Stamova, G. Venkov, T. Stamov, and C. Spirova. Global stability of integral manifolds for reaction–diffusion delayed neural networks of cohen–grossberg-type under variable impulsive perturbations. *Mathematics*, 8:1082, 07 2020.

[156] C. Popa and E. Kaslik. Finite-time mittag–leffler synchronization of neutral-type fractional-order neural networks with leakage delay and time-varying delays. *Mathematics*, 8:1146, 07 2020.

[157] Marina Tyunina, Jan Miksovsky, Tomas Kocourek, and Alexandr Dejneka. Hysteresis-free piezoresponse in thermally strained ferroelectric barium titanate films. *Electronic Materials*, 2(1):17–23, 2021.

[158] Wen Wang, Jian Wang, Zhanfeng Chen, Ruijin Wang, Keqing Lu, Zhiqian Sang, and Bingfeng Ju. Research on asymmetric hysteresis modeling and compensation of piezoelectric actuators with pmpi model. *Micromachines*, 11, 2020.

[159] Royson Dsouza, Bineesh Benny, Anil Sequeira, and Navin Karanth. Hysteresis modeling of amplified piezoelectric stack actuator for the control of the microgripper. *American Scientific Research Journal for Engineering, Technology, and Sciences*, 15:265–281, 01 2016.

[160] Bingxiao Ding, Yangmin Li, Xiao Xiao, and Yirui Tang. Optimized pid tracking control for piezoelectric actuators based on the bouc-wen model. In *2016 IEEE International Conference on Robotics and Biomimetics (ROBIO)*, pages 1576–1581, 2016.

[161] Yuxiang Ma and Yunhua Li. Active disturbance compensation based robust control for speed regulation system of permanent magnet synchronous motor. *Applied Sciences*, 10(2), 2020.

[162] Asif Sabanovic and Khalid Abidi. Sliding mode based piezoelectric actuator control. In *2004 IEEE International Conference on Industrial Technology, 2004. IEEE ICIT '04.*, volume 1, pages 425 – 430 Vol. 1, 01 2005.

[163] Rajko Svečko, Dušan Gleich, and Andrej Sarjaš. The effective chattering suppression technique with adaptive super-twisted sliding mode controller based on the quasi-barrier function; an experimentation setup. *Applied Sciences*, 10(2), 2020.

[164] Yumna Shahid and Minxiang Wei. Comparative analysis of different model-based controllers using active vehicle suspension system. *Algorithms*, 13(1), 2020.

[165] Sudipta Saha, Syed Muhammad Amrr, Abdelaziz Salah Saidi, Arunava Banerjee, and M. Nabi. Finite-time adaptive higher-order smc for the nonlinear five dof active magnetic bearing system. *Electronics*, 10(11), 2021.

[166] Xin Che, Dapeng Tian, Rui Xu, and Ping Jia. Finite-time control for piezoelectric actuators with a high-order terminal sliding mode enhanced hysteresis observer. *IEEE Access*, 8:223931–223940, 2020.

[167] Jazmín Zenteno-Torres, Jérôme Cieslak, Jorge Dávila, and David Henry. Sliding mode control with application to fault-tolerant control: Assessment and open problems. *Automation*, 2(1):1–30, 2021.

[168] Guangming Xue, Peilin Zhang, Zhongbo He, Dongwei Li, Zhaoshu Yang, and Zhenglong Zhao. Modification and numerical method for the jiles-atherton hysteresis model. *Communications in Computational Physics*, 21(3):763–781, 2017.

[169] Khubab Ahmed, Peng Yan, and Su Li. Duhem model-based hysteresis identification in piezo-actuated nano-stage using modified particle swarm optimization. *Micromachines*, 12(3), 2021.

[170] C.-Y. Su, Y. Stepanenko, J. Svoboda, and T.P. Leung. Robust adaptive control of a class of nonlinear systems with unknown backlash-like hysteresis. *IEEE Transactions on Automatic Control*, 45(12):2427–2432, 2000.

[171] Jinqiang Gan and Xianmin Zhang. Nonlinear hysteresis modeling of piezoelectric actuators using a generalized bouc–wen model. *Micromachines*, 10:183, 03 2019.

[172] Mengmeng Li, Qinglin Wang, Yuan Li, and Zhaoguo Jiang. Modeling and discrete-time terminal sliding mode control of a deap actuator with rate-dependent hysteresis nonlinearity. *Applied Sciences*, 9(13), 2019.

[173] Arie Levant. Principles of 2-sliding mode design. *Automatica*, 43(4):576–586, 2007.

[174] M. Kaiser. Time-delay neural networks for control. *IFAC Proceedings Volumes*, 27(14):967–972, 1994. Fourth IFAC Symposium on Robot Control, Capri, Italy, September 19-21, 1994.

[175] Yi-Chun Du and Alphin Stephanus. Levenberg-marquardt neural network algorithm for degree of arteriovenous fistula stenosis classification using a dual optical photoplethysmography sensor. *Sensors*, 18(7), 2018.

[176] Bingxiao Ding, Yangmin Li, Xiao Xiao, and Yirui Tang. Optimized pid tracking control for piezoelectric actuators based on the bouc-wen model. In *2016 IEEE International Conference on Robotics and Biomimetics (ROBIO)*, pages 1576–1581, 2016.

[177] Anis Kaci, Christophe Giraud-Audine, Frederic Giraud, Michel Amberg, and Betty Lemaire-Semail. Lqr based mimo-pid controller for the vector control of an underdamped harmonic oscillator. *Mechanical Systems and Signal Processing*, 134:106314, 2019.

[178] T. Tang, S. Xu Niu, T. Yang, B. Qi, and Q. Liang Bao. Vibration rejection of tip-tilt mirror using improved repetitive control. *Mechanical Systems and Signal Processing*, 116:432–442, 2019.

[179] Youhao Hu and Hai Wang. Robust tracking control for vehicle electronic throttle using adaptive dynamic sliding mode and extended state observer. *Mechanical Systems and Signal Processing*, 135:106375, 2020.

[180] Jin Zhang, Yiling Yang, Junqiang Lou, Yanding Wei, and Lei Fu. Development and hybrid position/force control of a dual-drive macro-fiber-composite microgripper. *Sensors*, 18(4), 2018.

[181] Jie Ling, Zhao Feng, Dongdong Zheng, Jun Yang, Haoyong Yu, and Xiaohui Xiao. Robust adaptive motion tracking of piezoelectric actuated stages using online neural-network-based sliding mode control. *Mechanical Systems and Signal Processing*, 150:107235, 2021.

[182] Vadim Utkin and Hoon Lee. Chattering problem in sliding mode control systems. *IFAC Proceedings Volumes*, 39(5):1, 2006. 2nd IFAC Conference on Analysis and Design of Hybrid Systems.

[183] M. Chandrashekhar and Ranjan Ganguli. Uncertainty handling in structural damage detection using fuzzy logic and probabilistic simulation. *Mechanical Systems and Signal Processing*, 23(2):384–404, 2009.

[184] André Sanches Fonseca Sobrinho and Francisco Granziera Junior. Type-1 fuzzy logic algorithm for low cost embedded systems. *Computers & Electrical Engineering*, 88:106861, 2020.

[185] M.H. Korayem, H. Khaksar, and A. Mousavi. Modeling and control of probe distance, substrate and probe of afm using afsmc in the presence of disturbances. *Mechanical Systems and Signal Processing*, 152:107458, 2021.

[186] Shengzheng Kang, Hongtao Wu, Xiaolong Yang, Yao Li, and Yaoyao Wang. Model-free robust finite-time force tracking control for piezoelectric actuators using time-delay estimation with adaptive fuzzy compensator. *Transactions of the Institute of Measurement and Control*, 42(3):351–364, 2020.

[187] Mohammed Altaher and Sumeet S. Aphale. Fuzzy-enhanced dual-loop control strategy for precise nanopositioning. In *2017 International Symposium on Computer Science and Intelligent Controls (ISCSIC)*, pages 73–81, 2017.

[188] Jerry M. Mendel. *Introduction*, chapter 1, pages 1–23. Springer International Publishing, 2017.

[189] J.M. Mendel and R.I.B. John. Type-2 fuzzy sets made simple. *IEEE Transactions on Fuzzy Systems*, 10(2):117–127, 2002.

[190] Jerry M. Mendel. *Sources of Uncertainty*, chapter 6, pages 245–258. Springer International Publishing, Cham, 2017.

[191] Dongrui Wu. On the fundamental differences between interval type-2 and type-1 fuzzy logic controllers. *IEEE Transactions on Fuzzy Systems*, 20(5):832–848, 2012.

[192] Prashant J. Gaidhane, Madhav J. Nigam, Anupam Kumar, and Pyari Mohan Pradhan. Design of interval type-2 fuzzy precompensated pid controller applied to two-dof robotic manipulator with variable payload. *ISA Transactions*, 89:169–185, 2019.

[193] Jian Huang, MyongHyok Ri, Dongrui Wu, and Songhyok Ri. Interval type-2 fuzzy logic modeling and control of a mobile two-wheeled inverted pendulum. *IEEE Transactions on Fuzzy Systems*, 26(4):2030–2038, 2018.

[194] K. A. Naik and C. P. Gupta. Performance comparison of type-1 and type-2 fuzzy logic systems. In *2017 4th International Conference on Signal Processing, Computing and Control (ISPCC)*, pages 72–76, 2017.

[195] Claudia-Adina Bojan-Dragos, Radu-Emil Precup, Stefan Preitl, Raul-Cristian Roman, Elena-Lorena Hedrea, and Alexandra-Iulia Szedlak-Stinean. Gwo-based optimal tuning of type-1 and type-2 fuzzy controllers for electromagnetic actuated clutch systems. *IFAC-PapersOnLine*, 54(4):189–194, 2021.

[196] Jyoti Ranjan Nayak, Binod Shaw, and Binod Kumar Sahu. Application of adaptive-sos (asos) algorithm based interval type-2 fuzzy-pid controller with derivative filter for automatic generation control of an interconnected power system. *Engineering Science and Technology, an International Journal*, 21(3):465–485, 2018.

[197] Mohammad Al Janaideh and Omar Aljanaideh. Further results on open-loop compensation of rate-dependent hysteresis in a magnetostrictive actuator with the prandtl-ishlinskii model. *Mechanical Systems and Signal Processing*, 104:835–850, 2018.

[198] Jerry Mendel. *Type-1 Fuzzy Systems: Design Methods and Applications*, chapter 4, pages 161–244. Springer International Publishing, 05 2017.

[199] Artur Movsessian, David García Cava, and Dmitri Tcherniak. An artificial neural network methodology for damage detection: Demonstration on an operating wind turbine blade. *Mechanical Systems and Signal Processing*, 159:107766, 2021.

[200] Xinyong Zhang and Liwei Sun. Optimization of optical machine structure by backpropagation neural network based on particle swarm optimization and bayesian regularization algorithms. *Materials*, 14(11), 2021.

[201] Eduard Sariev and Guido Germano. Bayesian regularized artificial neural networks for the estimation of the probability of default. *Quantitative Finance*, 20(2):311–328, 2020.

[202] L.A. Zadeh. The concept of a linguistic variable and its application to approximate reasoning—i. *Information Sciences*, 8(3):199–249, 1975.

[203] Masaharu Mizumoto and Kokichi Tanaka. Some properties of fuzzy sets of type 2. *Information and Control*, 31(4):312–340, 1976.

[204] Oscar Castillo, Leticia Amador-Angulo, Juan R. Castro, and Mario Garcia-Valdez. A comparative study of type-1 fuzzy logic systems, interval type-2 fuzzy logic systems and generalized type-2 fuzzy logic systems in control problems. *Information Sciences*, 354:257–274, 2016.

[205] Xiang-Ji Wei, Da-Qing Zhang, and Sheng-Juan Huang. A variable selection method for a hierarchical interval type-2 tsk fuzzy inference system. *Fuzzy Sets and Systems*, 438:46–61, 2022. Fuzzy and Neurofuzzy Models.

[206] Chunfeng Suo, Yongming Li, and Zhihui Li. On n-polygonal interval-valued fuzzy sets. *Fuzzy Sets and Systems*, 417:46–70, 2021. Fuzzy Intervals and Their Applications.

[207] W. Wang and J. M. Mendel. Multiple attribute group decision making with linguistic variables and complete unknown weight information. *Iranian Journal of Fuzzy Systems*, 16(4):145–157, 2019.

[208] Emanuel Ontiveros-Robles, Patricia Melin, and Oscar Castillo. New methodology to approximate type-reduction based on a continuous root-finding karnik mendel algorithm. *Algorithms*, 10(3), 2017.

[209] Nilesh N. Karnik and Jerry M. Mendel. Centroid of a type-2 fuzzy set. *Information Sciences*, 132(1):195–220, 2001.

[210] Dong An, Haodong Li, Ying Xu, and Lixiu Zhang. Compensation of hysteresis on piezoelectric actuators based on tripartite pi model. *Micromachines*, 9(2), 2018.

[211] Ting Zheng, Jiagang Wu, Dingquan Xiao, and Jianguo Zhu. Recent development in lead-free perovskite piezoelectric bulk materials. *Progress in Materials Science*, 98:552–624, 2018.

[212] Wenwen Han, Shubao Shao, Shuwen Zhang, Zheng Tian, and Minglong Xu. Design and modeling of decoupled miniature fast steering mirror with ultrahigh precision. *Mechanical Systems and Signal Processing*, 167:108521, 2022.

[213] Shuai Wang, Zhaobo Chen, Xiaoxiang Liu, and Yinghou Jiao. Feedforward Feedback Linearization Linear Quadratic Gaussian With Loop Transfer Recovery Control of Piezoelectric Actuator in Active Vibration Isolation System. *Journal of Vibration and Acoustics*, 140(4), 2018.

[214] Yi-Liang Yeh. Output feedback tracking sliding mode control for systems with state- and input-dependent disturbances. *Actuators*, 10(6), 2021.

[215] Fabrizio Vestroni and Paolo Casini. *Nonlinear Dynamics and Phenomena in Oscillators with Hysteresis*, chapter 8, pages 185–202. John Wiley & Sons, Ltd, 2021.

[216] Shengwei Quan, Ya-Xiong Wang, Xuelian Xiao, Hongwen He, and Fengchun Sun. Feedback linearization-based mimo model predictive control with defined pseudo-reference for hydrogen regulation of automotive fuel cells. *Applied Energy*, 293:116919, 2021.

[217] Jamshed Iqbal, Mukhtar Ullah, Said Ghani Khan, Baizid Khelifa, and Saša Ćuković. Nonlinear control systems - a brief overview of historical and recent advances. *Nonlinear Engineering*, 6(4):301–312, 2017.

[218] Catalin Dumitrescu, Petrica Ciotirnae, and Constantin Vizitiu. Fuzzy logic for intelligent control system using soft computing applications. *Sensors*, 21(8), 2021.

[219] Xiuyu Zhang, Xinkai Chen, Guoqiang Zhu, and Chun-Yi Su. Output feedback adaptive motion control and its experimental verification for time-delay nonlinear systems with asymmetric hysteresis. *IEEE Transactions on Industrial Electronics*, 67(8):6824–6834, 2020.

[220] Yajun Luo, Xue Zhang, Yahong Zhang, Yuandong Qu, Minglong Xu, Kunkun Fu, and Lin Ye. Active vibration control of a hoop truss structure with piezoelectric bending actuators based on a fuzzy logic algorithm. *Smart Materials and Structures*, 27(8):085030, jul 2018.

[221] Max Schwenzer, Ay Muzaffer, Thomas Bergs, and Abel Dirk. Review on model predictive control: an engineering perspective. *The International Journal of Advanced Manufacturing Technology*, 117:1327–1349, 2021.

[222] Zhangming Du, Chao Zhou, Zhiqiang Cao, Shuo Wang, Long Cheng, and Min Tan. A neural network-based model predictive controller for displacement tracking of piezoelectric actuator with feedback delays. *International Journal of Advanced Robotic Systems*, 18(6), 2021.

[223] Poornima M. Chanal, Mahabaleshwar S. Kakkasageri, and Sunil Kumar S. Manvi. Chapter 7 - security and privacy in the internet of things: computational intelligent techniques-based approaches. In Siddhartha Bhattacharyya, Paramartha Dutta, Debabrata Samanta, Anirban Mukherjee, and Indrajit Pan, editors, *Recent Trends in Computational Intelligence Enabled Research*, pages 111–127. Academic Press, 2021.

[224] Clara Marina Martínez and Dongpu Cao. 2 - integrated energy management for electrified vehicles. In Clara Marina Martínez and Dongpu Cao, editors, *Ihorizon-Enabled Energy Management for Electrified Vehicles*, pages 15–75. Butterworth-Heinemann, 2019.

[225] Cristian Napole, Oscar Barambones, Mohamed Derbeli, and Isidro Calvo. Advanced trajectory control for piezoelectric actuators based on robust control combined with artificial neural networks. *Applied Sciences*, 11(16), 2021.

[226] Cunman Liang, Fujun Wang, Beichao Shi, Zhichen Huo, Kaihuan Zhou, Yanling Tian, and Dawei Zhang. Design and control of a novel asymmetrical piezoelectric actuated microgripper for micromanipulation. *Sensors and Actuators A: Physical*, 269:227–237, 2018.

[227] Jun Yik Lau, Wenyu Liang, Hwee Choo Liaw, and Kok Kiong Tan. Sliding mode disturbance observer-based motion control for a piezoelectric actuator-based surgical device. *Asian Journal of Control*, 20(3):1194–1203, 2018.

[228] Zefeng Xu, Wenkai Huang, Zexuan Li, Linkai Hu, and Puwei Lu. Nonlinear nonsingular fast terminal sliding mode control using deep deterministic policy gradient. *Applied Sciences*, 11(10), 2021.

[229] Rui Xu and Miaolei Zhou. Sliding mode control with sigmoid function for the motion tracking control of the piezo-actuated stages. *Electronics Letters*, 53, 01 2017.

[230] Yuri B. Shtessel, Ilya A. Shkolnikov, and Mark D.J. Brown. An asymptotic second-order smooth sliding mode control. *Asian Journal of Control*, 5(4):498–504, 2003.

[231] Vadim Utkin, Alex Poznyak, Yury Orlov, and Andrey Polyakov. Conventional and high order sliding mode control. *Journal of the Franklin Institute*, 357(15):10244–10261, 2020.

[232] Leonid Fridman, Jaime A. Moreno, Bijnan Bandyopadhyay, Shyam Kamal, and Asif Chalanga. *Continuous Nested Algorithms : The Fifth Generation of Sliding Mode Controllers*, chapter 2, pages 5–35. Springer International Publishing, 2015.

[233] Deepika Deepika, Sandeep Kaur, and Shiv Narayan. Integral terminal sliding mode control unified with ude for output constrained tracking of mismatched uncertain non-linear systems. *ISA Transactions*, 101:1–9, 2020.

[234] Donya Ashtiani Haghighi and Saleh Mobayen. Design of an adaptive super-twisting decoupled terminal sliding mode control scheme for a class of fourth-order systems. *ISA Transactions*, 75:216–225, 2018.

[235] Chen Li, Yongji Wang, and Lei Liu. Path following control of ship based on time-varying threshold prescribed convergence law sliding mode. In *2018 37th Chinese Control Conference (CCC)*, pages 525–530, 2018.

[236] Qingsong Xu. Continuous integral terminal third-order sliding mode motion control for piezoelectric nanopositioning system. *IEEE/ASME Transactions on Mechatronics*, 22(4):1828–1838, 2017.

[237] Pengpeng Shi. One-dimensional magneto-mechanical model for anhysteretic magnetization and magnetostriction in ferromagnetic materials. *Journal of Magnetism and Magnetic Materials*, 537:168212, 2021.

[238] Gregor Thiele, Arne Fey, David Sommer, and Jorg Kruger. System identification of a hysteresis-controlled pump system using sindy. In *2020 24th International Conference on System Theory, Control and Computing (ICSTCC)*, pages 457–464, 10 2020.

[239] Mikhail Semenov, Olga Reshetova, Sergei Borzunov, and Peter Meleshenko. Self-oscillations in a system with hysteresis: the small parameter approach. *The European Physical Journal Special Topics*, 230, 07 2021.

[240] Zhi Li, Jinjun Shan, and Ulrich Gabbert. A direct inverse model for hysteresis compensation. *IEEE Transactions on Industrial Electronics*, 68(5):4173–4181, 2021.

[241] Mohammad Al Janaideh, Daniele Davino, Pavel Krejčí, and Ciro Visone. Comparison of prandtl–ishlinskiı˘ and preisach modeling for smart devices applications. *Physica B: Condensed Matter*, 486:155–159, 2016. 10th International Symposium on Hysteresis Modeling and Micromagnetics (HMM 2015).

[242] Li Zheng and Dong Weijie. Position and force self-sensing piezoelectric valve with hysteresis compensation. *Journal of Intelligent Material Systems and Structures*, page 1045389X2110116, 05 2021.

[243] Scorretti Riccardo, Francesco Riganti-Fulginei, Antonino Laudani, and Simone Quandam. Algorithms to reduce the computational cost of vector preisach model in view of finite element analysis. *Journal of Magnetism and Magnetic Materials*, 546:168876, 2022.

[244] Muyao Shao, Yiru Wang, Zhiyuan Gao, and Xiaojin Zhu. Discrete-time rate-dependent hysteresis modeling and parameter identification of piezoelectric actuators. *Transactions of the Institute of Measurement and Control*, 0(0):01423312211069364, 2022.

[245] Liu Yang, Zhongyang Zhao, Yi Zhang, and Dongjie Li. Rate-dependent modeling of piezoelectric actuators for nano manipulation based on fractional hammerstein model. *Micromachines*, 13(1), 2022.

[246] Xudong Zhu and Xilin Lu. Parametric identification of bouc-wen model and its application in mild steel damper modeling. *Procedia Engineering*, 14:318–324, 2011. The Proceedings of the Twelfth East Asia-Pacific Conference on Structural Engineering and Construction.

[247] J.J. Slotine and W. Li. *Sliding Surfaces*, chapter Sliding Control, pages 278–279. Prentice Hall, 1991.

[248] Cristian Napole, Oscar Barambones, Mohamed Derbeli, Isidro Calvo, Mohammed Yousri Silaa, and Javier Velasco. High-performance tracking for piezoelectric actuators using super-twisting algorithm based on artificial neural networks. *Mathematics*, 9(3), 2021.

[249] Bing Zhang, Kang Nie, Xinglong Chen, and Yao Mao. Development of sliding mode controller based on internal model controller for higher precision electro-optical tracking system. *Actuators*, 11(1), 2022.

[250] Y. Shtessel, C. Edwards, L. Fridman, and A. Levant. *Second-Order Sliding Mode Controllers and Differenciators*, chapter 4, pages 143–182. Springer New York, 2014.

[251] Raul Santiesteban, Leonid Fridman, and Jaime Moreno. Finite-time convergence analysis for "twisting" controller via a strict lyapunov function. In *2010 11th International Workshop on Variable Structure Systems (VSS)*, pages 1 – 6, 07 2010.

[252] Jaime Moreno, Héctor Ríos, Luis Ovalle, and Leonid Fridman. Multivariable super-twisting algorithm for systems with uncertain input matrix and perturbations. *IEEE Transactions on Automatic Control*, PP:1–1, 11 2021.

[253] Ismael Castillo, Martin Steinberger, Leonid Fridman, Jaime A. Moreno, and Martin Horn. *A Lyapunov based Saturated Super-Twisting Algorithm*, chapter 2, pages 47–68. Springer Singapore, Singapore, 2021.

[254] James E. Stott and Yuri B. Shtessel. Launch vehicle attitude control using sliding mode control and observation techniques. *Journal of the Franklin Institute*, 349(2):397–412, 2012. Advances in Guidance and Control of Aerospace Vehicles using Sliding Mode Control and Observation Techniques.

[255] Yuri Shtessel, Christopher Edwards, Leonid Fridman, and Arie Levant. *Introduction: Intuitive Theory of Sliding Mode Control*, chapter 1, pages 1–42. Springer New York, New York, NY, 2014.

[256] Yuri B. Shtessel, Malek Ghanes, and Roshini S. Ashok. Hydrogen fuel cell and ultracapacitor based electric power system sliding mode control: Electric vehicle application. *Energies*, 13(11), 2020.